# ABSTRACT

SINGH, SUGANDHA. Factors Affecting Seismic Response of Electrical Equipment in Nuclear Power Plants Subjected to High–Frequency Ground Motions. (Under the direction of Dr. Abhinav Gupta and Dr. Ashly Cabas).

Nuclear power plants in low–to–moderate seismicity regions are subjected to high–frequency ground motions. However, the safe shutdown earthquake for most of the plants is based on the low–frequency ground motions recorded in Western United States. The safety systems in nuclear power plants rely on electrical equipment which are sensitive to high–frequency accelerations. The electrical equipment are qualified by comparing their seismic capacity from shake table tests with the in–cabinet response spectrum (ICRS). This dissertation studies the effects of different factors such as localized nonlinearity in cabinet mounting arrangement such as gaps, interaction of building–cabinet system, etc., on ICRS. These factors are ignored by the conventional uncoupled linear elastic analysis. The effect of localized nonlinearities is not critical for low frequency ground motions but can be quite important in the case of high frequency ground motions. Analyses of SDOF cabinet models with gaps subjected to low frequency harmonic acceleration show that transient response due to localized impacts at cabinet base can increase the total response and lead to high–frequency peaks in the ICRS. For high frequency motions, the floor motions can be filtered out by gaps when floor displacements are smaller than the gap length. Furthermore, it is observed that building–cabinet interaction results in a reduction of the spectral amplitudes in ICRS but interaction occurs only when the gap is closed. The effect of interaction in nonlinear coupled systems with high–frequency tuned modes subjected to high–frequency ground motions is relatively lower as compared to that in a linear system. Characterization of high frequency design ground motions at a given site is difficult because only a few recorded ground motions may be available in low–to–moderate seismicity regions. Site–specific kappa ($\kappa_0$) is a site–specific attenuation parameter commonly used to capture near–surface in stochastic

simulations of ground motions and host–to–target adjustment methods. This dissertation proposes a closed–form equation to estimate probabilistic distributions of $\kappa_0$ using available site parameters such as shear–wave velocity and soil damping ratio in regions where recorded ground motions are not available. This analytical formulation to capture near–surface attenuation represents a step toward improving the characterization of high–frequency energy content at NPP located in CEUS.

# Factors Affecting Seismic Response of Electrical Equipment in Nuclear Power Plants Subjected to High–Frequency Ground Motion

by
Sugandha Singh

A dissertation submitted to the Graduate Faculty of
North Carolina State University
in partial fulfillment of the
requirements for the degree of
Doctor of Philosophy

Civil Engineering

Raleigh, North Carolina

2020

APPROVED BY:

| | |
|---|---|
| Dr. Abhinav Gupta<br>Co–Chair of Advisory Committee | Dr. Ashly Cabas<br>Co–Chair of Advisory Committee |
| Dr. Shamim Rahman | Dr. Mervyn Kowalsky |

# DEDICATION

*To My Mom, Dad and Brother*

# BIOGRAPHY

Sugandha Singh was born on January 23rd, 1991 in Haldwani, India. She grew up in the state of Uttarakhand, India. She joined the undergraduate program in Civil Engineering at College of Technology, G.B. Pant University of Agriculture & University, Pantnagar in July 2008 and graduated with the Bachelor of Technology (B.Tech.) degree in May 2012. Following graduation, she started working in Mumbai, India from July 2012 at Shapoorji Pallonji & Co. Ltd. (Construction Materials Group) as a Project Engineer/Coordinator for two years. She joined North Carolina State University to pursue Master of Science (M.S.) in Civil Engineering in August 2014. After graduating with a M.S. degree, she pursued her doctoral degree in Structural Engineering and Mechanics at North Carolina State University.

Sugandha worked as a teaching assistant for Structural Dynamics (graduate) and Structural Behavior and Measurements (undergraduate) courses at North Carolina State University. Sugandha's research interests so far include structural dynamics with focus on the behavior of electrical cabinets and control panels subjected to high–frequency ground motions; geotechnical earthquake engineering focusing on probabilistic seismic hazard and determination of spectral decay factor, kappa. In future, she plans on working in the fields of Fluid–Soil–Structure Interaction and Multi–Hazard Risk Assessment in Urban Planning.

In addition to coursework, Sugandha has received Teaching and Communication Certificate from Graduate School at North Carolina State University. She has also been associated with various administrative organizations at the university such as Graduate Student Association where she served as Vice President of Academic Affairs (2018–2019); Council on the Status of Women at NC State; Administrative Board of Graduate School, etc.

# ACKNOWLEDGEMENTS

To start with, I would like to express my genuine gratitude to Dr. Abhinav Gupta for giving me the opportunity to pursue MS and PhD studies at NCSU. This research would not have been possible without him for putting his valuable time in guiding me through the research and in writing this dissertation. I am very grateful to Dr. Ashly Cabas for her immense support and enthusiasm in guiding my work through the some very difficult times and having an unwavering belief in me. I would also like to thank Dr. Shamim Rahman, Dr. Mervyn Kowalsky, and Dr. Mihai Diaconeasa for graciously agreeing to serve on my committee and for their valuable suggestions.

My parents, Sanjay and Seema Kushwaha, and my brother, Devang, have always been instrumental in everything I have done in my life. None of this would have been remotely possible without the unconditional love, support, and encouragement from them. They have always inspired me at every step and gave me a direction in life. A would like to specially thank my friends Ankit, Mahita, John, and Judy for supporting me every step of the way. My life at NCSU would not have been complete if they had not been around me with their support. I also want to thank Saran, Chunyang, Pragya, and Ishika for helping me understand various concepts of my research. I thank my friends Shreya, Pallavi, Anushree, Kanchan, Ayesha, and Bharat for giving me hope and joy whenever I needed it. A heartfelt thanks to all of my colleagues especially, Nicholas, Abrahm, Sangwoo, Alexis, Harleen and Parth for their support.

Finally, the research was supported by the Center for Nuclear Energy Facilities & Structures at North Carolina State University. I am greatly indebted to the center for providing me with all the facilities and support throughout. I would also like to thank all the staff members of the Civil Engineering department for their help and support extended over the years.

# TABLE OF CONTENTS

# LIST OF TABLES

# LIST OF FIGURES

# Chapter 1

## Introduction

## 1. Introduction

Majority of nuclear power plants (NPP) in United States are located in Central and Eastern United States (CEUS). The CEUS is a low–to–moderate seismicity region and thus, lacks ground motion recordings for design safe–shutdown earthquake (SSE) spectrum at NPP site. The SSE recommended by United States Nuclear Regulatory Commission's Reg. Guide 1.60 is based on earthquake data recorded in Western United States (WUS) which has low–frequency content. However, as shown in Figure. 1, the ground motion studies (SSHAC, 1997; EPRI, 2013; PEER, 2015) conducted in low–to–moderate seismicity regions such as CEUS indicate that the ground motion response spectra at such regions exceed safe shutdown earthquake at high frequencies. A study by Electric Power Research Institute (EPRI, 2007) found that the high–frequency ground motions do not cause severe structural damage. However, the functionality of safety–related electrical equipment such as relays is affected by high–frequency accelerations. Therefore, the seismic response of electrical equipment when subjected to high–frequency ground motion must be studied. The safety–related electrical equipment such as relays initiate the safe shutdown procedure in nuclear power plants (NPP) during an earthquake. The electrical equipment are seismically qualified before use in NPPs, which requires comparisons of shake table test results for electrical equipment with the seismic response of electrical equipment obtained from analysis of NPP systems (EPRI, 2014).

Figure. 2 shows a schematic of the analysis procedure used to generate ICRS for seismic qualification of the safety–related electrical equipment. As shown in this figure, the analysis of building subjected to a ground motion yields floor accelerations. The safety–related electrical equipment are mounted on electrical cabinets. In-cabinet acceleration at the location of equipment is evaluated from the analysis of cabinet subjected to floor acceleration. A response spectrum

calculated from in-cabinet acceleration is known as In-cabinet Response Spectrum (ICRS). The acceleration capacity of electrical equipment from shake table tests is then compared with ICRS to seismically qualify electrical equipment.

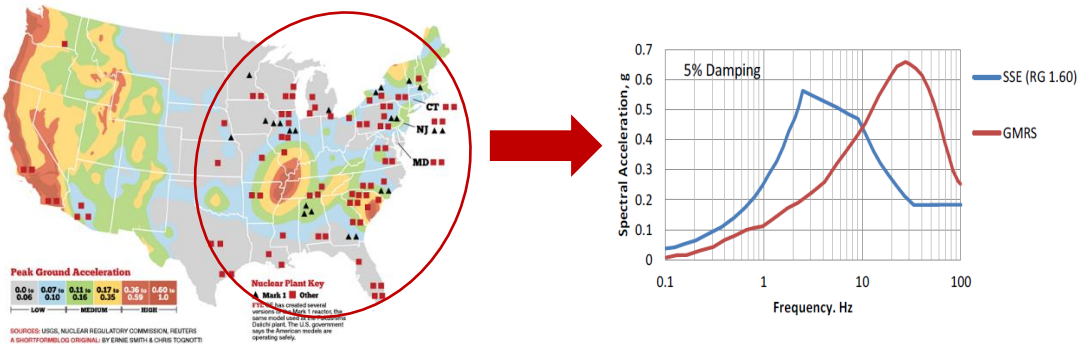


**(a)** **(b)**

**Figure. 1. (a)** United States Seismic Hazard Map and Nuclear Power Plant Locations. **(b)** Comparison of Safe Shutdown Earthquake and Ground Motion Response Spectrum at a CEUS site (EPRI, 2014)

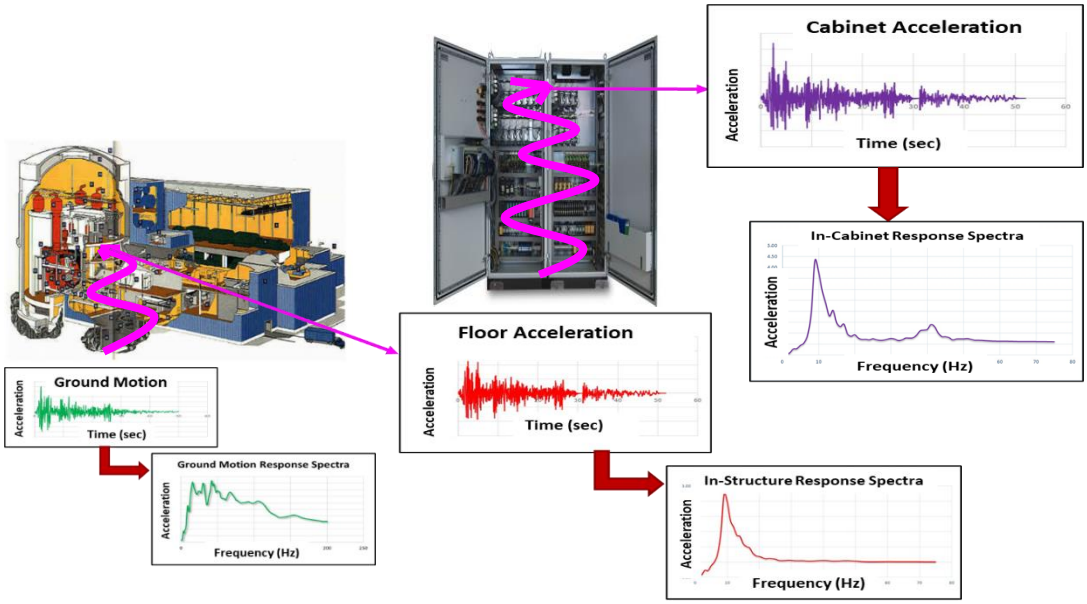


**Figure. 2.** Propagation of Ground Motion through NPP Building–Cabinet System

Conventionally, uncoupled linear analyses of building–cabinet systems are conducted to evaluate ICRS. The ICRS from linear analyses have high spectral amplitudes at high frequencies (Singh, 2017). However, the experimental study conducted by Vlaski et al. (2013, 2019) indicated that the high–frequency accelerations do not propagate to the electrical equipment. Herve (2014) suggested that a gap may be present at the bolted connection between the building floor and the electrical cabinet base plate. Since high–frequency accelerations induce low displacement, the seismic motion does not propagate to the electrical equipment. The analysis conducted by Singh (2017) shows that for most cases of building–cabinet systems, the high-frequency seismic motions do not propagate due to the gap.

The analysis conducted by Singh (2017) observed high–frequency peaks and valleys in the ICRS. Such an odd response of electrical equipment is explained to occur due to impact induced in the cabinet when the cabinet's base impacts with the anchor bolt head. However, the explanation for occurrence of peaks and valleys at periodic interval of frequencies requires greater investigation and explanation. Furthermore, Singh (2017) studied the response of electrical equipment of linear and nonlinear models of uncoupled single degree of freedom (SDOF) building and cabinet systems. The uncoupled analysis ignores the effects of building–cabinet interaction as well as contribution of high–frequency modes in a multi–degrees of freedom (MDOF) system on the ICRS. Therefore, it is important to explore the effect of these factors in a MDOF building–MDOF cabinet system. Finally, due to limited number of earthquake records available in regions such as CEUS, the characterization of appropriate ground motions needed in seismic qualification of equipment requires simulation-based approach. Site–specific kappa ($\kappa_0$) is an attenuation parameter which is commonly used in the stochastic simulation of ground motions and in host–to–target adjustments of ground motion models. Using traditional record-based methods, $\kappa_0$ can

only be evaluated in regions where abundant ground motion data are available. Further exploration of alternative methods for estimating $\kappa_0$ in regions with low–to–moderate seismicity (e.g., CEUS) is essential to further characterize near-surface attenuation and appropriate constraints to high-frequency seismic energy in the expected ground motions. To address these limitations, this research is divided into three main parts:

- Effects of boundary conditions on seismic response of electrical equipment subjected to high-frequency ground motions.
- Understanding the seismic response of MDOF building – MDOF electrical equipment subjected to high–frequency ground motions.
- Quantification of the contribution of sedimentary deposits to high–frequency attenuation in low–to–moderate seismicity regions via the site transfer function

## 2. Background

### 2.1. Effects of Boundary Conditions on Seismic Response of Electrical Equipment Subjected to High-Frequency Ground Motions

Singh (2017) shows that for nonlinear cabinet models with gaps, the spectral acceleration amplitudes are usually lower as compared to the linear analysis. The difference between linear and nonlinear cabinet models is rather significant for the case of high–frequency building (primary system) – high–frequency cabinet (secondary system) subjected to high–frequency ground motion. It is shown that in a particular case, the peak spectral acceleration from a linear analysis is 350g whereas that from the nonlinear cabinet model with gap is only 4g. Even though the nonlinear cabinet models with gap are found to have lower peak spectral accelerations, the ICRS shows

periodic pattern of peaks and valleys at high frequencies. This unique behavior of ICRS in nonlinear cabinet models must be studied and explained using fundamental principles. An analytical model of nonlinear single degree of freedom (SDOF) system is used to study this aspect and explain the observed behavior. The unique nature of ICRS in nonlinear cabinet model with gap is explained by studying the response of low– and high–frequency SDOF systems with gap subjected to harmonic excitations.

## 2.2. Understanding the Seismic Response of Electrical Equipment Subjected to High–Frequency Ground Motions

The study by Singh (2017) analyzed uncoupled SDOF building and SDOF cabinet systems. one of the assumptions in the study is that the majority of response is contributed by the fundamental building mode while for the electrical cabinet, a significant mode contributes to the response of the equipment (Gupta et al., 1999). Even though the high–frequency accelerations filter out due to the gap before reaching the equipment, many factors such as contribution of higher frequency modes of building and electrical cabinets, mass interaction between tuned modes of building and electrical cabinet, location of equipment, etc., are ignored in uncoupled SDOF systems analysis.

The current practice for seismic qualification of electrical equipment is to conduct linear uncoupled analysis of building–cabinet system. However, the results obtained from uncoupled analysis are conservative and many electrical devices often do not qualify for use in the nuclear power plant (EPRI, 2017; Dubey et al., 2019). A coupled analysis of building–cabinet system gives a realistic representation of in-cabinet motion and the ICRS. Various studies (Burdisso and Singh, 1987; Gupta and Gupta, 1997; EPRI, 2017; Dubey et al., 2019) to evaluate in-structure response

spectrum (ISRS) by conducting coupled analysis yields spectral ordinates which are 50% (sometimes even more) lower than those obtained from an uncoupled analysis.

For a coupled linear analysis, the effect of mass interaction has been studied quite widely. Moreover, the studies conducted to understand the effect of geometric nonlinearities (Rydell et al., 2014; Singh, 2017) on equipment response performed uncoupled analysis. However, it is important to study the combined effect of mass interaction and geometric nonlinearities on the response of electrical equipment. The study presented in this dissertation considers the modal frequencies of multiple degrees of freedom (MDOF) building that coincide with the peak frequencies of ground motion response spectra as well as the modal frequencies of MDOF electrical cabinet. The cabinet modes are either tuned or nearly tuned with different modes of the building. Hence, the effects of various factors such as mass interaction, gaps, tuning of different building–cabinet system modes, etc. are reflected in the ICRS.

## 2.3. Quantification of the Contribution of Sedimentary Deposits to High–Frequency Attenuation in Low–to–Moderate Seismicity Regions via the Site Transfer Function

The spectral decay parameter, kappa ($\kappa_{r\_AS}$; Anderson and Hough 1984) characterizes the attenuation of seismic waves at high frequencies as they travel from the source to ground surface. Kappa is usually calculated from a linear decay of the Fourier Amplitude Spectrum (FAS) for a recorded acceleration time history when plotted on natural log (amplitude) – linear (frequency) space. Kappa values evaluated from recorded motions at a particular site are linearly correlated to the epicentral distance, $R_{epi}$ (Anderson and Hough, 1984; Ktenidou et al., 2012). Site–specific kappa, $\kappa_{0\_AS}$, is evaluated at zero epicentral distance ($R_{epi}$=0) and represents the attenuation of

vertically propagating shear waves through the shallow geology of the soil profile (Anderson 1991, Ktenidou et al., 2012). $\kappa_{0\_AS}$ describes combined effects of anelastic attenuation (often captured by material damping ratios), and wave scattering at the site (Parolai and Bindi, 2004; Cabas et al. 2017, Pilz and Fäh, 2017). Estimates of kappa are useful in the stochastic simulation of ground motions (e.g., Boore, 2003) and in empirical ground motion prediction equations (e.g., Laurendau et al., 2013)

The value of $\kappa_{0\_AS}$ affects the response spectral shape and specifically the frequency at which peak spectral acceleration occurs (Silva and Darragh, 1995; Boore and Joyner, 1997; Malagnini et al., 2000; Biro and Renault, 2012; Laurendau et al., 2013). For a low value of $\kappa_{0\_AS}$, which is mostly observed at rock sites, the peak spectral accelerations occur at higher frequencies. The safety–related equipment used in critical facilities such as nuclear power plants, electrical substations, data centers, etc., are sensitive to high–frequency accelerations thus, affecting safety and functionality of the facility. Hence, $\kappa_{0\_AS}$ is an important factor required for stochastic simulation or host–to–target adjustment methods to evaluate ground motion response spectrum (GMRS) for engineering design purposes.

$\kappa_{0\_AS}$ can be easily evaluated at highly seismic regions because of the number of recorded strong ground motion records, but that is not the case at regions with low-to-moderate seismicity. The approach proposed by Drouet et al. (2010) evaluates $\kappa_0$ from the decaying slope of the site transfer function (hereafter referred to as $\kappa_{0\_TF}$) which measures the attenuation between the rock and the ground surface. A site's transfer function indicates changes in amplitude and frequency content in the ground motion as it propagates from a reference rock horizon to the ground surface; while accounting for the dynamic properties of the sedimentary column (namely, stiffness and anelastic attenuation). In this study, we propose a probabilistic distribution function for $\kappa_{0\_TF}$

values from a closed–form equation based only on-site parameters, namely shear wave velocity and material damping ratio. The equation is derived using a single-layer linear-elastic theoretical transfer function and uncertainty quantification analyses are conducted to provide a probabilistic description of $\kappa_0$ instead of the more common, yet limited, deterministic values available in the literature.

## 3. Research Objectives

The main objective of this research is to understand the effect of various factors such as geometric nonlinearity at cabinet base, interaction between building–cabinet system, subjected to high–frequency ground motions on the in–cabinet response spectrum and provide a better characterization of such high–frequency ground motions to further facilitate seismic qualification of electrical equipment. The primary objectives of proposed research are listed below:

- Study the response of single degree of freedom system with and without geometric nonlinearity at the base and understand the difference in the response of both systems.
- Understand the effects of building–cabinet interaction, localized geometric nonlinearity such as gaps, high–frequency modes of MDOF building and MDOF cabinets, and the ground motion characteristics such as peak ground acceleration and frequency content, on the ICRS.
- Investigate alternative methods of estimation of site-specific attenuation parameters for low-to-moderate seismicity regions, such CEUS.
- Provide a probabilistic characterization of the site-specific attenuation parameter based on readily available site conditions that can be further used in the adjustment of the high-frequency content of design ground motion spectra for NPP.

## 4. Proposed Tasks

Following research tasks are proposed to conduct this research:

### 4.1. Effects of Boundary Conditions on Seismic Response of Electrical Equipment Subjected to High-Frequency Ground Motion

- Consider a single degree of freedom (SDOF) system with gap at the base mounted on a frictionless surface. Identify the stages and conditions of contact and no contact of the SDOF base with the anchor bolt.
- Characterize each stage of SDOF by appropriate equations of motion and derive the solution for each equation.
- Develop a MATLAB code to obtain the total as well as transient and steady–state responses of the SDOF gap model subjected to harmonic ground motion.
- Analyze the nonlinear SDOF system with natural frequencies ranging from 0.01–100Hz subjected to harmonic ground motion with low, intermediate, and high excitation frequency. Examine the variation of maximum total acceleration response of the different SDOF systems with their natural frequencies.
- Conduct a parametric study by analyzing the linear and nonlinear SDOF systems with low- and high-frequencies same as that of the excitation frequencies of harmonic ground motions in the previous step. Based on the displacement response time history of linear and nonlinear SDOF systems, study the differences between transient, steady–state, and total responses.
- Utilize the response spectra obtained from the analysis to compare and explain the results obtained by Singh (2017).

### 4.2. Understanding the Seismic Response of Electrical Equipment Subjected to High–Frequency Ground Motions

- Create multi–degrees of freedom (MDOF) primary (building) systems such that a few modal frequencies coincide with frequencies at which peaks of selected low– and high–frequency ground motion response spectra occur.
- Create MDOF secondary (cabinet) systems with modal frequencies tuned with different modal frequencies of the primary systems. Calculate modal mass ratios for all the primary–secondary system combinations.
- Create cabinet systems with fixed–base, 1mm gap and 3mm gap at the cabinet base.
- Perform coupled as well as uncoupled analysis for all the systems.
- Compare results for linear and nonlinear coupled as well as uncoupled analyses for all cases. Summarize the effect of various factors such as mass interaction, gap, frequency, and amplitude of ground motions, etc., on the in–cabinet response spectrum.

### 4.3. Quantification of the Contribution of Sedimentary Deposits to High–Frequency Attenuation in Low–to–Moderate Seismicity Regions via the Site Transfer Function

- Select various study sites with linear soil response and different shear–wave velocity ($V_s$) profiles from the Kik–net database. Select at least ten recording pairs (recordings at bedrock and surface) at each site to evaluate site–specific kappa from both acceleration spectrum and transfer function method ($\Delta\kappa_{0\_AS}$ and $\kappa_{0\_TF}$). Find frequency bands using automated procedure of Ji et al. (2020) for each recording pair so that the frequencies for bedrock and surface recordings are same. Calculate and compare $\Delta\kappa_{0\_AS}$ and $\kappa_{0\_TF}$ to establish equivalency between the two methods.

- Conduct 1D linear-elastic site response analyses at each site to calculate theoretical transfer functions. Find estimates of theoretical $\kappa_{0\_TF}$ using frequency bands determined for site records. Quantify uncertainty in theoretical estimates of $\kappa_{0\_TF}$ by accounting for the variability in material damping ratio.
- Derive a closed–form equation to evaluate $\kappa_{0\_TF}$ for a single-layer approximation of the soil profile. Run Monte Carlo simulations to obtain $\kappa_{0\_TF}$ estimates by accounting for variability in both $V_s$ and damping ratio for a single layer.
- Plot and compare probability density functions for $\kappa_{0\_TF}$ estimates from site records, 1D linear-elastic site response analysis (accounting for uncertainty in damping ratio of each layer), and Monte Carlo simulations of closed–form equation (accounting for uncertainty in both $V_s$ and damping ratio for a single layer).

## 5. Organization

This dissertation consists of five chapters. Chapter 1 describes the introduction to problems faced by nuclear power plants in seismic qualification of electrical equipment due to high–frequency ground motions and further discusses the objectives of the research. Chapter 2 describes the effect of boundary conditions on response of electrical equipment. Chapter 3 discusses the effect of various factors such as coupled nonlinear analysis and amplitude of ground motion on ICRS. Chapter 4 proposes evaluation of probabilistic estimates of site–specific kappa using site parameters. Chapter 5 presents the overall summary and conclusions of the study conducted in chapters 2–4.

## 6. References


[1] Al Atik, L., Kottke, A., Abrahamson, N., Hollenback, J., (2014) "Kappa (κ) Scaling of Ground-Motion Prediction Equations Using an Inverse Random Vibration Theory Approach," *Bulletin of the Seismological Society of America,* Volume 104, pp. 336–346, February 2014, DOI: 10.1785/0120120200.

[2] Anderson, J.G., Hough, S.E., (1984) "A Model for the Shape of the Fourier Amplitude Spectrum of Acceleration at High-Frequencies," *Bulletin of the Seismological Society of America*, Vol. 74, No. 5, pp. 1969–1993, October 1984.

[3] Biasi, G., Smith, K.D., Final Project Report, (2001) "Site effects for seismic monitoring stations in the vicinity of Yucca Mountain, Nevada," Prepared for the US DOE/UCCSN Cooperative Agreement Number DE-FC08-98NV12081, Task 12, Southern Great Basin Seismic Network Operations (SGBSN), MOL.20011204.0045.

[4] Biro, Y., P. Renault, P., (2012) "Importance and impact of host-to-target conversions for ground motion prediction equations in PSHA," *In: Proc. of the 15th World Conference on Earthquake Engineering,* 1855, Lisbon, Portugal.

[5] Boore, D.M. (2003) "Simulation of Ground Motion Using the Stochastic Method," *Pure Appl. Geophys.,* Vol 160, pp. 635-676.

[6] Boore, D.M., (2016) "Determining Generic Velocity and Density Models for Crustal Amplification Calculations, with an Update of the Boore and Joyner (1997) Generic Site Amplification for $V_S(Z)$ 760 m/s," *Bulletin of the Seismological Society of America,* Vol. 106, No. 1, pp. 316–320, February 2016, doi: 10.1785/0120150229.

[7] Boore, D., Joyner, W., (1997) "Site amplifications for generic rock sites," *Bull. Seismol. Soc. Am.*, Vol. 87, No. 2, 1997, 327–341.

[8] Burdisso, R.A., and Singh, M.P. (1987) "Seismic Analysis of Multiply Supported Secondary Systems with Dynamic Interaction Effects." *Earthquake Engineering Structural Dynamics,* Volume 15, Pages 1005-1022.

[9] Cabas, A., Rodriguez-Marek, A., (2017) "Vs-κ0 Correction Factors for Input Ground Motions Used in Seismic Site Response Analyses," *Earthquake Spectra,* Volume 33, No. 3, Pages 917 – 941, August 2017, doi: 10.1193/22315EQS188M.

[10] Cabas, A., Rodriguez-Marek, A., Bonilla, L.F., (2017) "Estimation of Site-Specific Kappa ($\kappa_0$)-Consistent Damping Values at KiK-Net Sites to Assess the Discrepancy between Laboratory-Based Damping Models and Observed Attenuation (of Seismic Waves) in the Field," *Bulletin of the Seismological Society of America,* Vol. 107, No. 5, pp. 2258–2271, October 2017, doi: 10.1785/0120160370.

[1] Campbell, K.W. (2003) "Prediction of Strong Ground Motion Using the Hybrid Empirical Method and Its Use in the Development of Ground-Motion (Attenuation) Relations in Eastern North America," *Bulletin of the Seismological Society of America,* Vol. 93, No. 3, pp. 1012-1033, June 2003.

[2] Darendeli, M. B., (2001) "Development of a new family of normalized modulus reduction and material damping curves," Ph.D. Thesis, Department of Civil Engineering, University of Texas, Austin, Texas, 2001.

[3] Dubey, A.R., Bodda, S., Gupta, A., Vasquez, J., Bhargava, D., (2019) "Reduction in Seismic Demand by Using Equipment-Structure Interaction," *In: Transactions of Twenty Fifth International Conference on Structural Mechanics in Reactor Technology (SMiRT 25),* 2019.

[4] Drouet, S., Cotton, F., Gueguen, P., (2010) "$V_{s30}$, κ, regional attenuation and Mw from accelerograms: Application to magnitude 3-5 French earthquakes," *Geophysical Journal International,* 182, 880–898.

[5] EPRI, (2007) "Program on technology innovation: The effects of high-frequency ground motion on structures, components, and equipment in nuclear power plants," Palo Alto, CA: 2007.1015108.

[6] EPRI, (2013) "Seismic Evaluation Guidance: Screening, Prioritization and Implementation Details (SPID) for the Resolution of Fukushima Near-Term Task Force Recommendation 2.1: Seismic," Palo Alto, CA: 2013.1025287.

[7] EPRI, (2014) "High frequency program: High frequency testing summary," Palo Alto, CA, 2014.3002002997.

[8] EPRI, (2017) "Coupled Analysis of Primary – Secondary System to Generate Floor Response Spectra: Quantifying Reduction Factors for Coupled In-Structure Response Spectra Amplitudes," *3002010666,* Final Report, November 2017.

[9] Gupta, A., and Gupta, A. K. (1997). "Seismic response of tuned single degree of freedom secondary systems." *Nuclear Engineering and Design*, Volume 172, Pages 17–25.

[10] Gupta, A., Rustogi, S.K., Gupta, A.K., (1999) "Ritz Vector Approach for Evaluating Incabinet Response Spectra," *Nuclear Engineering and Design,* Vol. 199, pp. 255-272, March 1999. DOI: 10.1016/S0029-5493(99)00076-X.

[11] Herve, G., (2014) "Improvement of the evaluation of high frequency content in the calculation of impact floor response spectra," *In: 2nd Conference on Technical Innovation in Nuclear Civil Engineering TINCE 2014, Paris,* 2014.

[12] Ji, C., Cabas, A., Bonilla, F., Gelis, C., (2020) "Quantifying the High-Frequency Spectra Decay Parameter Beyond the Linear-Elastic Regime," *Manuscript in Preparation,* 2020.

[13] Ktenidou, O.-J., Gélis, C., Bonilla, L.-F., (2012) "A Study on the Variability of Kappa (κ) in a Borehole: Implications of the Computation Process," *Bulletin of the Seismological Society of America,* Vol. 103, No. 2a, 2012, doi: 10.1785/0120120093.

[14] Ktenidou, O.-J., Cotton, F., Abrahamson, N.A., Anderson, J.G., (2014) "Taxonomy of κ: A Review of Definitions and Estimation Approaches Targeted to Applications," *Seismological Research Letters,* Vol. 85, No. 1, January/February 2014, doi: 10.1785/0220130027.

[15] Ktenidou, O.-J., Abrahamson, N.A., Darragh, R.B., Silva, W.J., (2016) "A Methodology for the Estimation of Kappa (κ) from Large Datasets: Example Application to Rock Sites in the NGA-East Database and Implications on Design Motions," PEER Report No. 2016/01, April 2016.

[16] Laurendeau, A., Cotton, F., Ktenidou, O.-J., Bonilla, L.-F., Hollender, F., (2013) "Rock and Stiff-Soil Site Amplification: Dependency on $V_{S30}$ and Kappa ($\kappa_0$)," *Bulletin of the Seismological Society of America,* Vol. 103, No. 6, December 2013, doi: 10.1785/0120130020.

[17] Malagnini, L., Herrmann, R., Bona, M.D., (2000) "Ground-motion scaling in the Apennines (Italy)," *Bulletin of the Seismological Society of America,* Vol. 90, No. 4, 1062–1081.

[18] Parolai, S., Bindi, D., (2004) "Influence of Soil Layer Properties on κ evaluation," *Bulletin of the Seismological Society of America,* 94:349–356.

[19] PEER, (2015) "NGA-East: Median Ground-Motion Models for the Central and Eastern North America Region," *Pacific Earthquake Engineering Research Centre,* PEER Report No. 2015/04, April 2015.

[20] Pilz, M., Fäh, D., (2017) “The Contribution of Scattering to Near–Surface Attenuation,” *J Seismol (2017) 21:837-855,* DOI 10.1007/s10950-017-9638-4.

[21] Rydell, C., Malm, R., Ansell, A., (2014) “Piping System Subjected to Seismic Hard Rock High Frequencies,” *Nuclear Engineering and Design*, 278 (2014) 302–309.

[22] SSHAC, (1997) “Recommendations for Probabilistic Seismic Hazard Analysis: Guidance on Uncertainty and Use of Experts,” NUREG/CR-6372, UCRL-ID- 122160, Vol. 1.

[23] Singh, S., (2017) “Seismic Response of Electrical Equipment in Nuclear Power Plants,” M.S. Thesis, North Carolina State University.

[24] Silva, W., Darragh, R., (1995) “Engineering characterization of earthquake strong ground motion recorded at rock sites,” *Electric Power Research Institute*, 1995, Report TR-102261, Palo Alto, California.

[25] USNRC, (2014) "Design Response Spectra for Seismic Design of Nuclear Power Plants," Reg. Guide 1.60, July 2014.

[26] Vlaski, V., (2013) “Reduction of External Hazard (Fast Impact) Induced Vibrations,” F/AB-58, *In: 1st Conference on Technical Innovation in Nuclear Civil Engineering TINCE 2013, Paris,* October 28-31, 2013.

[27] Vlaski, V., Moersch, J., Sallmann, M., (2019) “Comparative Study for Reduction of APC Induced Vibrations,” *In: Transactions of 25$^{th}$ Conference on Structural Mechanics in Reactor Technology (SMiRT-25), Charlotte, NC, USA,* August 4-9, 2019.

# Chapter 2

## Effect of Boundary Conditions on Seismic Response of Electrical Equipment Subjected to High–Frequency Ground Motions

**Abstract**

In Central and Eastern United States (CEUS), the ground motion studies at various nuclear power plants sites have observed that the ground motion response spectra have high-frequency content contrary to the design spectrum suggested by United States Nuclear Regulatory Commission's Reg. Guide 1.60. The high-frequency ground motions do not damage the structures, however, the safety-related equipment such as relays are sensitive to high-frequency accelerations. The response of electrical equipment is given by an in-cabinet response spectrum which depends on the response the electrical cabinets as well as the buildings. The conventional linear analysis to evaluate in-cabinet response spectrum assumes a fixed-base connection between electrical cabinet and floor. The linear analysis may predict unnecessarily high peak spectral acceleration response of electrical equipment. However, modeling electrical cabinet with geometric nonlinearities such as a gap in the connection with building floor shows that high-frequency accelerations may not propagate to the electrical equipment. A closer look at the results from analysis of nonlinear cabinet model with a gap subjected to seismic ground motion shows periodic pattern of secondary peaks and valleys at higher frequencies. In this research, the unique nature of in-cabinet response spectra of nonlinear cabinet model with gap is explained by studying the response of low- and high-frequency single degree of freedom (SDOF) system with gap subjected to harmonic excitation. The in-cabinet response spectra obtained from analysis of nonlinear SDOF systems shows secondary high-frequency peaks similar to the ones obtained by seismic ground motion analysis of nonlinear electrical cabinet models. The occurrence of periodic pattern of peaks and valleys is found to be due to the interaction of transient and steady-state response of the nonlinear SDOF system.

## 1. Introduction

The safety-related electrical equipment such as relays in nuclear power plants are required to function adequately during and after an earthquake to maintain safe operation or to initiate safe shutdown of the plant. Seismic qualification of such electrical equipment and relays is typically conducted by shake table tests in which the earthquake input is defined in terms of an in-cabinet response spectra (ICRS). The ICRS is generated by a dynamic analysis of the electrical cabinet or control panel on which the relays are mounted. The earthquake input at the base of cabinets is defined by an in-structure response spectrum (ISRS) corresponding to the floor at which the cabinet is located. Historically, the design earthquake input at almost all nuclear power plant sites in the United States has been characterized by a safe shut down earthquake in accordance with USNRC's Reg. Guide 1.60 (USNRC, 2014). The spectrum shapes recommended in Reg. Guide 1.60 were derived using actual earthquake records from western United States. The earthquake records used for developing the spectrum shapes in Reg. Guide 1.60 contained primarily low frequency ground motions. Consequently, the first few low frequency modes of the building as well as the cabinets were sufficient to evaluate accurate ISRS and ICRS.

The ground motion studies conducted on Central & Eastern United States (CEUS) nuclear power plant sites after the Fukushima Daiichi nuclear accident along with other more recent studies (SSHAC, 1997; EPRI, 2013; PEER, 2015) have shown that the ground motion response spectra (GMRS) in CEUS contain significant high frequency content in the ground motions. A comparison of the Reg. Guide 1.60 spectra with a corresponding GMRS at one of the nuclear power plant sites in eastern US is shown in EPRI (2015). The recently determined GMRS has a spectral peak in the vicinity of 30 Hz whereas the Reg. Guide 1.60 spectrum curve has peak spectral accelerations in a much lower frequency region.

In general, the high frequency motions are not considered damaging in a relative sense when compared to the damaging potential of low frequency earthquakes. This is so because the displacements associated with the high frequency motions are much smaller compared to those during low frequency ground motions. However, the same is not true about the seismic response of electrical equipment like relays. It has been observed that the functionality of relays can be compromised during high frequency vibrations even if they have been seismically qualified for low frequency ground motions (EPRI, 2007). This is because the mechanical parts in the relays and other electrical equipment are sensitive to accelerations and not displacements. The mechanical parts tend to resonate with the high frequency accelerations but not with low frequency accelerations. Consequently, the electrical equipment must be qualified for high frequency earthquake motions. Seismic qualification of relays for high frequency ground motions has not been straightforward. A key limitation in this process is related to the availability of appropriate shake table facilities. Most of the commercial facilities have displacement-controlled shake tables and can conduct tests only for earthquake motions in the low frequency range. Availability of only a few appropriate high frequency shake table testing facilities makes the testing quite costly.

The state-of-the-art as well as the current practice for generating the ISRS and ICRS is based on a linear analysis of the building and the cabinet. It is important to note that a linear analysis is justified for low frequency ground motions. However, a linear analysis for high frequency ground motions cannot be completely justified. In order to fully explain this premise, one has to understand that in general there are many localized nonlinearities that exist in buildings, cabinets, and in the mounting region of the cabinet. Let us consider a structure with a nonlinearity due to a very small crack that might have resulted from any reason. Such cracks do not pose a problem for low frequency ground motions as the displacements associated with the low frequency

motions are much larger than the size of the cracks. The relatively small size of cracks do not interfere with the low frequency vibration shapes of a structure. However, the displacements due to high frequency motions can be of the same order as the size of cracks and in such a case, the cracks have the potential to filter out the high frequency displacements. Based on this understanding of differences between a structure's behavior when subjected to low frequency versus high frequency motions, one can argue that high frequency motions should not cause large accelerations. This should be particularly true for in-cabinet motions and the corresponding ICRS as several nonlinearities can exist in cabinets and control panels.

Singh (2017) presents an exploratory study to illustrate that a relatively small gap in the mounting arrangement at the base of cabinets can influence the ICRS significantly. In the case of high frequency motions, it is shown that such a nonlinearity due to gap can block the propagation of earthquake motion into the cabinet and thereby result in relatively much smaller values of spectral accelerations in ICRS. A linear analysis for such cases is shown to give excessively high values of spectral accelerations. One such case considered in Singh (2017) is presented in Figure. 2. In this example, a high frequency building modeled as a SDOF freedom system with a natural frequency of 35 Hz has a high frequency cabinet mounted on it. The cabinet is also represented as a SDOF system with a natural frequency of 35 Hz. A high frequency input ground motion applied at the base of building gives very high values of ICRS as evaluated from linear analysis whereas a nonlinear analysis by considering a very small gap of 1 mm gives much smaller values of ICRS. More specifically, the peak spectral acceleration from the linear analysis is as high as 350g but only about 4g from a nonlinear analysis. Experimental studies conducted by Vlaski (2013) and Vlaski et al. (2019) show that high seismic demands do not propagate to the relays for high

frequency input motions indicating existence of nonlinearities in the system. Herve et al. (2014) present a similar argument for high frequency vibrations in the case of aircraft impact.

While Singh (2017) effectively illustrates the importance of nonlinearities in the generation of ICRS, a careful look at the results from that study shows an unconventional behavior observed in the spectral shapes. To explain this further, the spectral accelerations for the case of 1 mm gap are plotted again at a smaller scale in Figure. 2. As can be seen in this figure, the spectral accelerations exhibit alternating peaks and valleys at frequencies greater than that of the peak spectral acceleration. This pattern cannot be seen in Figure. 1 as it is lost due to the scale of figure. At first, this behavior appears either erroneous or needs an explanation to justify its existence. In this paper, we discuss this problem in greater detail and use fundamentals of structural dynamics to explain the occurrence of this unconventional observation in ICRS from a nonlinear analysis. The safety-related electrical equipment such as relays in nuclear power plants are required to function adequately during and after an earthquake to maintain safe operation or to initiate safe shutdown of the plant. Seismic qualification of such electrical equipment and relays is typically conducted by shake table tests in which the earthquake input is defined in terms of an in-cabinet response spectra (ICRS). The ICRS is generated by a dynamic analysis of the electrical cabinet or control panel on which the relays are mounted. The earthquake input at the base of cabinets is defined by an in-structure response spectrum (ISRS) corresponding to the floor at which the cabinet is located. Historically, the design earthquake input at almost all nuclear power plant sites in the United States has been characterized by a safe shut down earthquake in accordance with USNRC's Reg. Guide 1.60 (USNRC, 2014). The spectrum shapes recommended in Reg. Guide 1.60 were derived using actual earthquake records from western United States. The earthquake records used for developing the spectrum shapes in Reg. Guide 1.60 contained primarily low

frequency ground motions. Consequently, the first few low frequency modes of the building as well as the cabinets were sufficient to evaluate accurate ISRS and ICRS.

The ground motion studies conducted on Central & Eastern United States (CEUS) nuclear power plant sites after the Fukushima Daiichi nuclear accident along with other more recent studies (SSHAC, 1997; EPRI, 2013; PEER, 2015) have shown that the ground motion response spectra (GMRS) in CEUS contain significant high frequency content in the ground motions. A comparison of the Reg. Guide 1.60 spectra with a corresponding GMRS at one of the nuclear power plant sites in eastern US is shown in EPRI (2015). The recently determined GMRS has a spectral peak in the vicinity of 30 Hz whereas the Reg. Guide 1.60 spectrum curve has peak spectral accelerations in a much lower frequency region.

In general, the high frequency motions are not considered damaging in a relative sense when compared to the damaging potential of low frequency earthquakes. This is so because the displacements associated with the high frequency motions are much smaller compared to those during low frequency ground motions. However, the same is not true about the seismic response of electrical equipment like relays. It has been observed that the functionality of relays can be compromised during high frequency vibrations even if they have been seismically qualified for low frequency ground motions (EPRI, 2007). This is because the mechanical parts in the relays and other electrical equipment are sensitive to accelerations and not displacements. The mechanical parts tend to resonate with the high frequency accelerations but not with low frequency accelerations. Consequently, the electrical equipment must be qualified for high frequency earthquake motions. Seismic qualification of relays for high frequency ground motions has not been straightforward. A key limitation in this process is related to the availability of appropriate shake table facilities. Most of the commercial facilities have displacement-controlled shake tables

and can conduct tests only for earthquake motions in the low frequency range. Availability of only a few appropriate high frequency shake table testing facilities makes the testing quite costly.

The state-of-the-art as well as the current practice for generating the ISRS and ICRS is based on a linear analysis of the building and the cabinet. It is important to note that a linear analysis is justified for low frequency ground motions. However, a linear analysis for high frequency ground motions cannot be completely justified. In order to fully explain this premise, one has to understand that in general there are many localized nonlinearities that exist in buildings, cabinets, and in the mounting region of the cabinet. Let us consider a structure with a nonlinearity due to a very small crack that might have resulted from any reason. Such cracks do not pose a problem for low frequency ground motions as the displacements associated with the low frequency motions are much larger than the size of the cracks. The relatively small size of cracks do not interfere with the low frequency vibration shapes of a structure. However, the displacements due to high frequency motions can be of the same order as the size of cracks and in such a case, the cracks have the potential to filter out the high frequency displacements. Based on this understanding of differences between a structure's behavior when subjected to low frequency versus high frequency motions, one can argue that high frequency motions should not cause large accelerations. This should be particularly true for in-cabinet motions and the corresponding ICRS as several nonlinearities can exist in cabinets and control panels.

Singh (2017) presents an exploratory study to illustrate that a relatively small gap in the mounting arrangement at the base of cabinets can influence the ICRS significantly. In the case of high frequency motions, it is shown that such a nonlinearity due to gap can block the propagation of earthquake motion into the cabinet and thereby result in relatively much smaller values of spectral accelerations in ICRS. A linear analysis for such cases is shown to give excessively high

values of spectral accelerations. One such case considered in Singh (2017) is presented in Figure. 2. In this example, a high frequency building modeled as a SDOF freedom system with a natural frequency of 35 Hz has a high frequency cabinet mounted on it. The cabinet is also represented as a SDOF system with a natural frequency of 35 Hz. A high frequency input ground motion applied at the base of building gives very high values of ICRS as evaluated from linear analysis whereas a nonlinear analysis by considering a very small gap of 1 mm gives much smaller values of ICRS. More specifically, the peak spectral acceleration from the linear analysis is as high as 350g but only about 4g from a nonlinear analysis. Experimental studies conducted by Vlaski (2013) and Vlaski et al. (2019) show that high seismic demands do not propagate to the relays for high frequency input motions indicating existence of nonlinearities in the system. Herve et al. (2014) present a similar argument for high frequency vibrations in the case of aircraft impact.

While Singh (2017) effectively illustrates the importance of nonlinearities in the generation of ICRS, a careful look at the results from that study shows an unconventional behavior observed in the spectral shapes. To explain this further, the spectral accelerations for the case of 1 mm gap are plotted again at a smaller scale in Figure. 2. As can be seen in this figure, the spectral accelerations exhibit alternating peaks and valleys at frequencies greater than that of the peak spectral acceleration. This pattern cannot be seen in Figure. 1 as it is lost due to the scale of figure. At first, this behavior appears either erroneous or needs an explanation to justify its existence. In this paper, we discuss this problem in greater detail and use fundamentals of structural dynamics to explain the occurrence of this unconventional observation in ICRS from a nonlinear analysis.

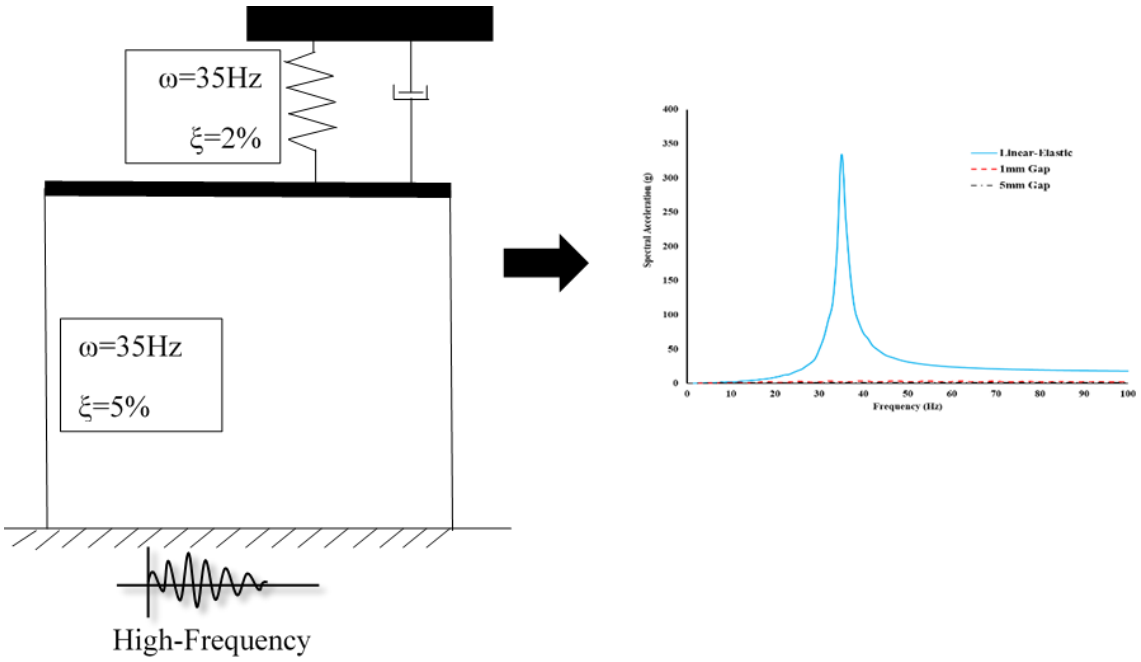


**Figure. 1.** ICRS of High-Frequency System subjected to High-Frequency Ground Motion (Singh, 2017)

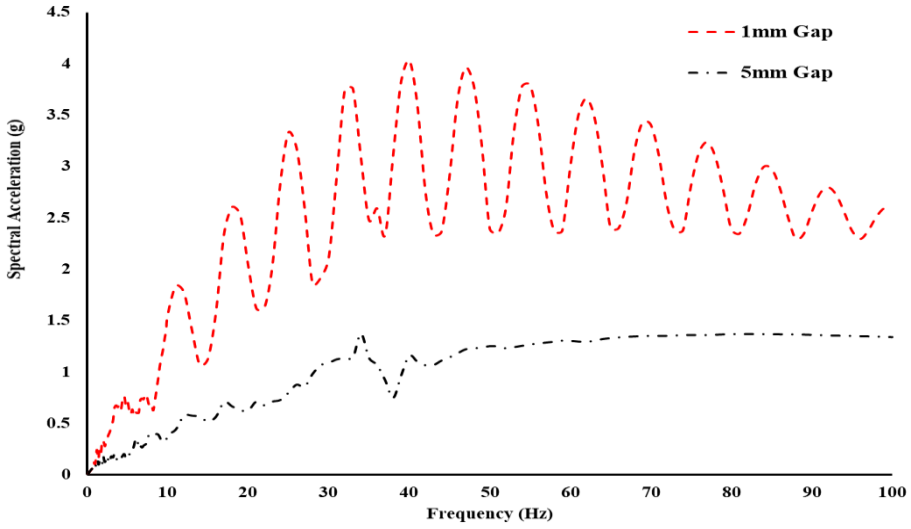


**Figure. 2.** ICRS of Nonlinear Cabinet Models with Gap for Figure 2 System showing High-Frequency Peaks and Valleys (Singh, 2017)

## 2. Description of Cabinet Mounting Arrangement

The response spectrum for an equipment is evaluated by conducting either finite element analysis or shake table test of the electrical cabinet. However, as outlined by Gupta et al. (1999), the response of electrical equipment mounted on an electrical cabinet, depends on factors such as dynamic properties of cabinet, location of equipment, etc. and can be represented by only a few modes termed as significant modes. A simplified analysis can thus be performed via Ritz Vector approach for cost efficiency. As per Gupta et al. (1999), a significant mode may either be a local mode, i.e., deformation of cabinet door, wall or frame where an equipment is mounted, or a global bending mode of the entire cabinet, or combination of both the local and the global modes. Llambias et al. (1989) and Gupta et al. (1999b) observed that differences between the experimentally and analytically evaluated dynamic properties of the cabinets are attributed to a difference in boundary conditions of the cabinet (Gupta and Yang, 2002). Most analysis models assume fixed-base boundary condition whereas the boundary conditions of the cabinet depend on the mounting arrangement.

The effect of mounting arrangement in a switchgear cabinet is explained by Gupta et al. (1999b). Sine sweep and random input shake table tests are conducted on the cabinet to plot transmissibility ratio and in-cabinet response spectra respectively at various locations of the electrical cabinet. The results obtained from tests are reconciled with finite element analysis. The cabinet consists of four individual units connected by bolts side-by-side. The corner angles at the base of each unit is bolted to tubular section which are then mounted on the shake table. The transmissibility plot in front–back direction shows two significant modes at 14Hz and 20Hz while the in-cabinet response spectrum in same direction shows a single peak at around 12.5Hz. The difference in peak frequencies from both tests is explained via finite element analysis and is

attributed to the mounting arrangement. In sine sweep test, the intensity of motion is fixed while frequency of excitation is changed. On the other hand, the random input has variable amplitudes and at higher amplitudes of load. The stiffness of mounting arrangement reduces due to various reasons such as tearing of base plate, yielding of bolts, gap in connections, etc. Also, at frequencies above 33Hz, the test data shows a significant amplification which the authors anticipate due to impacting and rattling of the cabinet which is similar to observations in figure. 2. The observation of high amplitudes at high frequencies is ignored by the authors. However, it must be addressed when studying the effects of high-frequency accelerations on equipment response.

Since the electrical cabinets are usually anchored to the building floor, as shown in figure. 3, the diameter of the bolt holes in the cabinet base plate are usually larger than the diameter of anchor bolt. Due to minor difference in the diameters of bolt holes and the bolt, the cabinet slides and responds in free vibration when not in contact with the anchor. The cabinet is subjected to the forced vibration when the base is in contact with the anchor bolt. In this paper, the reason of high-frequency secondary peaks in the in-cabinet response spectra is examined by studying the effect of gaps in bolted connections which leads to sliding of the cabinet.

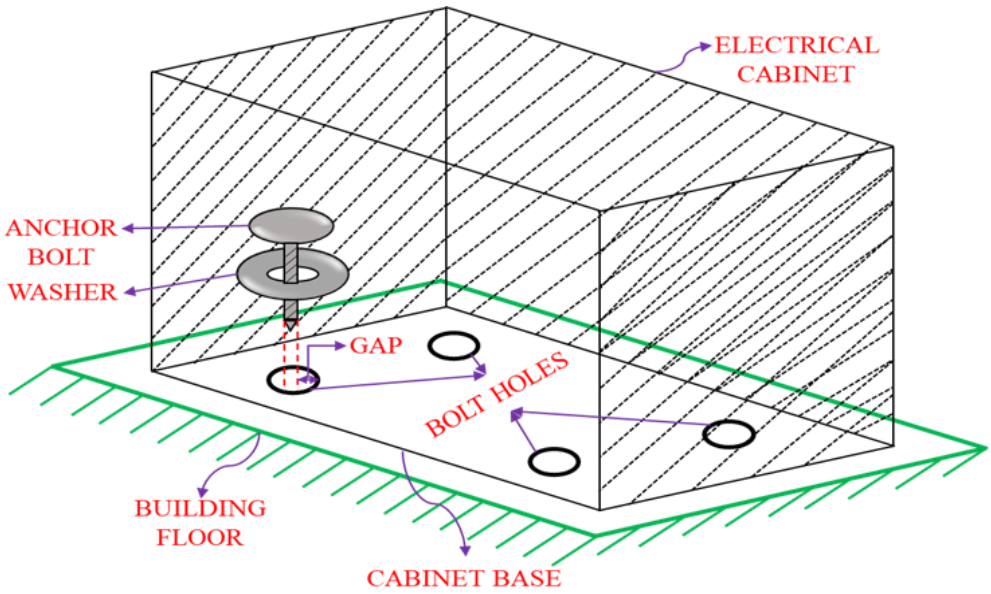


**Figure. 3.** Schematic Diagram of Electrical Cabinet Connection with the Floor

## 3. Sliding Behavior of Cabinets

### 3.1. Background

The sliding response of an SDOF system has been studied by several researchers. Newmark (1965) studied the sliding resistance of earth dams and derived the maximum displacement for an unanchored body subjected to rectangular ground motion pulses. Choi (2000) modified Newmark's formula for triangular ground motion pulses. Building further on the conclusions of Shao (1998) that sliding cannot be predicted with certainty, Choi (2000) proposed that sliding problem must be studied probabilistically as it is highly sensitive to multiple factors like ground motion amplitude, coefficient of friction, etc. Wilkins (2009) further looked into non-classical friction. He conducted an experimental study to propose a procedure for sliding analysis of unanchored objects. Recently, Hu and Nakashima (2017) studied the response of two DOF sliding

base system subjected to harmonic ground motion while Nikfar and Konstantinidis (2017) studied the demands on unanchored objects mounted on base-isolated buildings.

It is important to note that a very large number of studies on sliding behavior consider the behavior of rigid objects. Unlike these studies, the problem of a small gap at the base of an electrical cabinet is different. While the cabinet behaves like a rigid object when sliding occurs, the behavior changes to that of a fixed base cabinet once the gap closes and the cabinet behaves as a flexible structure. Once the oscillations begin, the cabinet continues to undergo free vibrations even during sliding until the motion comes to a complete stop or it changes to forced vibration when the gap closes again. Consequently, the solutions available in the literature cannot be used directly to understand the behavior of cabinets. Herve et al. (2014) and Singh (2017) represent this condition of geometric nonlinearity using a nonlinear elastic model as shown in Figure. 4 to represent the cabinet. As shown in this figure, the cabinet can undergo sliding on the tension side for a distance equal to the gap length. Once the gap closes, the cabinet exhibits a linear stiffness. On the compression side, the cabinet exhibits linear stiffness and no gap is considered. Singh (2017) uses a SDOF building with a nonlinear elastic SDOF cabinet model to create a suite of systems with different dynamic characteristics ranging from low frequency range to high frequency region. Each system is subjected to two types of earthquake inputs, a low frequency earthquake and a high frequency earthquake. It is shown that the presence of geometric nonlinearity at the building–cabinet interface, i.e. the mounting location of cabinet, filters out the high frequency motions which in turn results in significantly reduced amplitudes of accelerations in cabinet compared to the corresponding linear analysis. One such case is illustrated in Figure. 1 that shows a high frequency building model and a high frequency cabinet model (a generic representation of high frequency modes in building and cabinet). A linear analysis of this system

when subjected to a high frequency ground motion results in excessively high spectral amplitudes in the in-cabinet response spectra (ICRS) as shown in figure. 1. The corresponding values by considering the geometric nonlinearity at the cabinet base are vastly different and much lower.

The study discussed in Singh (2017) emphasizes the significance of geometric nonlinearities at the base of cabinets in the case of high frequency motions. However, a closer look at the plot of ICRS, given in figure. 2 for the case of nonlinear gap model, brings out an unusual behavior. The ICRS for the case of 1 mm gap shown in figure. 1 is plotted at an enlarged view in figure. 2 and shows a curve that is very different from a typical spectrum curve. The curve exhibits a periodic pattern with multiple peaks and valleys. This unusual pattern needs to be explained and a physical interpretation of this behavior needs to be established which is precisely the focus of this paper. The next few sections use a simple nonlinear elastic SDOF system (representing the cabinet) and a harmonic excitation to study this behavior theoretically. The harmonic excitation allows a detailed discussion on the physical behavior of such systems. More specifically, it addresses the following key aspects:

- What is the response of cabinet when the sliding stops upon contact with the anchor bolts?
- How does high-frequency ground motions affect the cabinet response when there is no sliding and the cabinet behaves as a flexible SDOF system?
- When and how is sliding initiated?
- What are the initial conditions at each instance of sliding?
- What is the response of cabinet during sliding?

### 3.2. Equation of Motion

Figure. 4 shows a SDOF cabinet model with a gap at its base. In this model, the diameter of the hole in cabinet's base plate is slightly larger than the diameter of the anchor bolt as is usually the case. This represents the nonlinear elastic model with the length of the gap between the anchor bolt and the cabinet's base plate being equal to the sliding distance used in the nonlinear elastic model shown in Figure. 5. For simplicity of problem description, in order to interpret the physical behavior of such a system during its vibration, all surfaces are assumed to be frictionless. This assumption means that initially the cabinet would slide as a rigid object until the gap is closed. The cabinet behaves as a SDOF freedom flexible system only after it comes in contact with the anchor bolt. Hence, the equations of motion for the model change with the displacement and also with the direction of the ground motion. The equations of motion and subsequent analytical solution is presented in this paper for harmonic base displacement where the amplitude of the ground displacement is assumed to be 10mm. This value of base displacement amplitude is selected for reasons mentioned below:

- In order to observe the effects of SDOF rigid body sliding, the closing of gap, initiation of flexible vibrations in the SDOF system, and restart of sliding, the displacement of the base must be more than that of the gap (1mm in this case).
- A cabinet is generally mounted on an elevated floor of a building. Depending on the frequency of the primary system and the ground, the total floor displacement could easily be as high as 10mm.

The equations of motion of the gap model will change based on the floor displacement and the direction of motion. For a SDOF cabinet model with mass $m$, stiffness $k$, and damping $c$, the following steps define the complete motion which is divided into different states. It is assumed

that prior to the application of base motion, the anchor bolt and the cabinet base are in contact with each other as shown in figure. 4. Starting from this state, the equation of motion would depend upon the direction of ground motion which can be in either direction. Therefore,

1. If $\dot{u}_g < 0$ at time, $t = 0$, the equation of motion is given by:

$$m\ddot{u} + c\dot{u} + ku = m\Omega^2 u_{go} sin\Omega t \quad \textbf{(1)}$$

where $\Omega$ is the frequency of harmonic ground displacement and $u_{go}$ is the amplitude of the harmonic base displacement. Since the SDOF system is at rest before application of the load, the initial condition are zero.

2. When $\dot{u}_g \geq 0$ at $t = t_0$ the equation of motion for $t \geq t_0$ is given by:

$$m\ddot{u} + c\dot{u} + ku = 0 \quad \textbf{(2)}$$

3. At $t=t_1$, where $t_1 \geq t_0$ the relative displacement of the base between the two time instances, $\Delta_{g1}$, is given by:

$$\Delta_{g1} = u_g(t_1) - u_g(t_0) \quad \textbf{(3)}$$

4. Let $\delta_g$ be the length of gap at the anchor bolt location (considered as 1mm in this case).

   *If* $\delta_g \leq \Delta_{g1}$ and, $\dot{u}_g > 0$ – *Go to step-5*

   *If* $\delta_g > \Delta_{g1}$ and, $\dot{u}_g < 0$ – *Go to step-7*

5. System is in contact with anchor bolt. Equation of motion for $t \geq t_1$ is given by Eq. (1).
6. When $\dot{u}_g < 0$ at $t = t_2$ the equation of motion is given by Eq. (2). Repeat the process starting at step 3 above.
7. System is not in contact with anchor bolt. Equation of motion for $t \geq t_1$ is given by Eq. (2).

8. Repeat the process starting at step-3 above.

As seen in the process described above, only two equations of motion govern the entire system behavior. The solution of Eq. (1) consists of both transient and steady-state parts whereas the solution of Eq. (2) consists only of transient part. It is important to note that the change in support conditions introduce new initial conditions every time the equation of motion changes. The velocity and displacement at the instant of the change from the solution of one equation act as the new initial conditions for the solution of the transient response in the other equation.

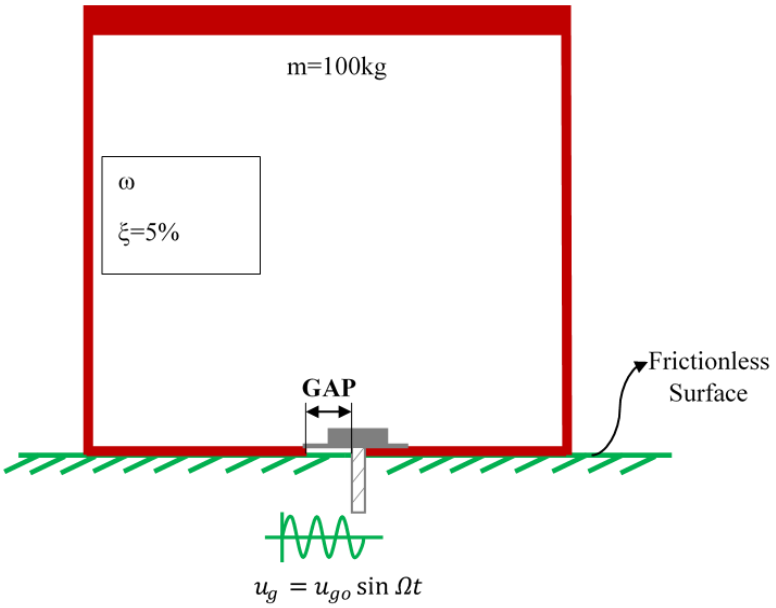


**Figure. 4.** Nonlinear Single Degree of Freedom System with Gap

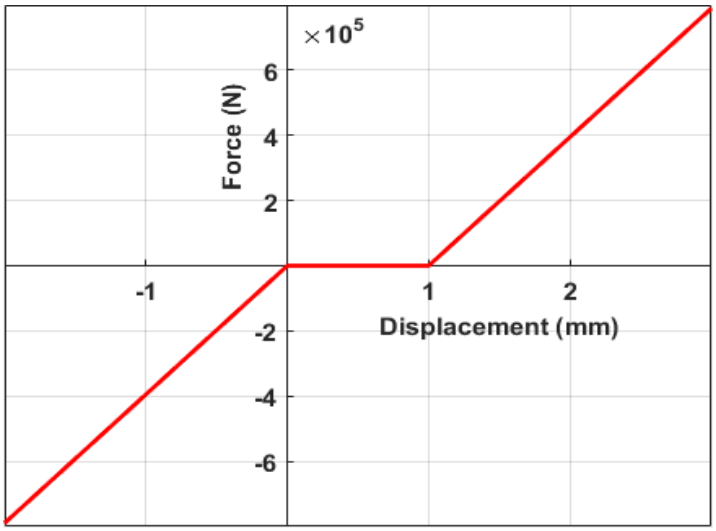


**Figure. 5.** Nonlinear Elastic Force–Displacement Plot

## 4. Application and Discussion of Results

Next, we consider three different SDOF systems with natural frequencies, $\omega$ = 3Hz (low frequency system) and 35Hz (high frequency system) in order to study the influence of a small gap at the base on their response when subjected to harmonic base excitation. Furthermore, we consider three different harmonic base excitation frequencies that range from low to high frequency excitations and also represent resonance conditions. For each system and the excitation, the total (absolute) acceleration response is evaluated by solving the differential equations of motions described in the previous section. The time history of absolute acceleration is then used to obtain the in-cabinet response spectra (ICRS). The ICRS are generated for both cases of fixed base and the nonlinear base with a small gap of 1 mm.

### 4.1. Effect of Nonlinearity Due to Gap

The main difference between ICRS of nonlinear and linear models is the occurrence of secondary peaks at higher frequencies in the case of nonlinear model. To examine this effect closely, let us look at the transient response in the solution of equations of motion. In the case of linear analysis, the transient response diminishes rapidly, and the cabinet response is dominated by the steady-state part of the solution. However, in the case of a nonlinear analysis with a small gap, a new transient response is introduced every time the boundary condition changes, i.e. at every closing of the gap. For example, figures. 6–7 show the displacement response of nonlinear and linear systems with natural frequency of 35Hz subjected to ground motion of excitation frequency 10Hz. For the linear SDOF, the transient response amplitude is less than the steady-state response and thus, does not contribute significantly to the total response. On the contrary, the transient response in the case of nonlinear SDOF system is relatively much larger and governs the total response. Every repeated closing of the gap in a nonlinear model introduces (and in this case increases) the transient response. The interaction between the transient response and the steady-state response of a nonlinear SDOF system is discussed in greater detail below to explain the occurrence of secondary peaks as seen in Figure. 8. The displacement response for different ratios of natural and excitation frequencies is also evaluated and discussed in detail in order to understand the impact of nonlinearity due to gaps on the ICRS.

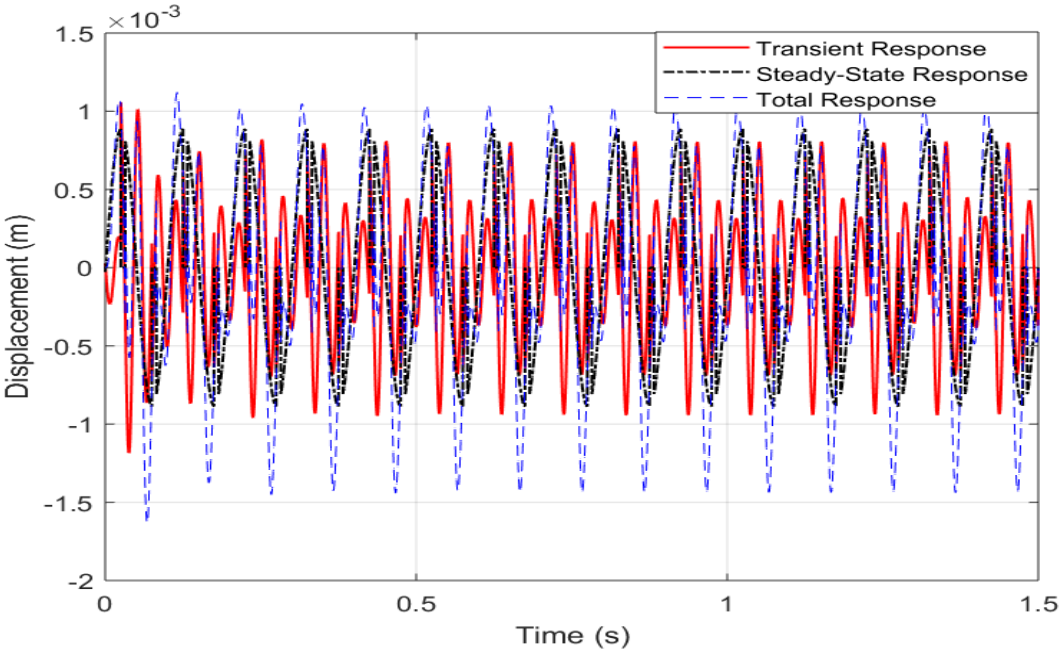


**Figure. 6.** Transient, Steady–State and Total Displacement Time History of Nonlinear SDOF System

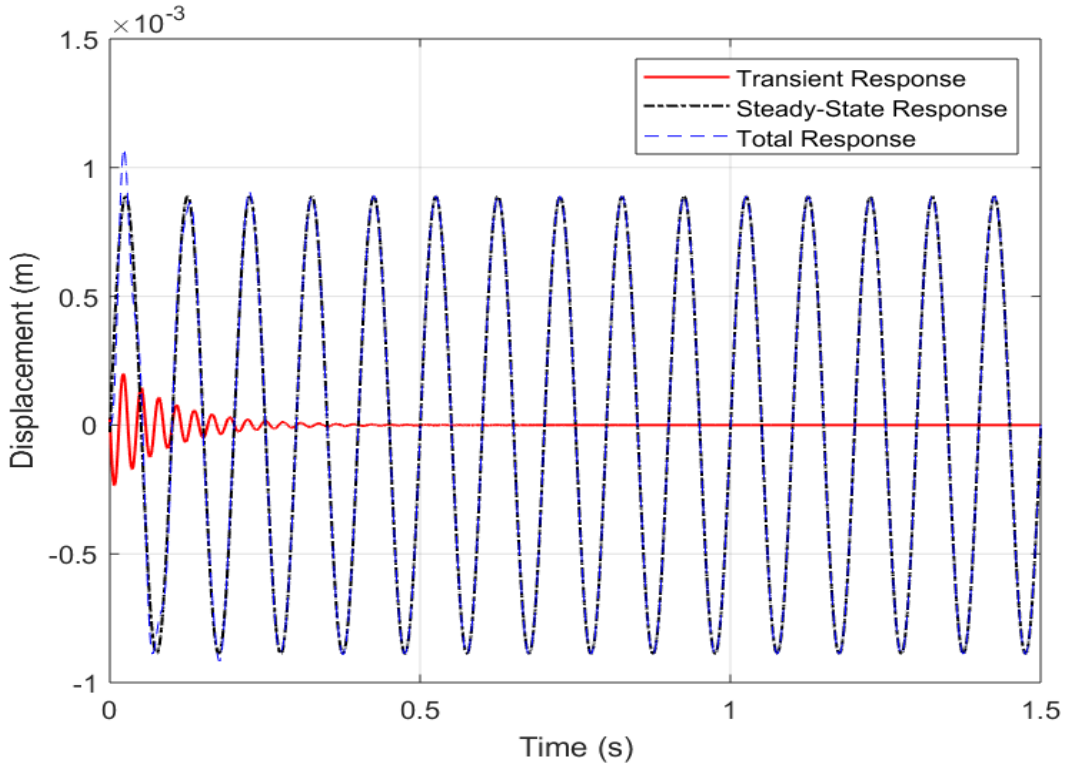


**Figure. 7.** Transient, Steady–State and Total Displacement Time History of Linear SDOF System

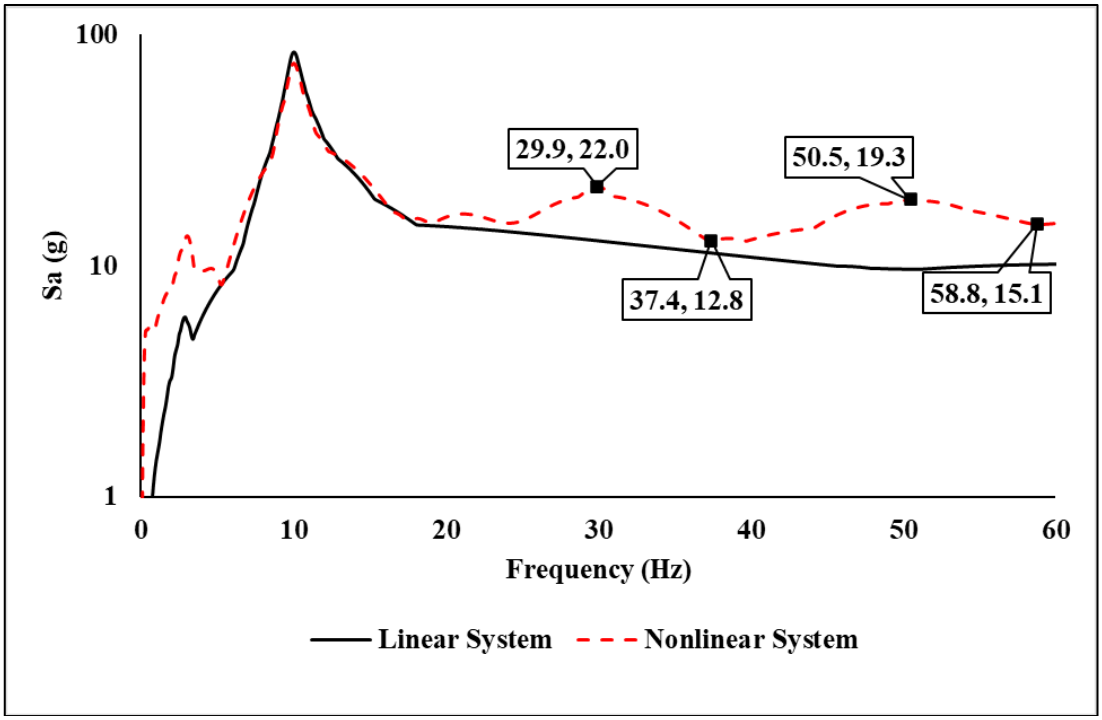


**Figure. 8.** In-Cabinet Response Spectrum of Linear and Nonlinear SDOF Systems

### 4.1.1. Secondary Peaks

As mentioned earlier in this manuscript, the ICRS obtained for the case of a nonlinear gap model exhibits a strange periodic behavior with secondary peaks and troughs at higher frequencies. Upon careful examination, it is found that the peaks have a strong periodic behavior. The peaks occur for SDOF systems with natural frequencies which are odd multiples of the excitation frequency. Such systems would be referred to as case *A* in the remainder of this manuscript. Furthermore, the troughs occur for SDOF systems with natural frequencies that are approximately even multiples of the excitation frequency. Such systems would be referred to as case *B*. To illustrate this, figure. 9 shows the spectra for the case of nonlinear SDOF system when subjected to a 3Hz harmonic excitation showing secondary peaks and the points of peak and troughs. Same trend can be observed in figure. 10 for the case of 10 Hz excitation.

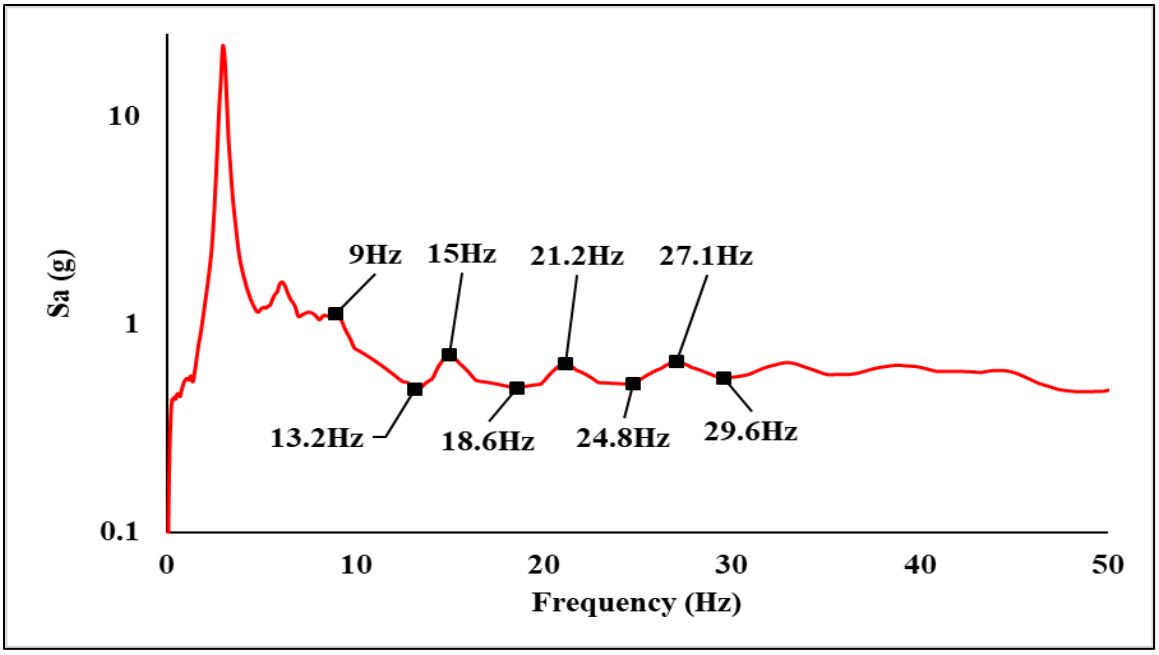


**Figure. 9.** Ground Motion Response Spectrum of GAP SDOF for Excitation Frequency, $\Omega$ = 3Hz

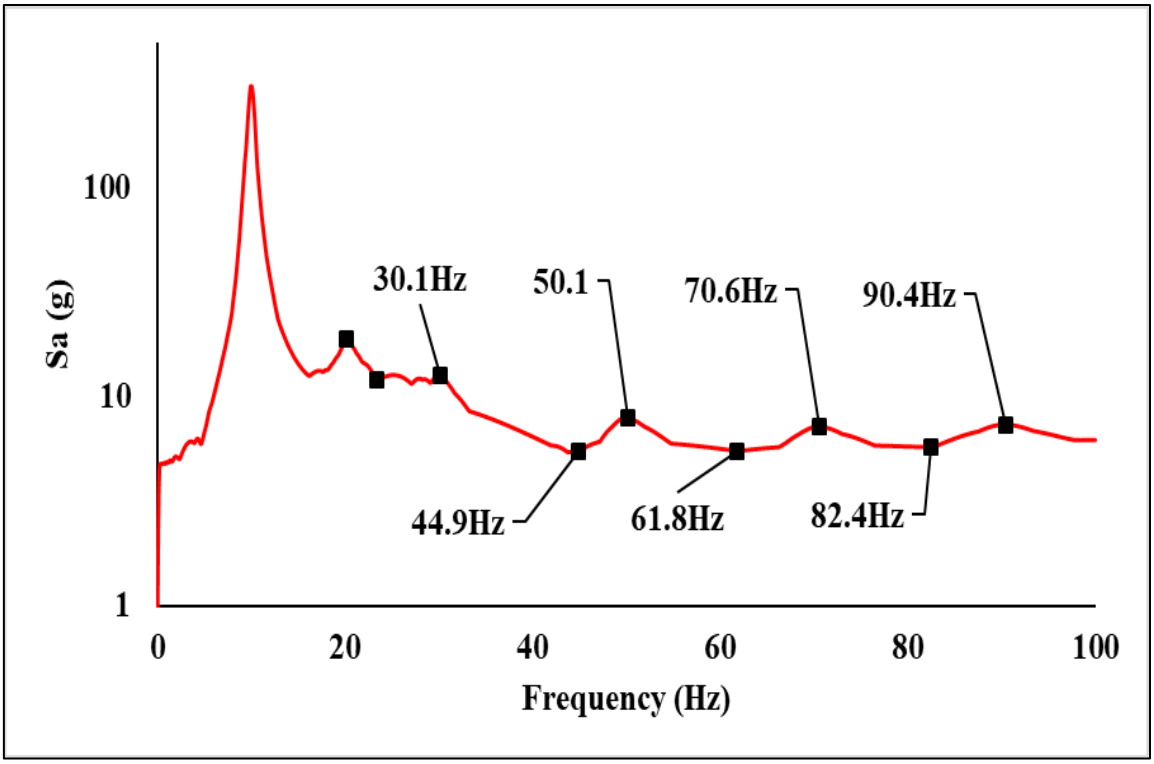


**Figure. 10.** Ground Motion Response Spectrum of GAP SDOF for Excitation Frequency,

The steady-state response depends on the excitation frequency whereas the transient response is governed by the natural frequency of SDOF system. Figure. 11 shows interaction between the transient and steady-state responses for case *A*. The maxima of transient response coincide with the maxima of steady-state response; hence the total responses are higher for cases *A* when transient and steady-state responses are added which leads to occurrence of peaks for these natural frequencies. On the other hand, Figure. 12 shows the responses for case *B* where the maxima of transient response does not coincide with the maxima of steady-state response. Therefore, the total response is lower for cases *B*.

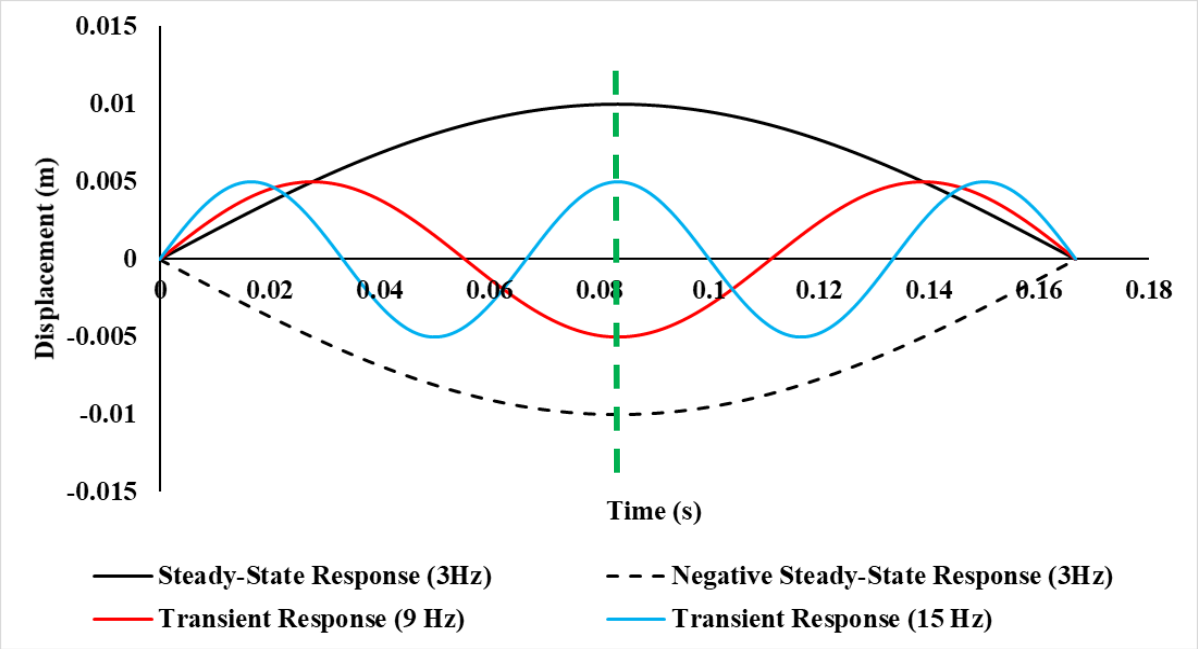


**Figure. 11.** Interaction of Steady-State Response with Transient Response of Odd Multiple Natural Frequencies

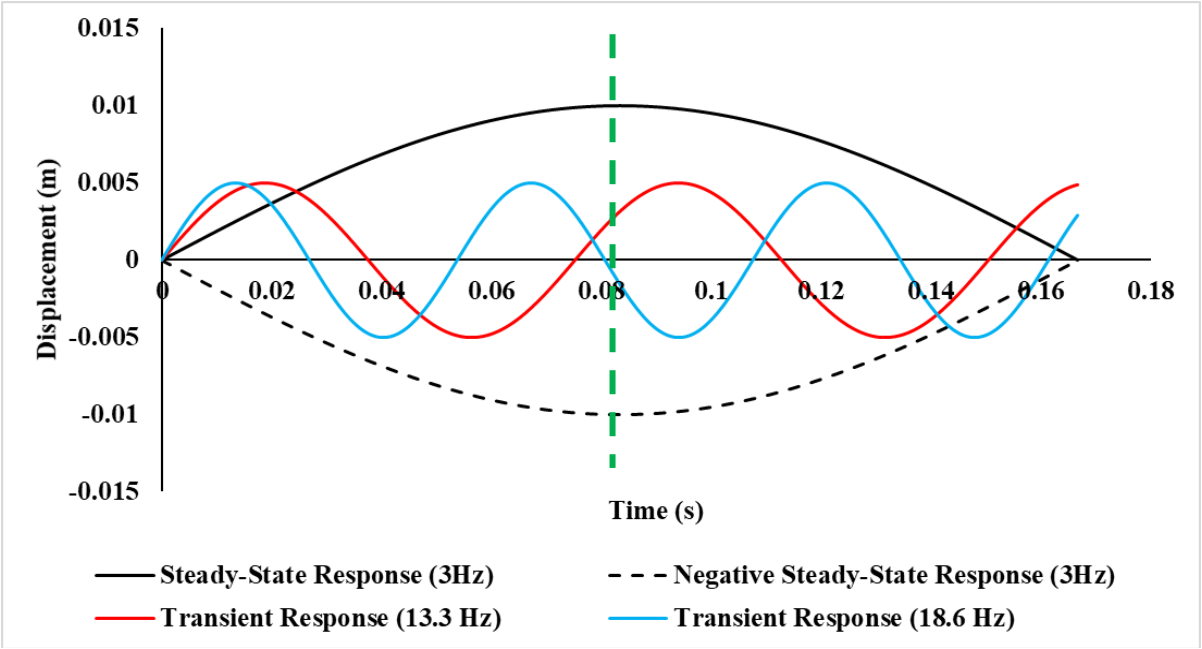


**Figure. 12.** Interaction of Steady-State Response with Transient Response of Even Multiple Natural Frequencies

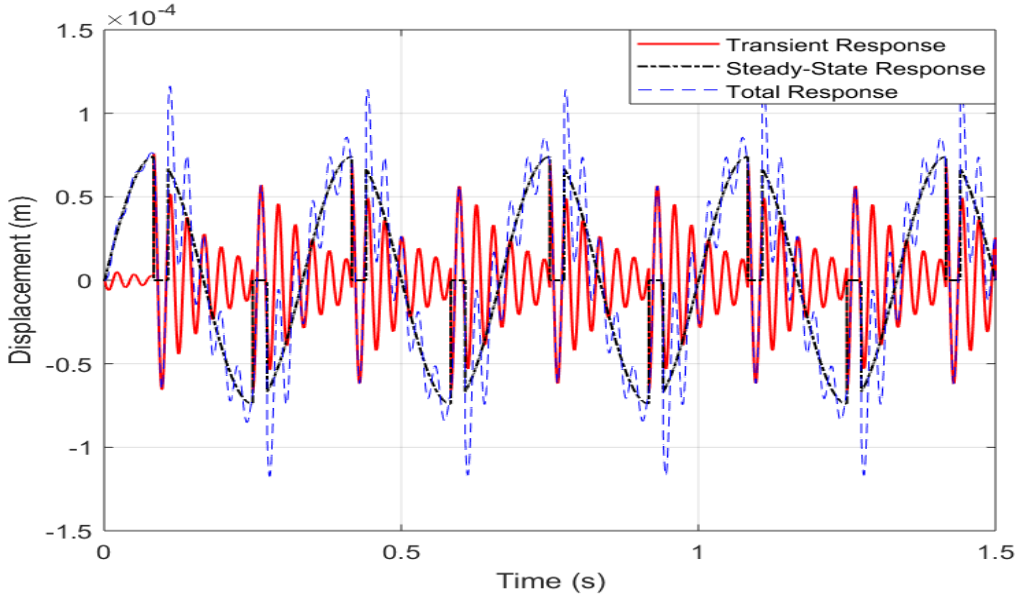


**Figure. 13.** Transient, Steady-State and Total Displacement of Nonlinear System with $\omega$ = 35Hz Relative to Ground Motion with $\Omega$ = 3Hz

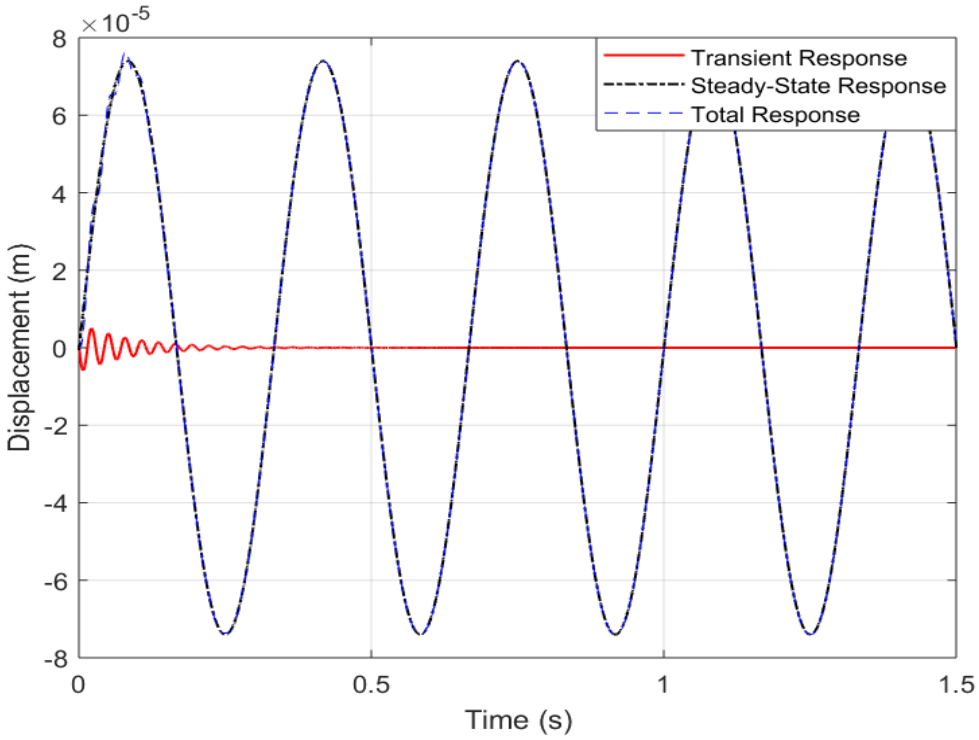


**Figure. 14.** Transient, Steady-State and Total Displacement of Linear System with $\omega$ = 35Hz Relative to Ground Motion with $\Omega$ = 3Hz

### 4.1.2. Displacement Response of cases where $\Omega < \omega$

In the cases where the excitation frequency $\Omega$ is lower than the natural frequency $\omega$ of SDOF (figures. 13, 14), the transient response in the linear cases decays and does not have significant contribution in the SDOF response. In the case of nonlinear SDOF system, however, the transient response contributes to the total response about the same as the steady-state response. The transient response decays until the SDOF vibrates freely when the bolt is not in contact with the SDOF base.

### 4.1.3. Displacement Response of cases where $\Omega = \omega$

In the cases where the excitation and SDOF frequencies are same (figures. 15, 16), the transient response in the linear cases decays whereas the transient response of nonlinear SDOF system increases. It must be noted that for linear SDOF cases, the transient and steady-state responses

cancel each other, and the total response increases as the transient response decreases. For the nonlinear SDOF cases, the transient and steady-state responses add with each other, and the total response increases as the transient response increases. Hence, the total response of nonlinear SDOF system is higher than the linear SDOF system. Thus, the peak spectral amplitude of nonlinear SDOF system is higher than the linear SDOF system.

### 4.1.4. Displacement Response of cases where $\Omega > \omega$

In the cases where the excitation frequency is higher than the SDOF system frequency (figures. 17, 18), the transient response is dominant for both linear and nonlinear SDOF systems. The difference in the response of linear and nonlinear SDOF systems is that while the linear SDOF system oscillates about the initial position, the nonlinear SDOF system does not. This behavior is observed because the boundary condition of the nonlinear system changes more frequently due to high-frequency excitation which prevents the nonlinear SDOF system from returning to the initial position.

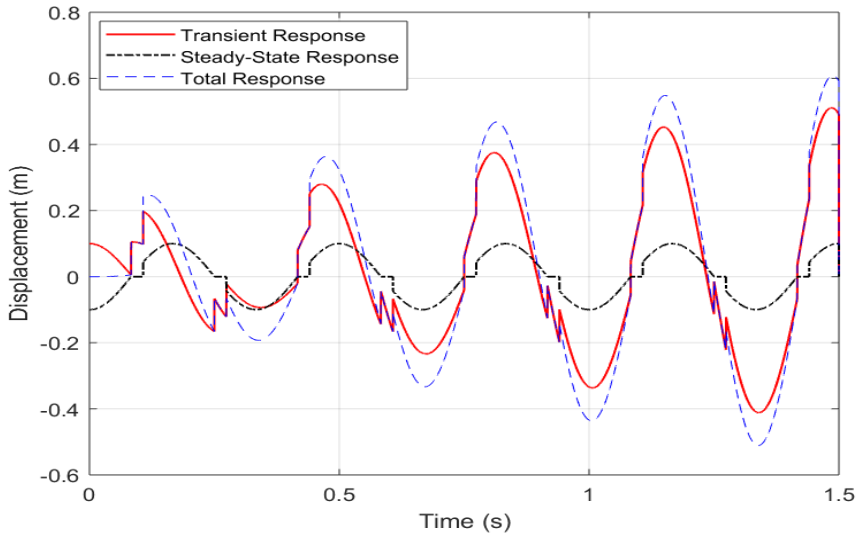


**Figure. 15.** Transient, Steady-State and Total Displacement of Gap SDOF with $\omega$ = 3Hz Relative to Ground Motion with $\Omega$ = 3Hz

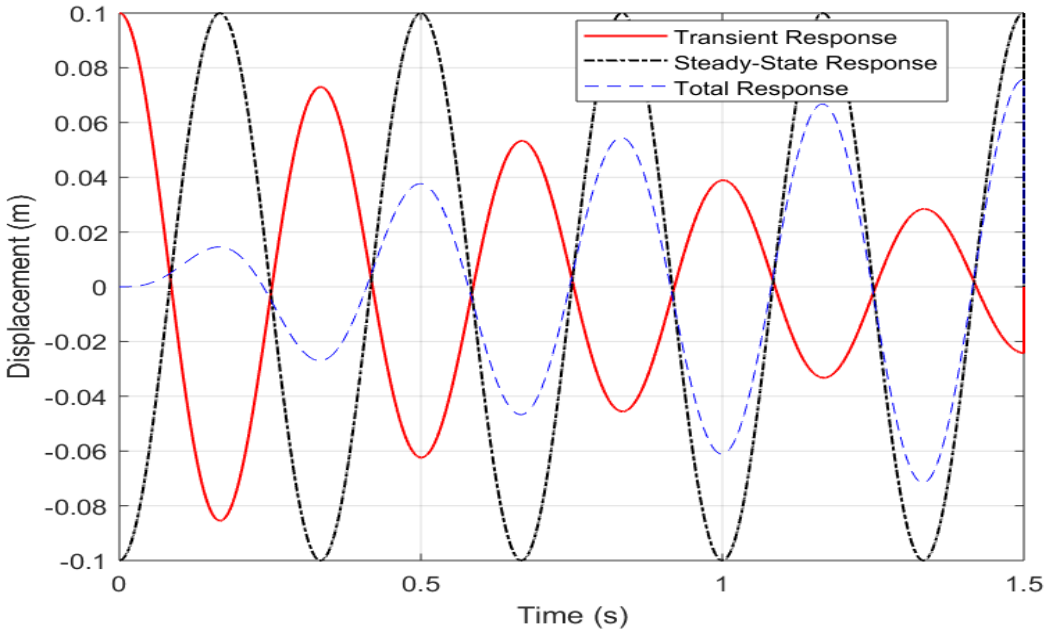


**Figure. 16.** Transient, Steady-State and Total Displacement of Linear SDOF with $\omega$ = 3Hz Relative to Ground Motion with $\Omega$ = 3Hz

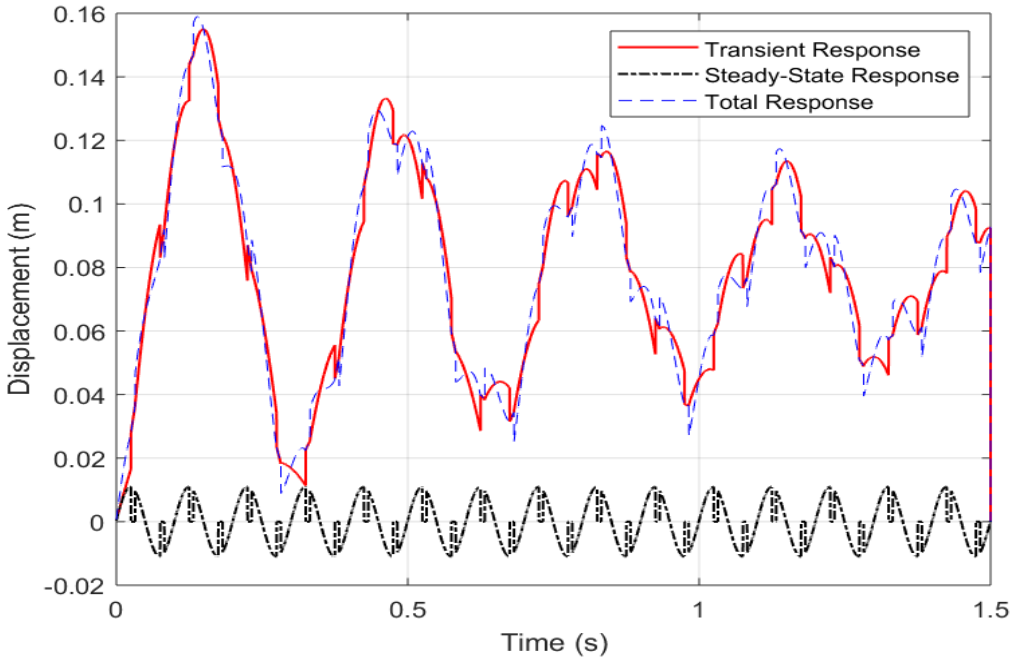


**Figure. 17.** Transient, Steady-State and Total Displacement of Gap SDOF with $\omega$ = 3Hz Relative to Ground Motion with $\Omega$ = 10Hz

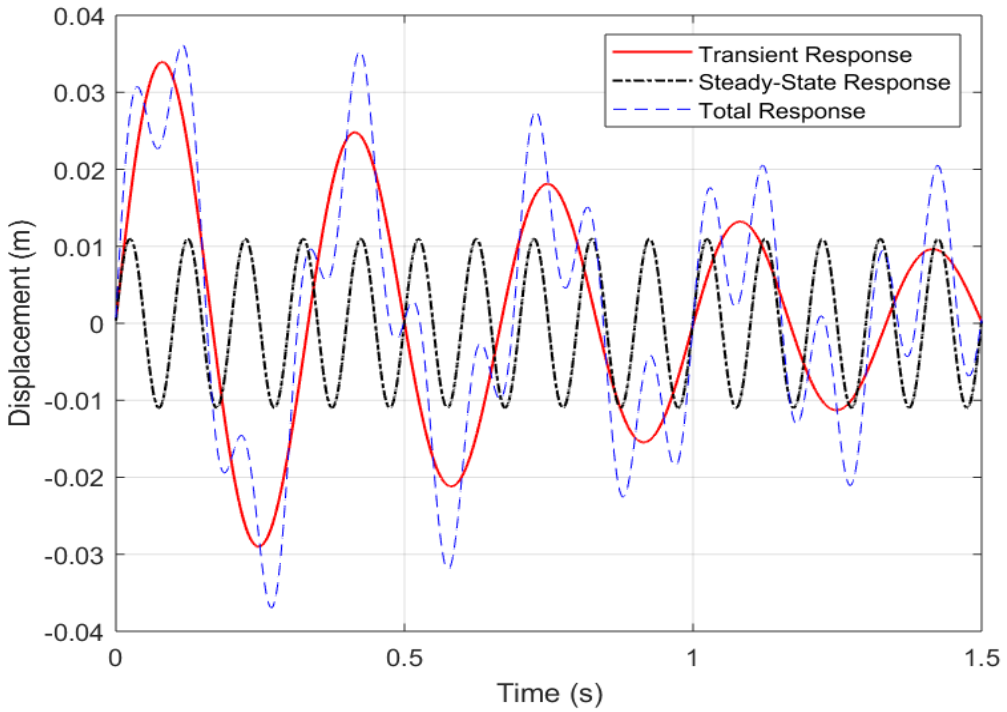


**Figure. 18.** Transient, Steady-State and Total Displacement of Linear SDOF with $\omega$ = 3Hz Relative to Ground Motion with $\Omega$ = 10Hz

## 5. Conclusions

The ground motion studies conducted on Central and Eastern United States nuclear power plant sites indicate that the ground motion response spectra contains high-frequency content. The high-frequency ground motions are relatively not damaging compared to low-frequency ground motions because the displacements associated with high-frequency ground motions are small. However, the functionality of safety-related equipment such as relays can be compromised for high-frequency accelerations. In order to qualify electrical equipment for high-frequency ground motions, the in-cabinet response spectra (ICRS) are usually evaluated by linear analysis of building and electrical cabinets. However, as discussed by Singh (2017), there is often a significant

difference in the ICRS obtained from linear and nonlinear models. The ICRS of nonlinear models with gap show a periodic pattern with multiple peaks and valley at higher frequencies. The reasons for the unique nature of ICRS of nonlinear gap model are explained in this research.

The results obtained from the analysis of linear single degree of freedom (SDOF) system and nonlinear SDOF system with gap can be concluded as follows:

- The transient response of linear SDOF system decays and does not contribute significantly to the total response of the SDOF (except for cases when excitation frequency is more than the natural frequency of SDOF system). The major contribution to the total response of the nonlinear SDOF system comes from the transient response.
- The periodic pattern of secondary peaks and valleys are observed in the ICRS for harmonic excitation similar to the observations made by Singh (2017) for actual earthquake excitations. The general pattern for all the cases shows that the peaks occur for oscillators whose natural frequencies are odd multiple of the excitation frequency while the valleys occur for oscillators whose natural frequencies are even multiple of the excitation frequency.
- The pattern of multiple secondary peaks and valleys is explained by the interaction of steady-state response with the transient response for the oscillators. For an oscillator with natural frequency which is an odd multiple of the excitation frequency, the maximum amplitude of steady-state response coincides with maximum amplitude of transient response. On the other hand, for an oscillators with natural frequency which is an even multiple of the excitation frequency, the maximum amplitude of steady-state response does not coincide with the maximum amplitude of transient response. Thus, the total response of an oscillator with natural frequency which is an odd multiple of the excitation frequency

is more than that of an oscillator with natural frequency which is an even multiple of the excitation frequency. This leads to a periodic pattern of spectral values in the ICRS for nonlinear SDOF system.

- The differences in displacement response of linear and nonlinear SDOF systems is also affected by the interaction of excitation and natural frequency of the oscillator. For cases where excitation frequency is less than the natural frequency of SDOF system, the transient response does not affect the total response of linear SDOF system whereas for cases where excitation frequency is more than the natural frequency of SDOF system, the total response of linear SDOF is contributed mainly by the transient response. On the other hand, the transient response of nonlinear SDOF for both the cases mentioned above, plays a major role in total response and hence peak spectral acceleration of ICRS as well as the occurrence of secondary peaks. For the cases where excitation frequency is equal to the natural frequency of SDOF system, the total response of both linear and nonlinear SDOF systems increases up to a maximum amplitude. However, the transient response of nonlinear SDOF systems increase in each cycle while that of linear SDOF decays. Thus, the peak spectral acceleration of nonlinear SDOF systems is much higher than that of linear SDOF systems.

## 6. Acknowledgement

This research was supported by Center for Nuclear Energy Facilities and Structures at North Carolina State University. Resources for the Center come from the dues paid by member organizations and from the Civil, Construction, and Environmental Engineering Department and College of Engineering in the University.

## 7. References


[1] Choi, B., (2000) “Sliding Response of an Unfastened Body subjected to a Ground Motion,” M.S. Thesis, North Carolina State University.

[2] EPRI, (2007) "Program on technology innovation: The effects of high-frequency ground motion on structures, components, and equipment in nuclear power plants," Palo Alto, CA: 2007.1015108.

[3] EPRI, (2013) “Seismic Evaluation Guidance: Screening, Prioritization and Implementation Details (SPID) for the Resolution of Fukushima Near-Term Task Force Recommendation 2.1: Seismic,” Palo Alto, CA: 2013.1025287.

[4] EPRI, (2014) "High frequency program: High frequency testing summary," Palo Alto, CA, 2014.3002002997.

[5] EPRI, (2015) "High frequency program: Application guidance for functional confirmation and fragility evaluation," Palo Alto, CA, 2015.3002004396.

[6] Gupta, A., Rustogi, S.K., Gupta, A.K., (1999) “Ritz Vector Approach for Evaluating Incabinet Response Spectra,” *Nuclear Engineering and Design,* Vol. 199, pp. 255-272, March 1999. DOI: 10.1016/S0029-5493(99)00076-X.

[7] Gupta, A., Rustogi, S.K., Gupta, A.K., (1999b) “Reconciliation of Experimental and Analysis Results of Switchgear Incabinet Spectra,” *In: Transactions of Tenth International Conference on Structural Mechanics in Reactor Technology (SMiRT-10),* 1999b.

[8] Gupta, A., Yang, J., (2002) “Modified Ritz vector approach for dynamic properties of electrical cabinets and control panels,” *Nuclear Engineering and Design 217(1),* pp. 49-62. DOI: 10.1016/S0029-5493(02)00133-4.

[9] Herve, G., (2014) "Improvement of the evaluation of high frequency content in the calculation of impact floor response spectra," *In: 2nd Conference on Technical Innovation in Nuclear Civil Engineering TINCE 2014, Paris*.

[10] Hu, H-S., Nakashima, M., (2017) “Responses of Two-Degree-of-Freedom Sliding Base Systems Subjected to Harmonic Ground Motions,” *Journal of Structural Engineering 143(2),* 2017, DOI: 10.1061/(ASCE)ST.1943-541X.0001653.

[11] Llambias, J.M., Sevant, C.J., Shepherd, D.J., (1989) "Non-linear response of electrical cubicles for fragility estimation," *In: Transactions of Tenth International Conference on Structural Mechanics in Reactor Technology (SMiRT-10)*, 1989.

[12] Newmark, N.M., (1965) “Effects of Earthquakes on Dams and Embankments,” Geotechnique, Vol. XV, No. 2, pp. 139-159, June 1965.

[13] Nikfar, F., Konstantinidis, D., (2017) “Peak Sliding Demands on Unanchored Equipment and Contents in Base-Isolated Buildings under Pulse Excitation,” *Journal of Structural Engineering 143(9),* DOI: 10.1061/(ASCE)ST.1943-541X.0001811.

[14] PEER, (2015) “NGA-East: Median Ground-Motion Models for the Central and Eastern North America Region,” *Pacific Earthquake Engineering Research Centre,* PEER Report No. 2015/04, April 2015.

[15] SSHAC, (1997) “Recommendations for Probabilistic Seismic Hazard Analysis: Guidance on Uncertainty and Use of Experts,” NUREG/CR-6372, UCRL-ID- 122160, Vol. 1.

[16] Shao, Y., (1998) “Seismic Response of Unanchored Bodies,” Doctoral dissertation, North Carolina State University, Raleigh, North Carolina.

[17] Singh, S., (2017) “Seismic Response of Electrical Equipment in Nuclear Power Plants,” M.S. Thesis, North Carolina State University.

[18] USNRC, (2014) "Design Response Spectra for Seismic Design of Nuclear Power Plants," Reg. Guide 1.60, July 2014.

[19] Vlaski, V., (2013) “Reduction of External Hazard (Fast Impact) Induced Vibrations,” F/AB-58, *In: 1st Conference on Technical Innovation in Nuclear Civil Engineering TINCE 2013, Paris,* October 28-31, 2013.

[20] Vlaski, V., Moersch, J., Sallmann, M., (2019) “Comparative Study for Reduction of APC Induced Vibrations,” *In: Transactions of 25$^{th}$ Conference on Structural Mechanics in Reactor Technology (SMiRT-25), Charlotte, NC, USA,* August 4-9, 2019.

[21] Wilkins, J.K., (2009) “The Influence of Classical and Non-Classical Friction on Sliding,” Doctoral Dissertation, North Carolina State University.

# Chapter 3

## Understanding the Seismic Response of Electrical Equipment Subjected to High–Frequency Ground Motions

**Abstract**

Ground motion studies in Central and Eastern United States (CEUS) show that the ground motion response spectra exceeds design spectrum of nuclear power plants in high–frequency range. To ensure safe shutdown of nuclear power plants in events where design spectrum is exceeded, the safety–related electrical equipment such as relays must be seismically qualified for high–frequency ground motions. Conventionally, uncoupled linear analysis of building and electrical cabinet is conducted and then seismic demands on equipment are evaluated. The conventional analysis ignores effects of various factors such as geometric nonlinearities, mass interaction between primary (building) and secondary (electrical cabinet) systems, etc. Ignoring such factors lead to unnecessarily high seismic demands on equipment. In this study, the seismic demands on equipment are evaluated by conducting both coupled and uncoupled analysis of linear primary system and linear as well as nonlinear secondary system. Various cases are analyzed where at least one mode of primary system is tuned with one mode of secondary systems. Each case is subjected to both low–frequency and high–frequency ground motions to compare the difference in response to each ground motion. The seismic demands on equipment are compared for coupled and uncoupled analysis as well as for linear and nonlinear systems. The results show reduction in seismic demands on electrical equipment for various nonlinear coupled analysis cases. The high seismic demands evaluated from linear uncoupled analysis may lead to disqualification of electrical equipment which can be avoided by conducting coupled nonlinear analysis of primary–secondary systems and obtaining the realistic seismic demands on equipment.

## 1. Introduction

It has been observed that the ground motions recorded at nuclear power plant sites in Central and Eastern United States (CEUS) have exceeded the design spectrum at frequencies above 10Hz. A study conducted by Electric Power Research Institute (EPRI, 2007) presents the effect of such high frequency ground motions on the safety–related electrical equipment such as relays. The 1986 Northeastern Ohio Earthquake, the 2011 Mineral, Virginia earthquake and most recently the 2016 Gyeongju earthquake in South Korea represent events in which nuclear power plants were subjected to high–frequency ground motions and various electrical systems tripped even though they were seismically qualified to continue operation during and after the earthquake. In another example, the design spectrum of Perry Nuclear Power Plant was exceeded by ground motion response spectrum (GMRS) of 1986 Northeastern Ohio earthquake in frequency range over 10Hz (EPRI, 2007). The plant was under construction and therefore a full extent of the effects of high–frequency ground motion could not be observed. However, operational testing of plant was underway and three non–safety related electrical systems experienced trips due to relay activation. Therefore, it is important to understand the behavior of electrical equipment when subjected to high–frequency ground motions.

Recent studies (SSHAC, 1997; EPRI, 2013; PEER, 2015) have proposed that earthquakes at nuclear power plant sites in CEUS are likely to comprise of a dominant frequency content between 15–30Hz. The response spectrum for such an earthquake would exceed the safe shutdown earthquake spectrum recommended by United States Nuclear Regulatory Committee (USNRC, 2014) Regulatory Guide 1.60 as illustrated in EPRI (2014). As per the recommendation 2.1 of Near–Term Task Force (NTTF) report on Fukushima Daiichi disaster, the nuclear power plants in the United States are required to re–evaluate seismic hazards on their sites and reassess the safety

of existing structures, systems and components against the updated hazard (USNRC, 2011). In general, the high–frequency ground motions do not cause structural damage as the displacements induced by such motions are relatively small (EPRI 2007, 2014). The high–frequency seismic accelerations, on the other hand, can adversely affect the functionality of electrical instruments mounted on cabinets and control panels. Historically, the electrical instruments are qualified for low–frequency seismic accelerations only (EPRI, 2014).

EPRI (2014, 2015) conducted a shake table study to determine the capacity of a few sensitive electrical instruments subjected to high frequency accelerations in the range of 16–48Hz. Engineers at a nuclear power plant qualify the electrical instruments by evaluating the seismic demands for a given hazard at the plant site and comparing it with the instrument capacities. The method to evaluate seismic demands according to EPRI (2015) multiplies the GMRS at the site with empirically obtained amplification factors for the structure and the electrical cabinet. The amplification of GMRS in the structure is based on the height of the floor at which cabinet is placed. The amplified floor response spectrum thus obtained is known as in–structure response spectrum (ISRS). Further amplification of ISRS due to the electrical cabinet is based on the type of the cabinet. The amplified spectrum is called in–cabinet response spectrum (ICRS) which gives the seismic demands on the devices like relays. The method suggested in EPRI (2015) uses empirical data to calculate the amplification factors. The amplification factors do not consider the natural frequency of either the structure or the electrical cabinet. The approach also ignores many other factors such as cabinet mounting arrangement, location of equipment on the cabinet, geometric nonlinearities, interaction between the structure and the cabinet, etc. In general, the use of empirical amplification factors have been found to be inaccurate which can often render some devices seismically unacceptable for use in a plant.

Preliminary studies have shown that geometric nonlinearities such as a gap between the anchor bolt and the cabinet base plate can filter out the high–frequency excitations resulting in much less spectral values of ICRS (Vlaski et al., 2013; Herve et al., 2014; Singh, 2017; Vlaski et al., 2019). The study by Singh (2017) has indicated that such small gaps can also increase the amplifications in the cabinet when subjected to low frequency ground motions due to localized impacts. The key observations from this study are preliminary as they are based on a SDOF representation of the building and a SDOF model of the cabinet. In addition, almost all existing studies on understanding the seismic behavior of electrical cabinets and generation of ICRS are based on an uncoupled analysis of the cabinets. Even though cabinets are heavy structural systems that can exhibit significant mass interaction with the supporting buildings, such interactions are not considered in an uncoupled analysis. It has now been well established that a linear analysis of the coupled system that accounts for equipment-structure interaction can result in more than 50% reduction in ISRS which in turn would lead to significantly less spectral accelerations in ICRS (Burdisso et al., 1987; Dubey et al., 2019).

In this paper, the work presented in Singh (2017) is extended further by considering the effect of localized nonlinearities at the cabinet base in MDOF building – MDOF cabinet systems. Consideration of MDOF systems is essential to study the effects of tuning between different modes of the buildings and cabinets as well as the distribution of mass participation across multiple modes. Unlike previous studies, both an uncoupled and a coupled analysis of the building–cabinet system are considered to assess the effect of mass interaction on ICRS. Ground motions with both low frequency and high frequency contents are considered to study these effects.

## 2. Dynamic Characteristics of Electrical Cabinet

### 2.1 Observations from Linear Models

Detailed analytical and experimental studies on electrical cabinets have shown that accurate ICRS can be calculated by using only a single "significant" mode of the cabinet (Gupta et al., 1999; Gupta et al., 2019; Salman et al., 2020). A significant mode can be either a global rocking mode or a local mode (cabinet door/panels, internal frame, etc.). Sometimes, it can also be a combination of both. As illustrated in various studies (Gupta et al., 1999; Gupta et al., 2019; Salman et al., 2020), a significant mode may not necessarily be the fundamental mode of a cabinet. Also, the peak spectral acceleration in ICRS varies based on the location of devices within the cabinet. Gupta et al. (1999) shows that ICRS on the top of a cabinet can be much less than that at the mid height when a local mode of the plate or frame is significant.

Initial studies by Gupta et al. (1999) assumed the electrical cabinet to be fixed at the base. A fixity at the cabinet base restricted the observation on significant cabinet mode to either a local mode or a global bending mode. It could not capture a global rocking mode. A comparison between the experimental and analytical results conducted by different studies (Rustogi and Gupta, 2004; Lee and Jung, 2020) shows the importance of considering the flexibility of mounting arrangement at the cabinet base. The significant mode can also be a combination of rigid–body rocking of the cabinet either by itself or in combination with a local mode. High mass participation in rocking mode can sometimes result in overturning of the cabinet (Yim and Chopra, 1985). Various studies (Yang et al., 2002; Han et al., 2018) study the flexibility of different mounting arrangements in cabinets and presents a formulation for evaluating the rotational stiffness for each case. The results obtained from an analysis after incorporating the rocking mode show an improved agreement between the experimental and the finite element analysis results.

## 2.2 Observations from Nonlinear Models

A few recent studies (Vlaski et al., 2013; Herve et al., 2014; Singh, 2017; Vlaski et al., 2019) have focused on the propagation of high frequency motions from ground through the nuclear power plant structure, systems, and components. EPRI (2007) concludes that high–frequency ground motions induce small displacements which do not lead to structural damage but the high–frequency accelerations can adversely affect the output signal of electrical devices. Vlaski et al. (2013) uses observations from experimental tests to infer that high–frequency accelerations may not necessarily propagate to the electrical systems. Herve et al. (2014) and Singh (2017) studied the effect of geometric nonlinearities such as those due to gaps between the cabinet base and the floor as shown in Figure. 1. These studies illustrate that small displacements from high frequency motions may not necessarily propagate across the gap and are filtered out. Consequently, the spectral accelerations in ICRS are much less than those obtained from a linear analysis. At the same time, it is also shown that a low frequency ground motion with floor displacements greater than the gap can lead to spectral accelerations that are much larger than those calculated from a linear analysis. Such an increase occurs due to the transient motions imparted by impact between the anchor bolts and the cabinet base plate. It is important to note that these recent studies are based on SDOF representations of the cabinet as well as buildings. Also, these studies consider the buildings and the cabinet to be uncoupled thereby ignoring the effect of mass interaction between the two systems.

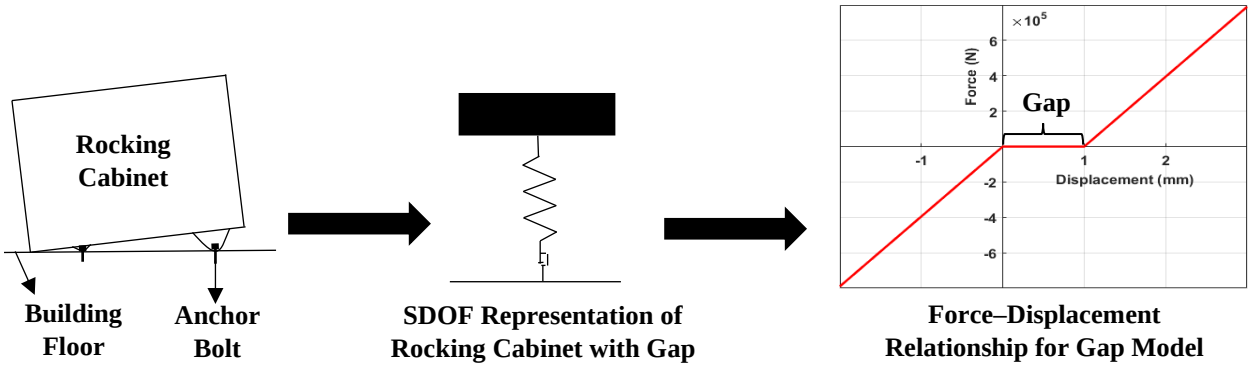


**Figure. 1.** Nonlinear Gap Model for Rigid Body Rocking of Cabinet

## 3. Modeling the Behavior of Coupled Systems

The concept of modeling the seismic behavior of coupled building–equipment or building–piping systems has been studied extensively (Xu et al., 1999; Xu et al., 2004; Dubey et al., 2019). It has been shown that a coupled analysis can result in a significant reduction of ISRS or the seismic response of equipment and piping. Such a reduction occurs due to mass interaction between the modes of the building (primary) system and the modes of the equipment (secondary) system. The effect of mass interaction is more pronounced when the modes of the primary and the secondary system are tuned or nearly tuned. The complexity in modeling the behavior of a coupled systems increases due to the effect of nonclassical damping which can lead to an additional reduction in the response of secondary system. This effect is significant in systems with tuned or nearly tuned modes when the mass interaction is very small and damping characteristics of the building are different from that of the equipment which is usually the case (Xu et al., 2004; Gupta and Bose, 2017). In this study, we study the effect of mass-interaction only. The effect of nonclassical damping is not considered.

The equation of motion of a coupled primary–secondary system (Gupta and Gupta, 1997) is given by equation (1):

` $$[M]\{\ddot{U}\} + [C]\{\dot{U}\} + [K]\{U\} = -[M]\{U_b\}\ddot{u}_g \quad \textbf{(1)}$$

Where, $[M]$, $[C]$ and $[K]$ are the mass, damping and stiffness matrices of the coupled primary–secondary system; $\{\ddot{U}\}$, $\{\dot{U}\}$ and $\{U\}$ are acceleration, velocity and displacement vectors of the coupled system; $\{U_b\}$ is the influence vector of coupled system and $\ddot{u}_g$ is the ground acceleration time history. Equation (1) can further be expressed as:

$$\begin{bmatrix}[M_P] & [O]\\ [O] & [M_S]\end{bmatrix}\begin{Bmatrix}\{\ddot{U}_P\}\\ \{\ddot{U}_S\}\end{Bmatrix} + \begin{bmatrix}[C_P] + [C_P^S] & [C_{PS}]\\ [C_{SP}] & [C_S]\end{bmatrix}\begin{Bmatrix}\{\dot{U}_P\}\\ \{\dot{U}_S\}\end{Bmatrix} + \begin{bmatrix}[K_P] + [K_P^S] & [K_{PS}]\\ [K_{SP}] & [K_S]\end{bmatrix}\begin{Bmatrix}\{U_P\}\\ \{U_S\}\end{Bmatrix} = -\begin{bmatrix}[M_P] & [O]\\ [O] & [M_S]\end{bmatrix}\begin{Bmatrix}\{U_{bP}\}\\ \{U_{bS}\}\end{Bmatrix}\ddot{u}_g \quad \textbf{(2)}$$

Where, $[M_P]$ and $[M_S]$ are uncoupled mass matrices of primary and secondary systems respectively; $[C_P]$ and $[C_S]$ are uncoupled damping matrices of primary and secondary systems respectively; $[K_P]$ and $[K_S]$ are uncoupled stiffness matrices of primary and secondary systems respectively; $[C_P^S]$ and $[K_P^S]$ are the damping and stiffness contributions of the secondary system for the primary system's connecting DOF; $\{\ddot{U}_P\}$, $\{\dot{U}_P\}$ and $\{U_P\}$ are the acceleration, velocity and displacement respectively of the primary system; $\{\ddot{U}_S\}$, $\{\dot{U}_S\}$ and $\{U_S\}$ are the acceleration, velocity and displacement respectively of the secondary system; $\{U_{bP}\}$ and $\{U_{bS}\}$ are the influence vectors for primary and secondary systems respectively.

The above equation written in a conventional form does not provide a straightforward inference of mass interaction between the primary and the secondary systems as the mass matrix is diagonal and the off-diagonal terms that would establish interaction are zero. This initial

perception can be clarified by a closer look at the definition of degrees of freedom in the equations of motion. The secondary system displacement vector $\{U_S\}$ in the above equations expresses the displacements with respect to the fixed base of the entire coupled structure, i.e., with respect to the fixed based of the primary system. In contrast, the equations of motion in an uncoupled analysis consider the displacements with respect to the primary system DOFs which are also the base of secondary systems. Equations (1) and (2) above can be transformed and rewritten in a form that considers secondary system displacements with respect to the base of secondary system. To do so, the displacement vector of secondary system, $\{\bar{U}_s\}$ can be given by equation (3).

$$\{\bar{U}_s\} = \{U_s\} - [U_{sc}]\{U_c\} \quad \textbf{(3)}$$

Where, $\{U_s\}$ and $\{U_c\}$ are the displacement vectors for secondary system and the primary system connecting DOF relative to the base of the primary system, respectively. The matrix $[U_{sc}]$ represents the static deformation shape of the secondary system when the corresponding primary system connecting DOF undergoes a unit displacement the calculation of which is described by Gupta and Gupta (1998). The displacement vector of coupled system may be expressed by equation (4).

$$\{U\} = \begin{Bmatrix}\{U_p\}\\ \{U_s\}\end{Bmatrix} = \begin{bmatrix}[I] & [O]\\ [U_{sp}] & [I]\end{bmatrix}\begin{Bmatrix}\{\bar{U}_p\}\\ \{\bar{U}_s\}\end{Bmatrix};\ \{U\} = [T]\{\bar{U}\} \quad \textbf{(4)}$$

Where, $\{U_p\} = \{\bar{U}_p\}$, $[U_{sp}]$ is an extension of matrix $[U_{sc}]$ where zeros are added for DOF of primary system not connected to the secondary system. Substituting equation (4) in equation (1) and pre–multiplying by $[T]^T$, the equation of motion is written as:

$$[\bar{M}]\{\ddot{\bar{U}}\} + [\bar{C}]\{\dot{\bar{U}}\} + [\bar{K}]\{\bar{U}\} = -[\bar{M}]\{\bar{U}_b\}\ddot{u}_g \quad \textbf{(5)}$$

Where,

$$[\bar{M}] = [T]^T[M][T] = \begin{bmatrix} [\bar{M}_p] & [\bar{M}_{ps}] \\ [\bar{M}_{sp}] & [\bar{M}_s] \end{bmatrix}$$

$$[\bar{C}] = [T]^T[C][T] = \begin{bmatrix} [\bar{C}_p] & [\bar{C}_{ps}] \\ [\bar{C}_{sp}] & [\bar{C}_s] \end{bmatrix}$$

$$[\bar{K}] = [T]^T[K][T] = \begin{bmatrix} [\bar{K}_p] & [\bar{K}_{ps}] \\ [\bar{K}_{sp}] & [\bar{K}_s] \end{bmatrix}$$

$$\{\bar{U}_b\} = [T]^{-1}\{U_b\} = \begin{Bmatrix} \{\bar{U}_{bp}\} \\ \{\bar{U}_{bs}\} \end{Bmatrix} = \begin{bmatrix} [I] & [O] \\ -[U_{sp}] & [I] \end{bmatrix} \begin{Bmatrix} \{U_{bp}\} \\ \{U_{bs}\} \end{Bmatrix}$$

$$\left[\bar{M}_p\right] = \left[M_p\right] + \left[U_{sp}\right]^T [M_s][U_{sp}]$$

$$\left[\bar{M}_{ps}\right] = \left[\bar{M}_{sp}\right]^T = \left[U_{sp}\right]^T [M_s]$$

$$[\bar{M}_s] = [M_s]$$

$$\left[\bar{C}_p\right] = \left[C_p\right] + \left[C_p^s\right] + \left[U_{sp}\right]^T \left[C_{sp}\right] + \left[C_{ps}\right]\left[U_{sp}\right] + \left[U_{sp}\right]^T [C_s][U_{sp}]$$

$$[\bar{C}_{ps}] = \left[\bar{C}_{sp}\right]^T = [C_{ps}] + \left[U_{sp}\right]^T [C_s] = [O]$$

$$[\bar{C}_s] = [C_s]$$

$$\left[\bar{K}_p\right] = \left[K_p\right] + \left[K_p^s\right] + \left[U_{sp}\right]^T \left[K_{sp}\right] + \left[K_{ps}\right]\left[U_{sp}\right] + \left[U_{sp}\right]^T [K_s][U_{sp}]$$

$$[\bar{K}_{ps}] = \left[\bar{K}_{sp}\right]^T = [K_{ps}] + \left[U_{sp}\right]^T [K_s] = [O]$$

$$[\bar{K}_s] = [K_s]$$

As can be seen from the transformed equations of motion above, the off–diagonal terms in the mass matrix account for mass interactions between the two systems. The above equations for a linear system can be transformed further using the mode shapes of the primary and the secondary system as described in Gupta and Gupta (1998). Such a transformation can be used to show that

the mass interaction between the $i^{th}$ mode of the primary system and the $j^{th}$ mode of the secondary system can be expressed as (Gupta and Jaw, 1986):

$$\sqrt{r_{ij}} = [\gamma_{cj}]\{\phi_{ci}\}, \quad [\gamma_{cj}] = \{\phi_{sj}\}^T [M_s][U_{sc}] \tag{6}$$

Where, $r_{ij}$ is the modal mass ratio; $\{\phi_{ci}\}$ is the vector consisting of $i^{th}$ primary mode shape at connecting DOF; $\{\phi_{sj}\}$ is the $j^{th}$ mode shape of secondary system. For a nonlinear system, the stiffness of the secondary system is not proportional to the displacement but rather a function of the secondary system displacement ($\{U_s\}$). Hence, equation (5) can be rewritten as equation (7).

$$\begin{bmatrix} [\bar{M}_p] & [\bar{M}_{ps}] \\ [\bar{M}_{sp}] & [\bar{M}_s] \end{bmatrix} \begin{Bmatrix} \{\ddot{\bar{U}}_p\} \\ \{\ddot{\bar{U}}_s\} \end{Bmatrix} + \begin{bmatrix} [\bar{C}_p] & [O] \\ [O] & [\bar{C}_s] \end{bmatrix} \begin{Bmatrix} \{\dot{\bar{U}}_p\} \\ \{\dot{\bar{U}}_s\} \end{Bmatrix} + \begin{bmatrix} [\bar{K}_p] & [O] \\ [O] & [\bar{K}_s(\{U_s\})] \end{bmatrix} \begin{Bmatrix} \{\bar{U}_p\} \\ \{\bar{U}_s\} \end{Bmatrix} = -\begin{bmatrix} [\bar{M}_p] & [\bar{M}_{ps}] \\ [\bar{M}_{sp}] & [\bar{M}_s] \end{bmatrix} \begin{Bmatrix} \{\bar{U}_{bp}\} \\ \{\bar{U}_{bs}\} \end{Bmatrix} \ddot{u}_g \tag{7}$$

## 4. Application Case Studies

Representative MDOF building and MDOF cabinet models are considered in this study to evaluate the effects of: (i) localized nonlinearity in a MDOF secondary system, (ii) mass interaction between the primary and secondary systems, (iii) frequency content and magnitude of accelerations in the earthquake ground motion records, and (iv) degree of nonlinearity due to different gaps in the cabinet mounting arrangement.

A 10–DOF primary system representing the building and a 6–DOF secondary system representing the cabinet is considered for this study. The mass and stiffness properties of these systems are varied to create seven different MDOF primary–secondary systems. Each system is subjected to two earthquake ground motions, a low–frequency and a high–frequency ground

motion. The peak spectral acceleration in low–frequency ground motion occurs at 4Hz as compared to 16Hz for the high–frequency ground motion. The ground motions are normalized to same peak ground acceleration (PGA) in order to study the effect of frequency content. Figure 2 shows the comparison between the spectra of the two ground motions normalized to 1g PGA. The response of a nonlinear system is highly dependent upon the amplitude of excitation as it cannot be scaled proportionally with the ground motion. Therefore, the magnitude of the ground acceleration in terms of PGA also affects the seismic demands on the electrical equipment. Two different amplitudes are considered by normalizing the ground motions to 0.2g which is typical of the design PGAs in nuclear power plants around the world as well as 1g.

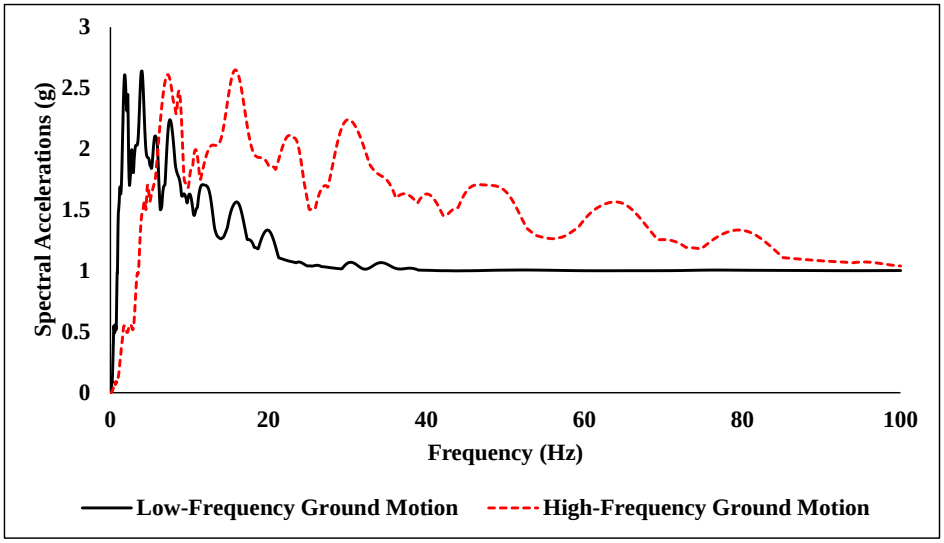


**Figure. 2.** Comparison of Low–Frequency and High–Frequency Ground Motion Response Spectra

For brevity, results from only two different systems are presented in this study but the observations made for these systems are also applicable for other systems. The primary systems are created such that their modal frequencies coincide with the frequencies of spectral peaks in the ground motion response spectra. In the System–1, the fundamental modes of primary and

secondary systems are tuned at a frequency of 4Hz which also resonates with the frequency of the spectral peak in the low–frequency ground motion. In System–2, the second and third modes of the primary and secondary system are tuned with each other at 16Hz and 33Hz frequency, respectively, which coincide with the frequencies of spectral peaks of high–frequency ground motion. Figure 3 shows a typical primary and secondary system and table 1 shows the mass and stiffness at each DOF for both systems. Table 2 gives the frequencies of the uncoupled primary and secondary systems in the two cases. The connection between the primary and secondary system is modeled as linear as well as nonlinear. In nonlinear secondary systems, the force–displacement relationship of the connecting stiffness is modeled as nonlinear elastic gap whose force–displacement relationship is shown in figure 1. Two different values of gaps considered are 1mm and 3mm. The two systems are connected at the top ($10^{th}$ floor) of primary system. The uncoupled analysis is conducted by evaluating the response of the primary system excited by the ground motion and then calculating the response of secondary system subjected to absolute acceleration obtained at the tenth DOF of primary system. In a coupled analysis, the coupled primary–secondary system is subjected to the ground motion at the base of primary system. The modal damping ratio for all the modes in the coupled or uncoupled systems is assumed to be 5%. For nonlinear direct integration of both systems, the damping matrix is developed by using mode superposition method (CSI, 2011) according to the equation (8).

$$[C] = \sum_{i=1}^{N} \frac{4\pi}{T_i} \xi_i ([M]\{\phi_i\})([M]\{\phi_i\})^T \quad \textbf{(8)}$$

Where, $T_i$, $\xi_i$, and $\{\phi_i\}$ are the modal period, damping ratio, and mode shape for $i^{th}$ mode of the coupled or uncoupled primary or secondary system. $N$ is the total number of modes. The ICRS from both uncoupled and coupled analysis are generated at different elevations within the

secondary systems but results for only the first (bottom floor) and the sixth (top floor) DOFs are presented in this paper for brevity.

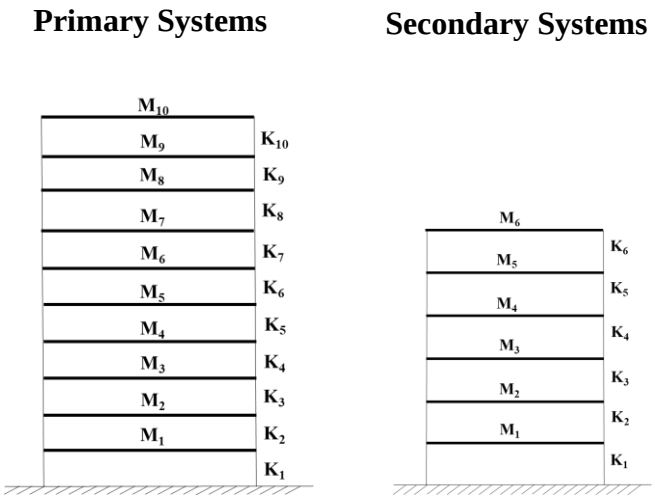


**Figure. 3.** Primary and Secondary Systems used in Analysis. Secondary System is Connected at $10^{th}$ Floor of Primary System

**Table 1.** Primary and Secondary System Properties

| DOF | Primary System | | | | DOF | Secondary System | | | |
|---|---|---|---|---|---|---|---|---|---|
| | Mass (kg) | | Stiffness ($N/m^2$) | | | Mass (kg) | | Stiffness ($N/m^2$) | |
| | System 1 | System 2 | System 1 | System 2 | | System 1 | System 2 | System 1 | System 2 |
| 1 | 1000 | 1000 | 2.84E7 | 4E7 | 1 | 10 | 10 | 1.14E5 | 3.96E5 |
| 2 | 100 | 100 | 2.84E6 | 1.09E7 | 2 | 1 | 1 | 1.14E4 | 3.96E4 |
| 3 | 100 | 1000 | 2.84E6 | 4E7 | 3 | 10 | 10 | 1.14E5 | 3.96E5 |
| 4 | 1000 | 100 | 2.84E7 | 1.09E7 | 4 | 1 | 1 | 1.14E4 | 3.96E4 |
| 5 | 100 | 100 | 2.84E6 | 1.09E7 | 5 | 1 | 1 | 1.14E4 | 3.96E4 |
| 6 | 100 | 100 | 2.84E6 | 1.09E7 | 6 | 1 | 1 | 1.14E4 | 3.96E4 |
| 7 | 100 | 100 | 2.84E6 | 1.09E7 | | | | | |
| 8 | 100 | 100 | 2.84E6 | 1.09E7 | | | | | |
| 9 | 100 | 100 | 2.84E6 | 1.09E7 | | | | | |
| 10 | 100 | 100 | 2.84E6 | 1.09E7 | | | | | |

**Table 2.** Uncoupled Primary and Secondary System Modal Frequencies (Hz)

| Mode No. | Primary System | | Mode No. | Secondary System | |
|---|---|---|---|---|---|
| | System–1 | System–2 | | System–1 | System–2 |
| 1 | 4.00 | 8.27 | 1 | 4.00 | 7.47 |
| 2 | 8.42 | 16 | 2 | 7.74 | 16.30 |
| 3 | 19.52 | 33.20 | 3 | 17.79 | 33.20 |
| 4 | 26.84 | 35.98 | 4 | 21.40 | 39.94 |
| 5 | 30.72 | 52.98 | 5 | 30.63 | 57.17 |
| 6 | 38.42 | 70.45 | 6 | 58.62 | 109.42 |
| 7 | 40.32 | 84.97 | | | |
| 8 | 47.57 | 95.85 | | | |
| 9 | 52.12 | 102.58 | | | |
| 10 | 93.02 | 117.35 | | | |

## 5. Results

### 5.1. Comparison of Coupled and Uncoupled Linear Analysis

The mass interaction between the tuned modes of primary and secondary systems in the coupled analysis reduces peak spectral acceleration in the ICRS. For system–1, the modal mass ratio between the tuned modes calculated in accordance with equation (6) is 1.04%. For system–2, the modal mass ratio between the tuned modes is 1.48% for the second mode pair and 1.71% for the third mode pair. To illustrate the effect of mass interaction between tuned modes, the comparison between the coupled and uncoupled analysis is shown in figure 4 and 5 for system–1 and figure 6 and 7 for system–2.

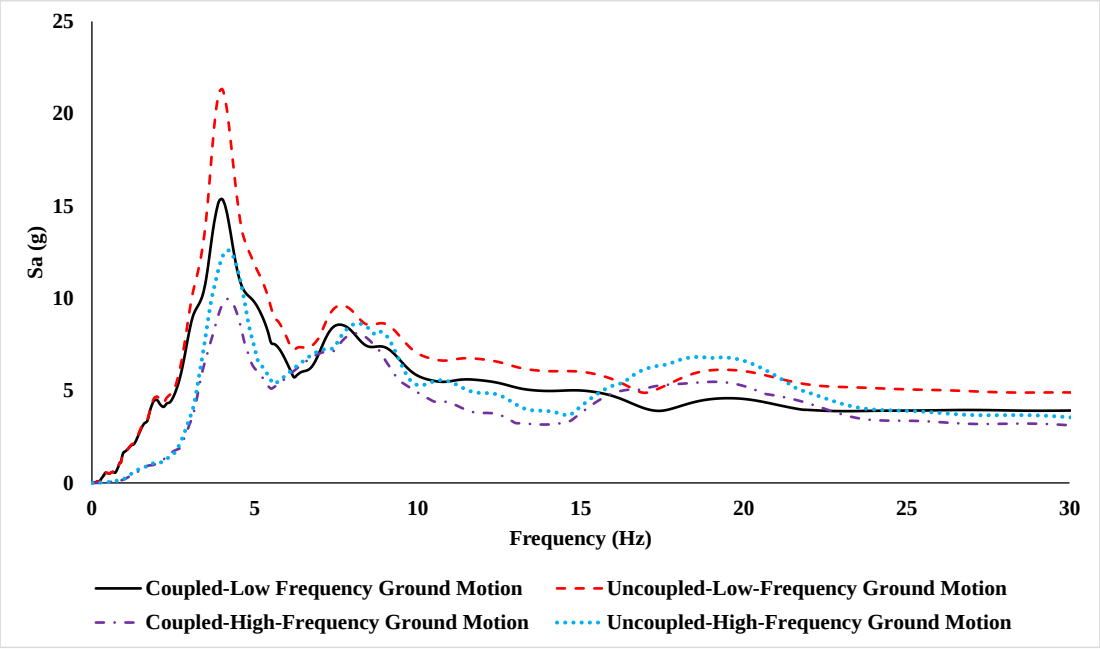


**Figure. 4.** Comparison of ICRS obtained at First Story of Secondary System from Coupled and Uncoupled Linear Analysis of System–1 subjected to both Low–Frequency and High–Frequency Ground Motions

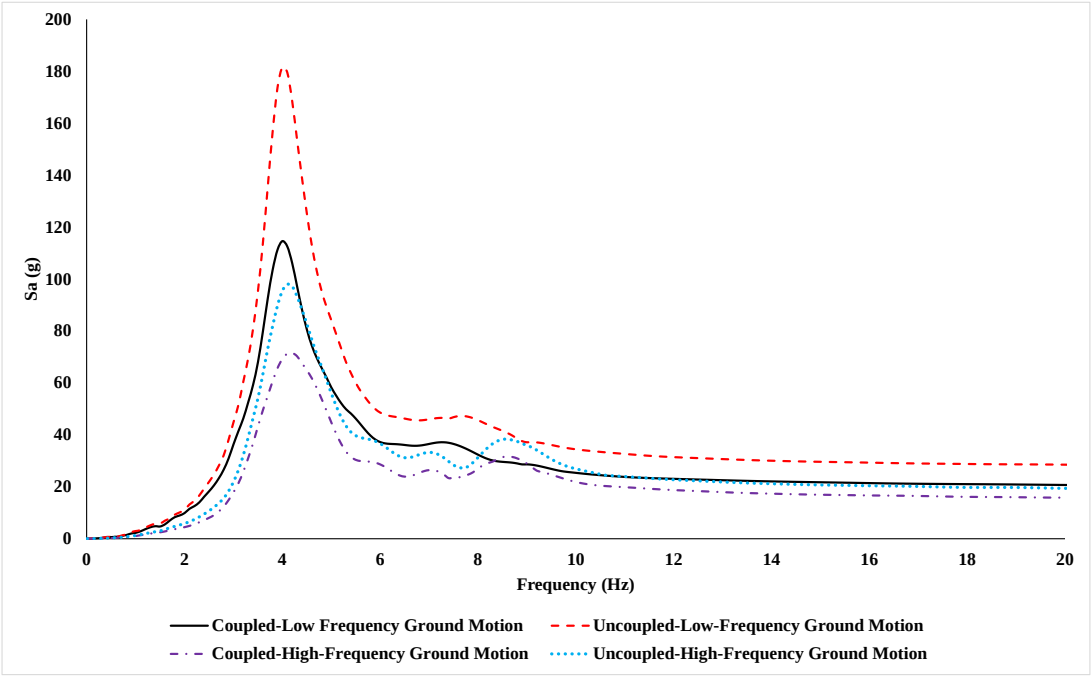


**Figure. 5.** Comparison of ICRS obtained at Sixth DOF of Secondary System from Coupled and Uncoupled Linear Analysis of System–1 subjected to both Low–Frequency and High–Frequency Ground Motions

As shown in figure 4 and 5, the peak spectral acceleration for all cases of system–1 occur at 4Hz. Overall, the amplitudes of ICRS are higher when the system is subjected to low–frequency ground motion. The peak spectral accelerations are significantly lower for coupled analysis as compared to uncoupled analysis for both ground motions at both the stories. Unlike system–1, the spectral amplitudes of ICRS obtained for system–2 and shown in figures 6 and 7, are higher when system is subjected to high–frequency ground motion. Similar to system–1, system–2 also shows a significant reduction in spectral accelerations from a coupled analysis. For system–2, figure 6 shows an important observation. The peak spectral values occurs at 7.6Hz from a coupled as well as uncoupled analysis for the low frequency ground motion case. For the high frequency ground motion case, the peak spectral acceleration for the uncoupled analysis occurs at 33Hz which is the frequency of the third primary and the third secondary system modes. Both of these modes are also tuned with a peak in ground motion response spectrum. The coupled analysis on the other hand gives a relatively much less spectral acceleration. This observation illustrates the significance of using a coupled analysis especially in the case of high frequency ground motions. An uncoupled analysis for such systems can lead to excessive conservatism. This observation is limited to lower floors of the secondary system because the high frequency modes contribute significantly to the total response on these floors. This observation cannot be made in figure 7 for the top floor because the response at top floor comes primarily from the fundamental mode of secondary system.

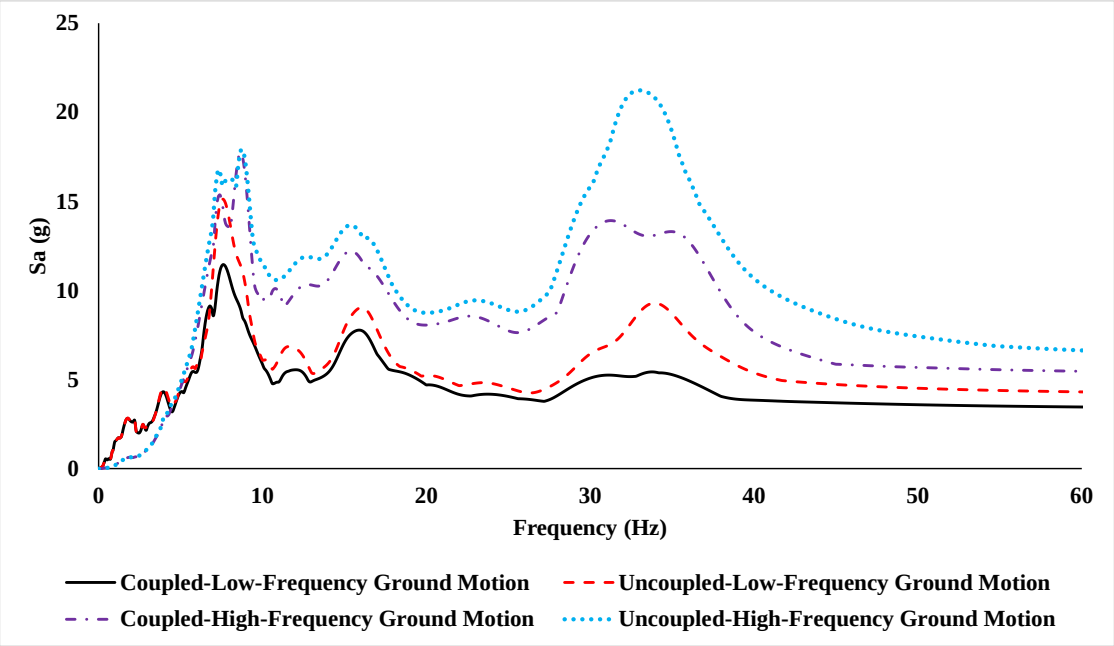


**Figure. 6.** Comparison of ICRS obtained at First DOF of Secondary System from Coupled and Uncoupled Linear Analysis of System–2 subjected to both Low–Frequency and High–Frequency Ground Motions

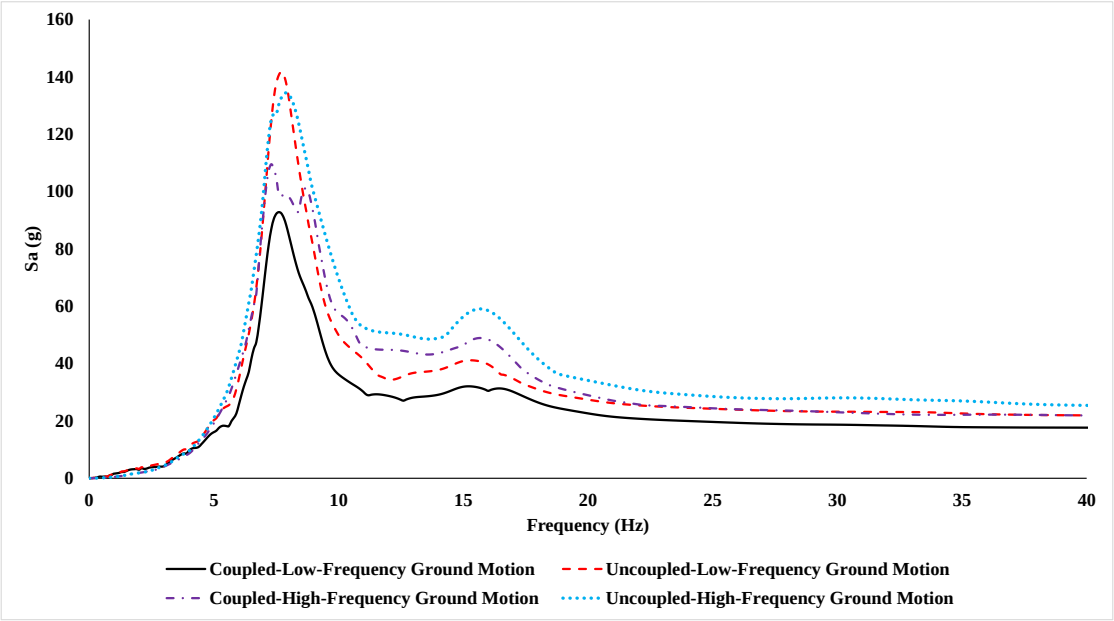


**Figure. 7.** Comparison of ICRS obtained at Sixth DOF of Secondary System from Coupled and Uncoupled Linear Analysis of System–2 subjected to both Low–Frequency and High–Frequency Ground Motions

## 5.2. Comparison of Uncoupled Linear and Nonlinear Analysis

Next, the effect of base nonlinearity is studied using uncoupled analysis and comparing the results to the corresponding linear analysis. The purpose is to study the effect of multiple modes on the observations made by Singh (2017) using only SDOF primary and SDOF secondary systems. Figures 8–11 show the results obtained for both the systems. For system–1 in which the fundamental modes of primary and secondary systems are tuned, there is negligible difference between spectral amplitudes from linear and nonlinear analysis at frequencies of fundamental modes. However, the ICRS evaluated at first floor from a nonlinear analysis shows significantly higher values of spectral accelerations in the high frequency as seen in figure 8. The same is not true for the top floor as seen in figure 9. This observation is quite interesting, and the particular behavior occurs because the nonlinearity results in an impact at cabinet base. Physically, this impact occurs between the anchor bolt and the cabinet base plate whenever the gap closes. The impact results in high frequency transient vibrations which in turn can get amplified by the high frequency modes. The high frequency modes contribute significantly to the total response at first floor but not at the top (sixth) floor where the total response comes primarily from the fundamental mode.

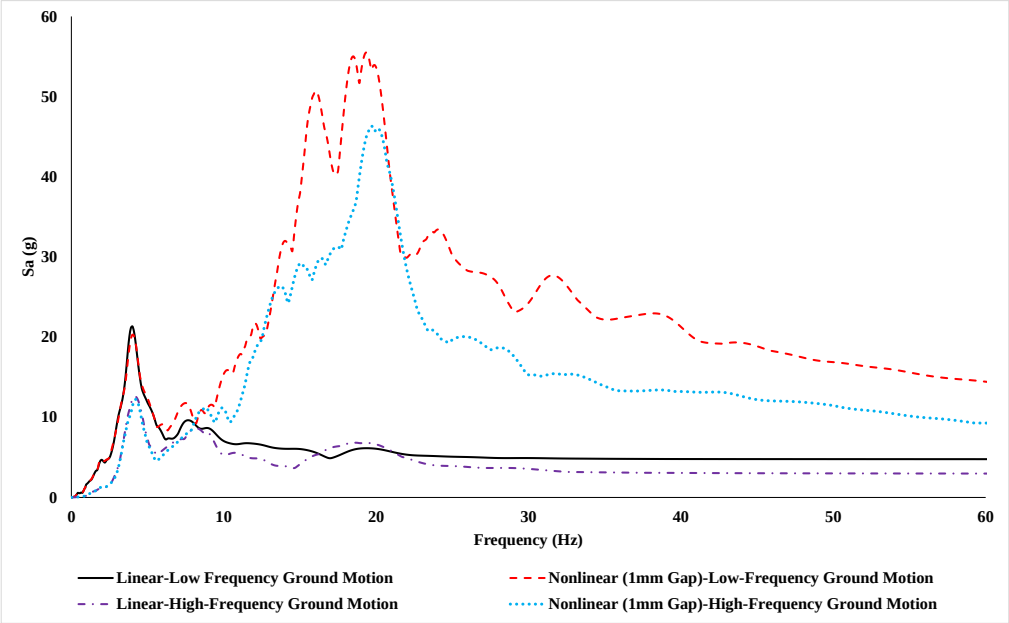


**Figure. 8.** Comparison of ICRS obtained at First DOF of Secondary System from Uncoupled Linear and Nonlinear Analysis of System–1 subjected to both Low–Frequency and High–Frequency Ground Motions

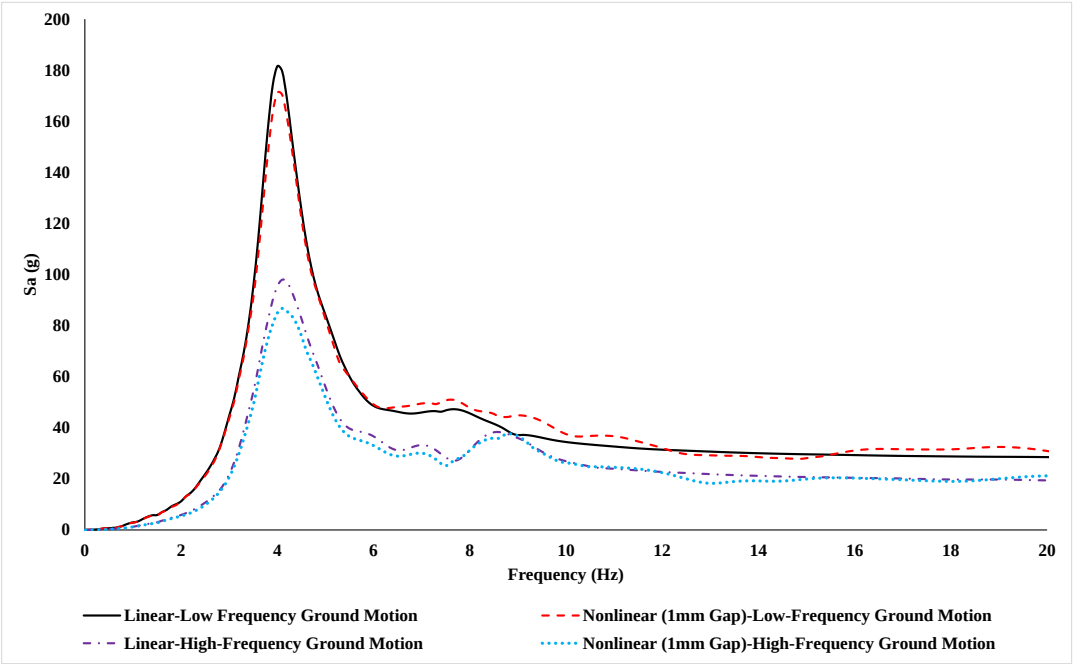


**Figure. 9.** Comparison of ICRS obtained at First DOF (Left) and Sixth DOF (Right) of Secondary System from Uncoupled Linear and Nonlinear Analysis of System-1 subjected to both Low–Frequency and High–Frequency Ground Motions

For system–2, the behavior seen in figure 10 is similar to that seen in figure 8 for system-1. In fact, the spectral accelerations in the high frequency region exhibit even greater amplifications because the second and the third mode of the primary and secondary systems are tuned with each other and much of the response at the first floor comes from these high frequency modes. Since the response of primary system in this case also comes primarily from high frequency modes, the total displacements at the top floor of primary system are relatively less. Consequently, a nonlinearity at the secondary system base filters greater amount of earthquake motion even for a small gap of 1 mm. This filtering results in much smaller values of spectral accelerations at the top floor of secondary system as seen from the curves for nonlinear analysis in figure 11.

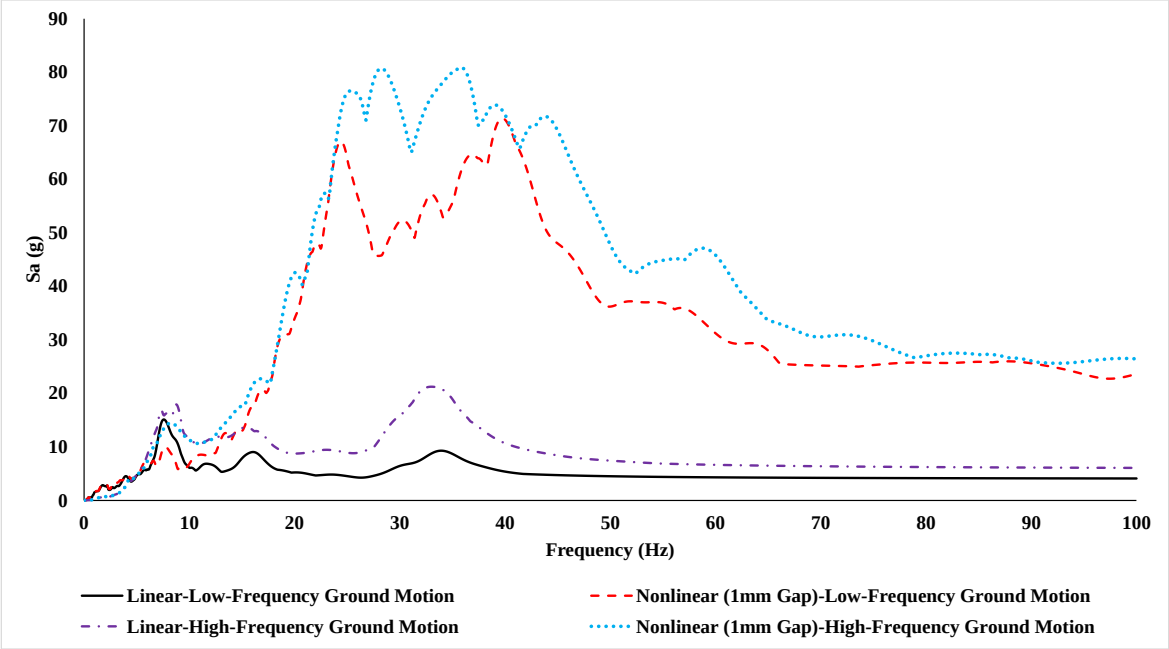


**Figure. 10.** Comparison of ICRS obtained at First DOF of Secondary System from Uncoupled Linear and Nonlinear Analysis of System–2 subjected to both Low–Frequency and High–Frequency Ground Motions

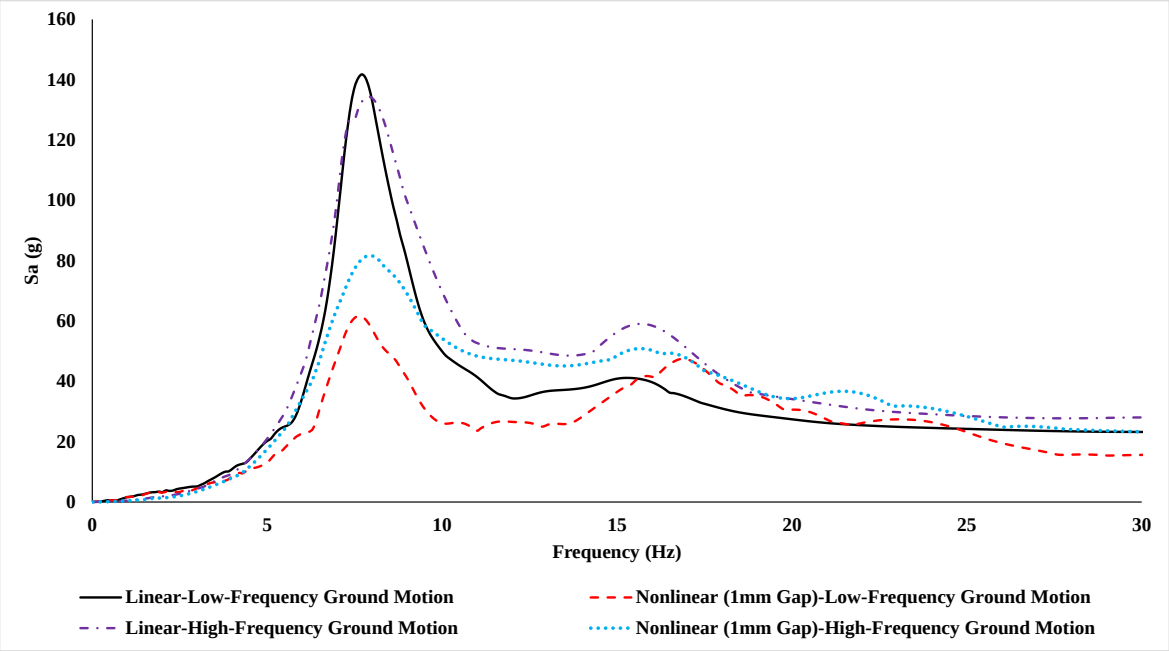


**Figure. 11.** Comparison of ICRS obtained at Sixth DOF of Secondary System from Uncoupled Linear and Nonlinear Analysis of System–2 subjected to both Low–Frequency and High–Frequency Ground Motions

### 5.3. Comparison of Coupled and Uncoupled Nonlinear Analysis

This section compares the results for nonlinear cases from coupled and uncoupled analysis in order to evaluate the significance of equipment–structure interaction. Figures 12–15 compare the results from the two systems. The ICRS obtained from a coupled analysis for both the systems at the two elevations (first and sixth floors) are lower than the corresponding ICRS evaluated from an uncoupled analysis. However, it is also observed that the differences between the coupled and uncoupled analysis reduces when systems are subjected to high–frequency ground motion as compared to the differences observed for the low–frequency ground motion. In coupled analysis, the mass interaction between primary and secondary system reduces the spectral amplitudes of the ICRS. The primary reason for this observation is related to a reduced degree of equipment-structure interaction (or mass interaction) between the primary and secondary systems due to

nonlinearity. In a coupled nonlinear analysis, interaction between the modes of primary and secondary system occurs only when the gap closes, and the two systems are physically connected. During the time that the two systems are disengaged due to the presence of a gap, the interaction between the two systems ceases. Since the high–frequency ground motion induces low displacements, the gap closes less often and hence the effect of mass interaction is lower as compared to the low–frequency ground motion case.

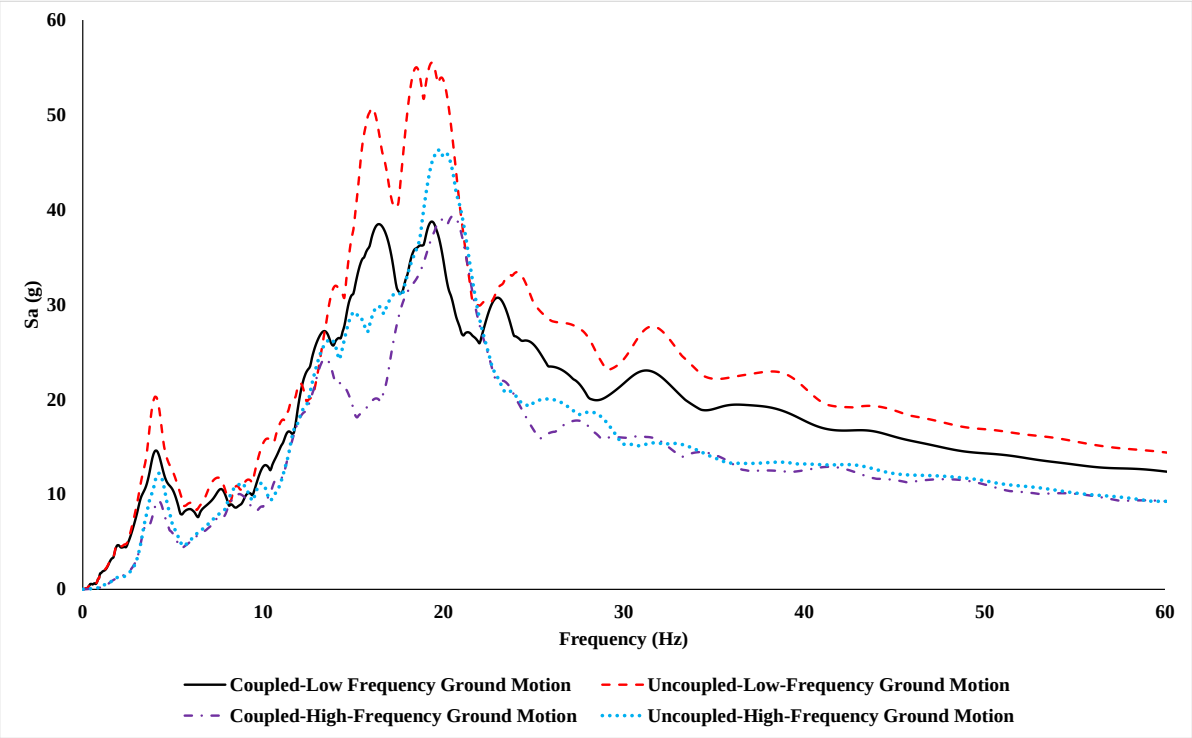


**Figure. 12.** Comparison of ICRS obtained at First DOF of Secondary System from Coupled and Uncoupled Nonlinear Analysis of System–1 subjected to both Low–Frequency and High–Frequency Ground Motions

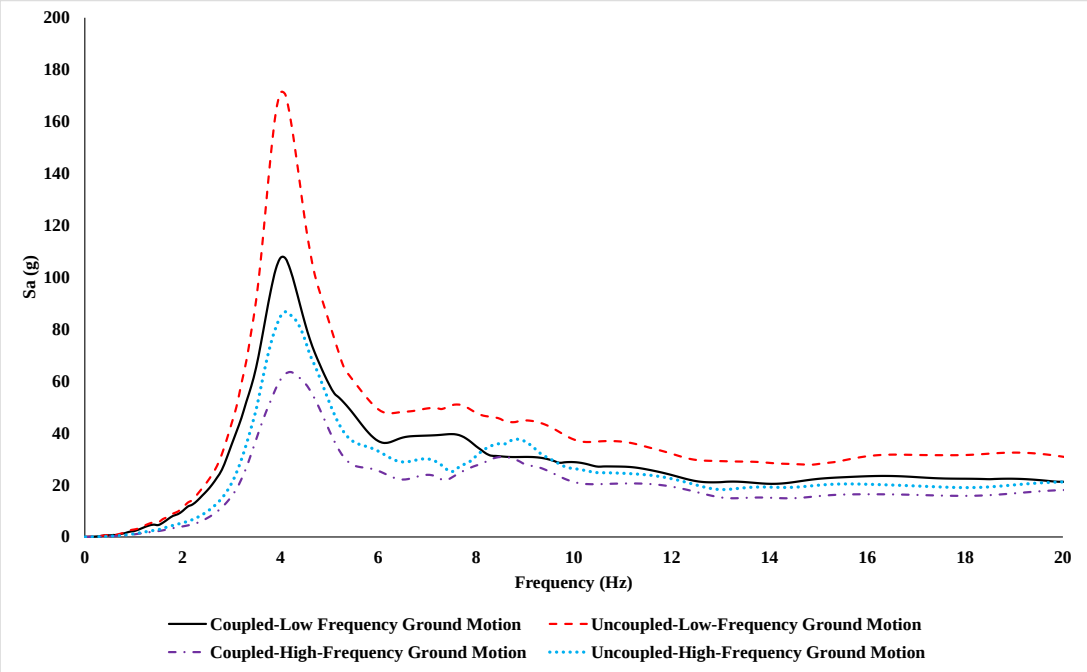


**Figure. 13.** Comparison of ICRS obtained at Sixth DOF of Secondary System from Coupled and Uncoupled Nonlinear Analysis of System–1 subjected to both Low–Frequency and High–Frequency Ground Motions

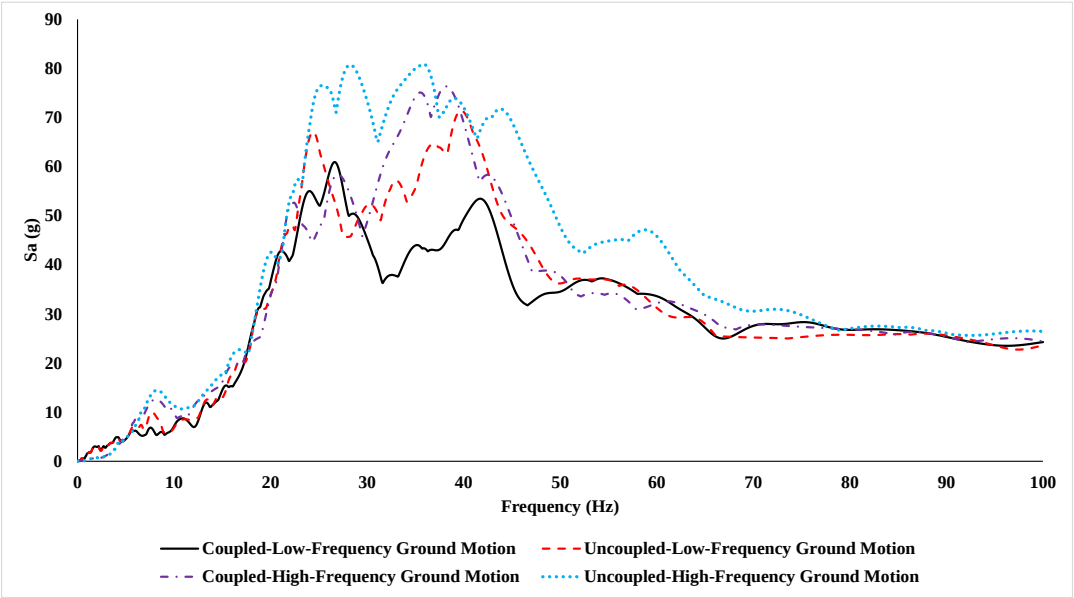


**Figure. 14.** Comparison of ICRS obtained at First DOF of Secondary System from Coupled and Uncoupled Nonlinear Analysis of System–2 subjected to both Low–Frequency and High–Frequency Ground Motions

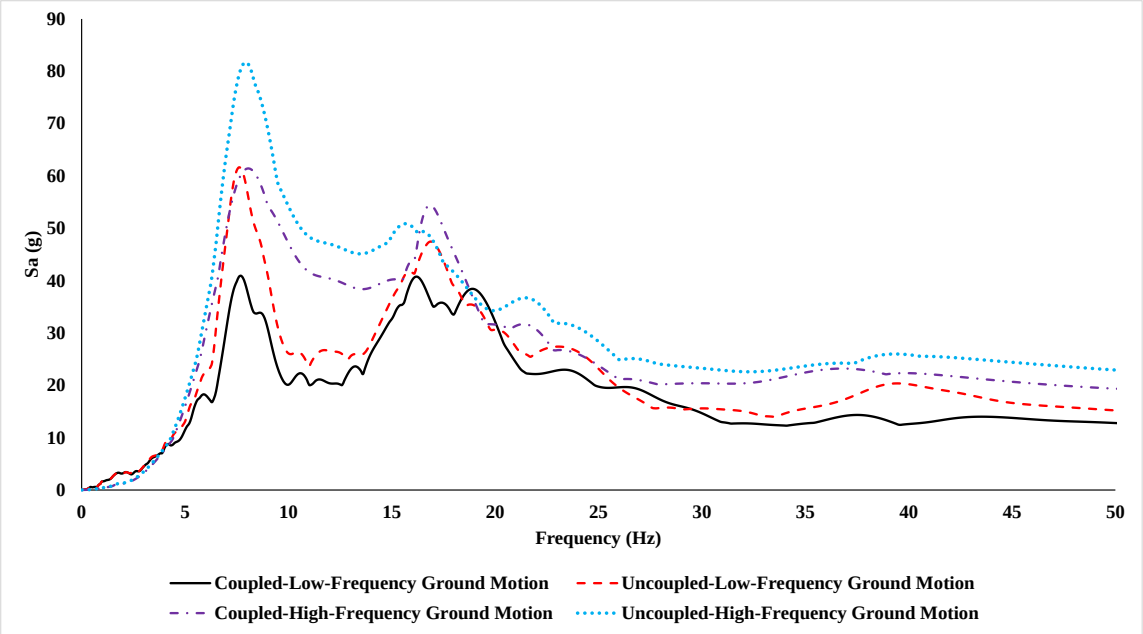


**Figure. 15.** Comparison of ICRS obtained at Sixth DOF of Secondary System from Coupled and Uncoupled Nonlinear Analysis of System–2 subjected to both Low–Frequency and High–Frequency Ground Motions

### 5.4. Amplitude of Ground Motion

The results presented in the sections above considered ground motions to be normalized to 1g peak ground acceleration (PGA). The PGAs of design ground motion at a nuclear plant are much lower. This can be a significant aspect because the nonlinear behavior is highly dependent upon the amplitude of the ground motion and the associated displacements in the primary and secondary systems. The displacement amplitudes would also govern the duration of free sliding in secondary system, the number of impacts, and the velocity of impacts at the secondary system base. Figures 16–19 show the comparison of coupled nonlinear analysis results for both the systems subjected to ground motions normalized to 1g and 0.2g PGA. It is interesting to note that a reduction by a factor of 5 in the ground motion results in a reduction by factor of only 2 in the figure 16 for the low frequency ground motion case. This is so because the peak spectral accelerations at first floor

result from the transient motion due to impact. The number of impacts and the velocity of impact are less for the case of 0.2g PGA but the reduction does not result in a proportional reduction in ICRS. On the contrary, the reductions observed in figure 17 for the top (sixth) floor are greater than a factor of 5 because the response comes primarily from fundamental mode which is tuned with the fundamental mode of primary system and these tuned modes of the two systems undergo significant modal mass interaction. Figures 18 and 19 show that peak spectral accelerations for a 0.2g PGA earthquake are lower than the corresponding values for a 1g PGA earthquake by a factor that is almost as large as 20. This behavior is observed because higher modes contribute significantly to the response of primary system in system-2. Consequently, the displacements at the top ($10^{th}$) floor of the primary system are relatively much less than in the case of system-1. Such smaller displacements are then filtered out for a large part in the case of 0.2g PGA earthquake records and, therefore, a significant reduction is observed.

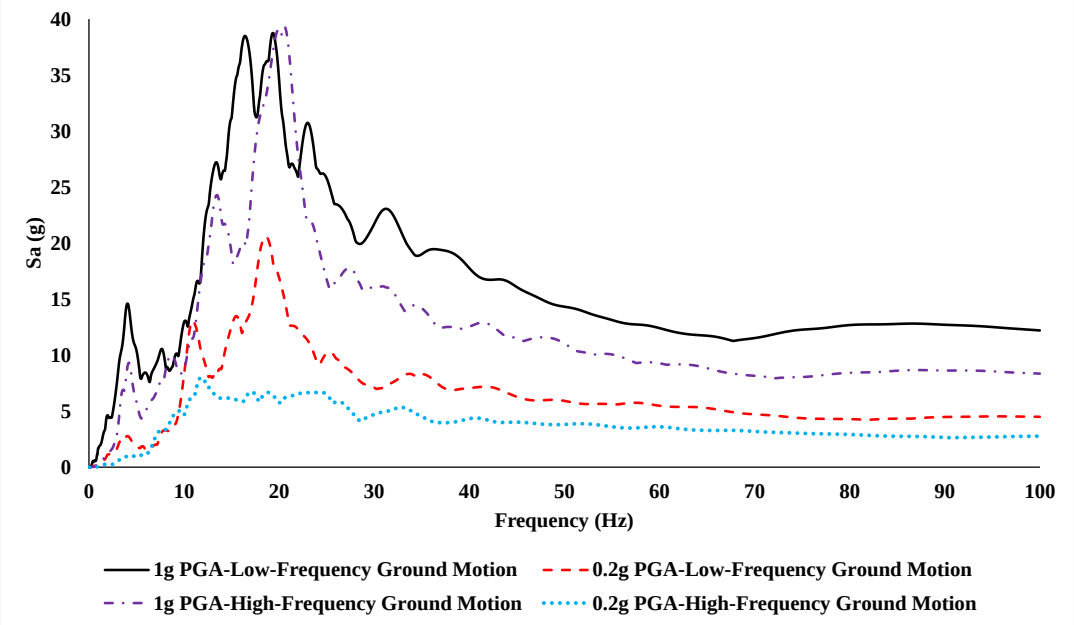


**Figure. 16.** Comparison of ICRS obtained at First DOF of Secondary System from Coupled Nonlinear Analysis of System–1 subjected to both Low–Frequency and High–Frequency Ground Motions Normalized to 1g and 0.2g PGA

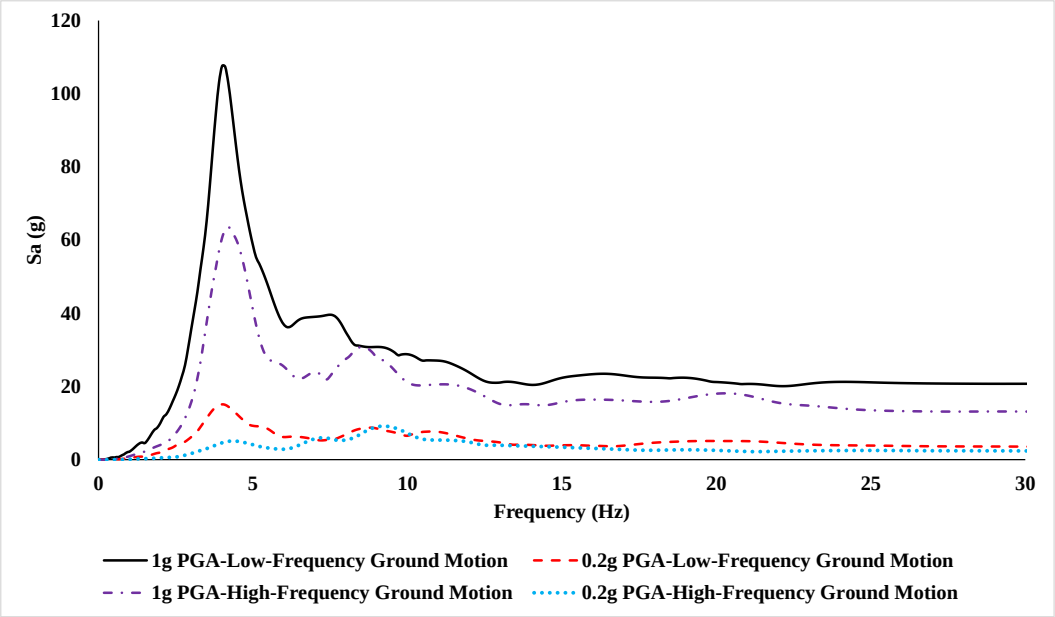


**Figure. 17.** Comparison of ICRS obtained at Sixth DOF of Secondary System from Coupled Nonlinear Analysis of System–1 subjected to both Low–Frequency and High–Frequency Ground Motions Normalized to 1g and 0.2g PGA

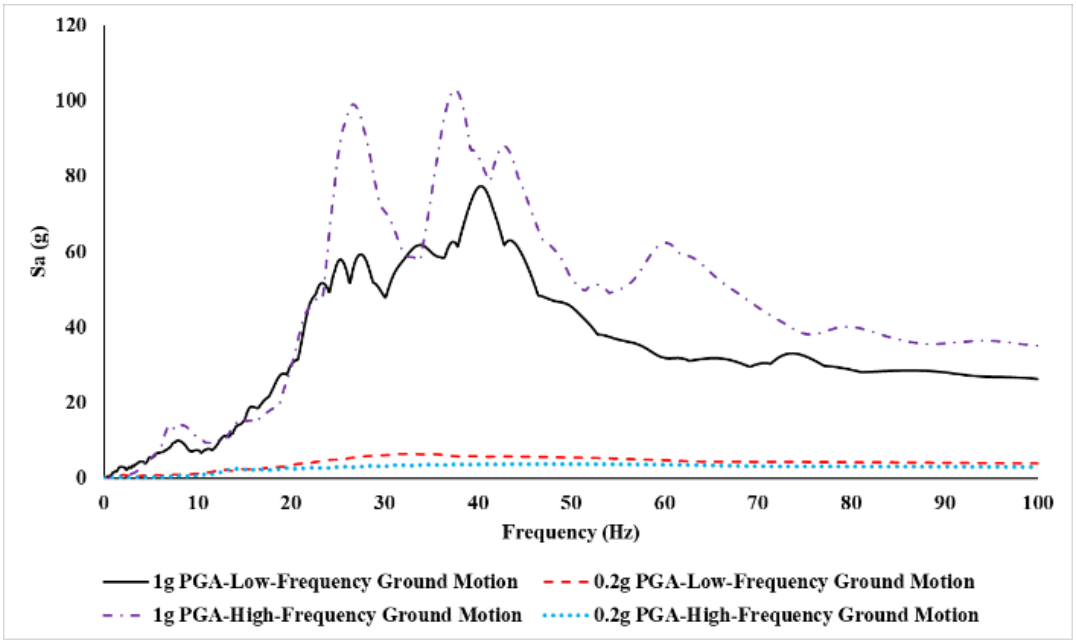


**Figure. 18.** Comparison of ICRS obtained at First DOF of Secondary System from Coupled Nonlinear Analysis of System–2 subjected to both Low–Frequency and High–Frequency Ground Motions Normalized to 1g and 0.2g PGA

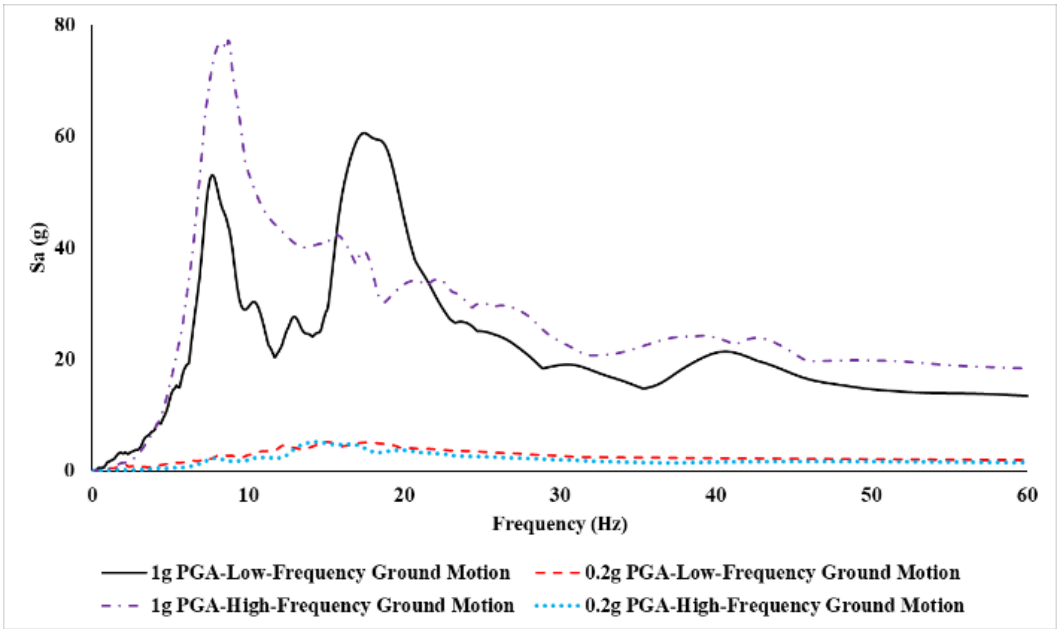


**Figure. 19.** Comparison of ICRS obtained at Sixth DOF of Secondary System from Coupled Nonlinear Analysis of System–2 subjected to both Low–Frequency and High–Frequency Ground Motions Normalized to 1g and 0.2g PGA

### 5.5. Gap Length

As observed in the previous section, a gap at the base of secondary system can filter out the ground motions particularly the high frequency ground motions. Therefore, the effect of gap length is evaluated, and the results presented in this section. Figures 20–27 compare the ICRS obtained for 1mm and 3mm gap model at first and sixth DOF of systems 1 and 2. In almost all cases, the results show the spectral amplitudes of ICRS obtained from 3mm gap model are lower than that of 1mm gap model which reinforces the concept of earthquake motions being filtered out by a gap in the mounting region. However, it is important to note that the spectral accelerations around 10 Hz in figure 22 are greater for the 3 mm case compared to those from 1 mm case. This observation appears to be strange at first. It is determined that even though a 3 mm gap results in a relatively smaller duration of contact between the primary and secondary systems, the maximum

displacements at the top floor of primary system due to a low frequency ground motion (figure 22) are much greater than 3 mm. A larger gap of 3 mm results in higher impact velocities compared to the 1 mm case which in turn leads to larger response. Another important observation can be made in figure 25 that shows periodic peaks and valleys in the spectral values in the high frequency region. This reasons for such a behavior are explained in Singh and Gupta (2020) which explains that a constructive interference of transient response with the steady–state response results in a peak and a destructive interference in a valley. Interestingly, such a pattern is difficult to observe in other figures because of the contribution from multiple modes in a MDOF system which can result in more complex interference of modal responses.

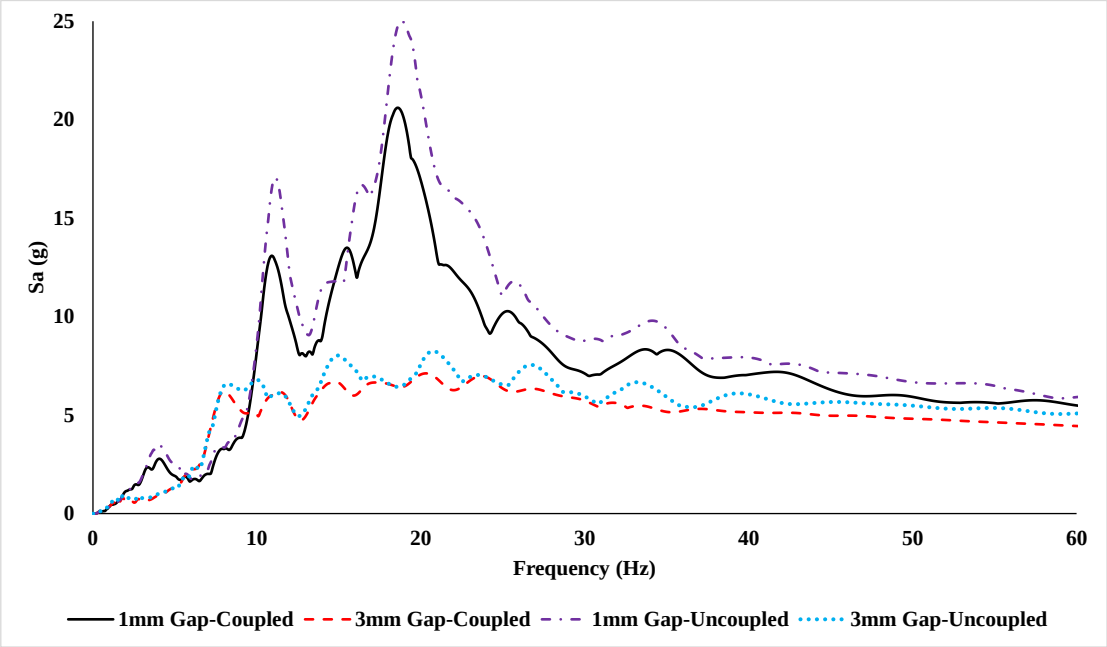


**Figure. 20.** Comparison of ICRS obtained at First DOF of Secondary System from Coupled and Uncoupled Nonlinear Analysis of System–1 subjected to Low–Frequency Ground Motion

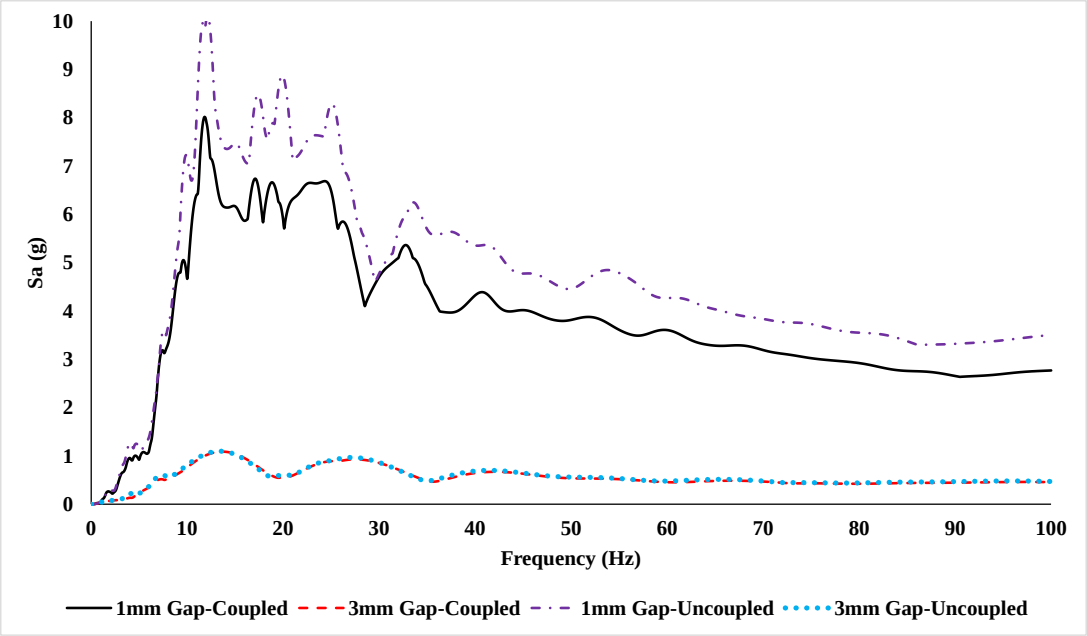


**Figure. 21.** Comparison of ICRS obtained at First DOF of Secondary System from Coupled and Uncoupled Nonlinear Analysis of System-1 subjected to High–Frequency Ground Motions

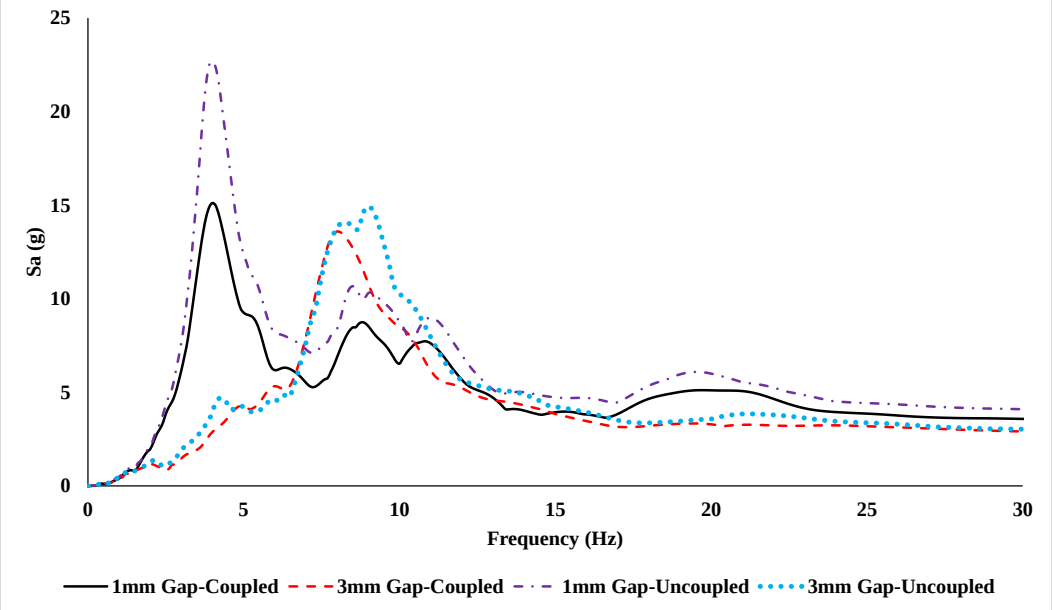


**Figure. 22.** Comparison of ICRS obtained at Sixth DOF of Secondary System from Coupled and Uncoupled Nonlinear Analysis of System–1 subjected to Low–Frequency Ground Motions

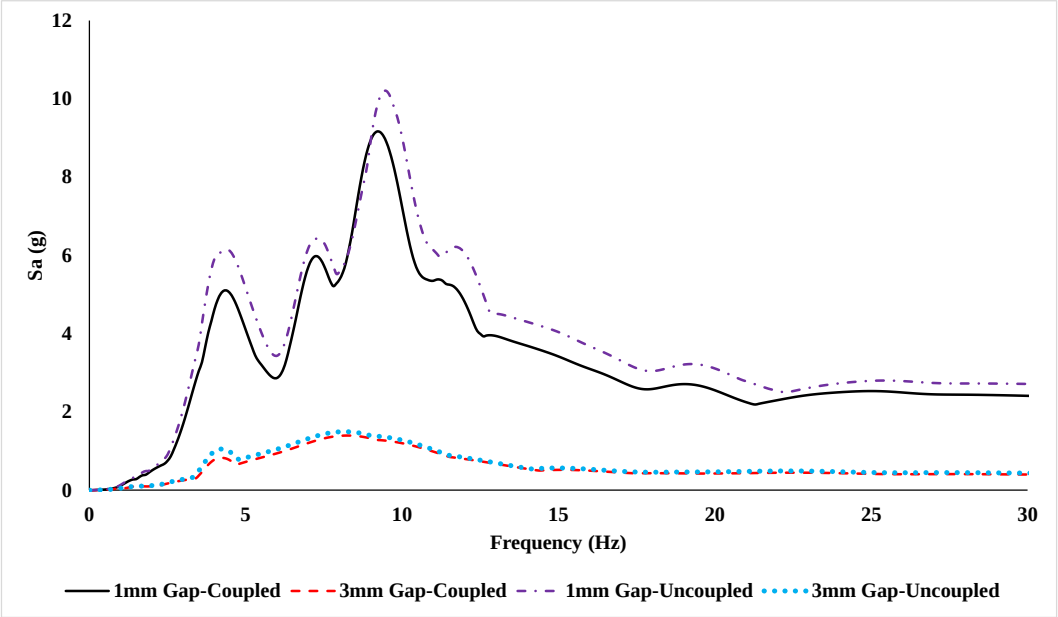


**Figure. 23.** Comparison of ICRS obtained at Sixth DOF of Secondary System from Coupled and Uncoupled Nonlinear Analysis of System–1 subjected to High–Frequency Ground Motions

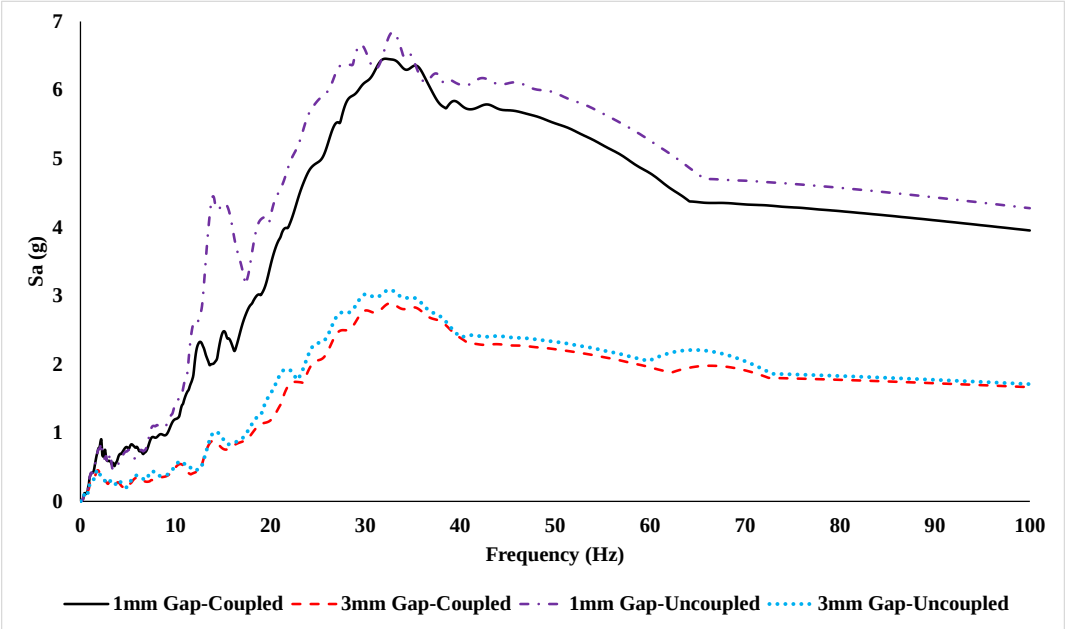


**Figure. 24.** Comparison of ICRS obtained at First DOF of Secondary System from Coupled and Uncoupled Nonlinear Analysis of System–2 subjected to Low–Frequency Ground Motions

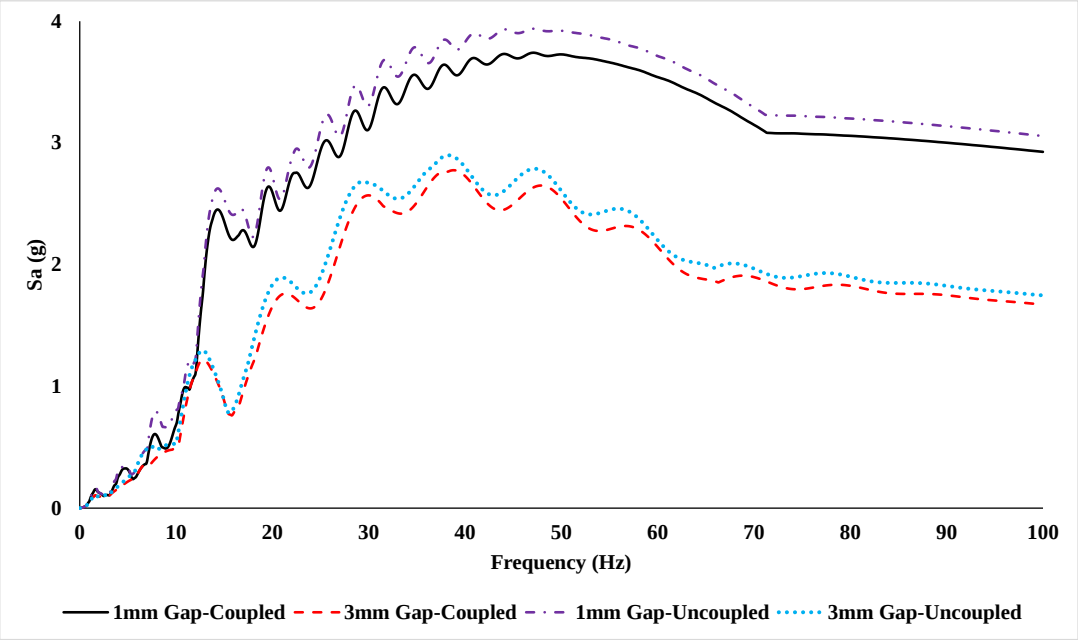


**Figure. 25.** Comparison of ICRS obtained at First DOF of Secondary System from Coupled and Uncoupled Nonlinear Analysis of System–2 subjected to High–Frequency Ground Motions

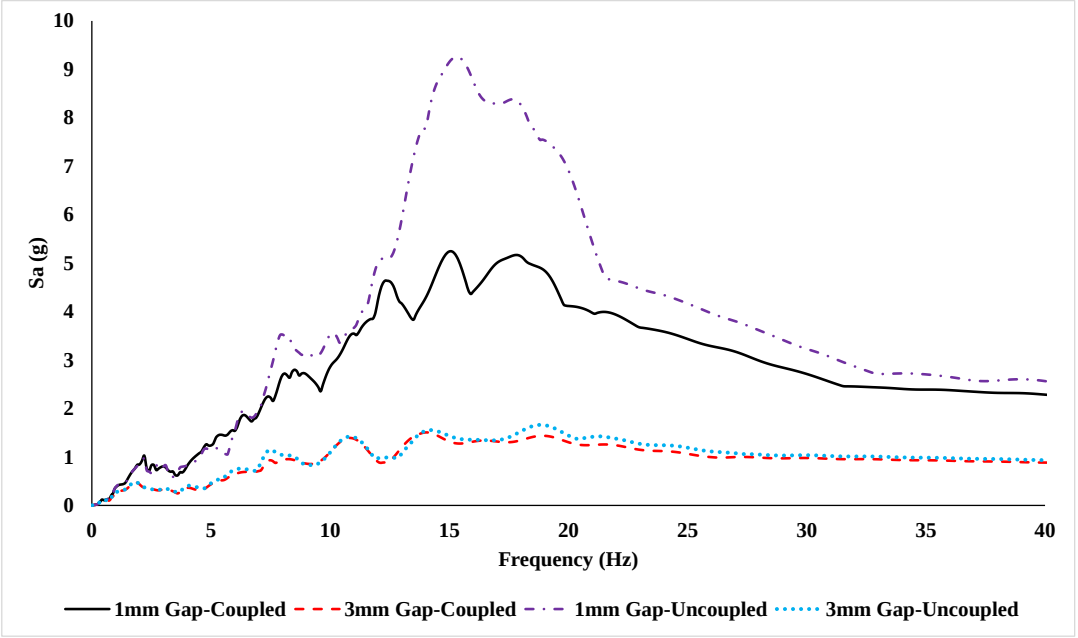


**Figure. 26.** Comparison of ICRS obtained at Sixth DOF of Secondary System from Coupled and Uncoupled Nonlinear Analysis of System–2 subjected to Low–Frequency Ground Motions

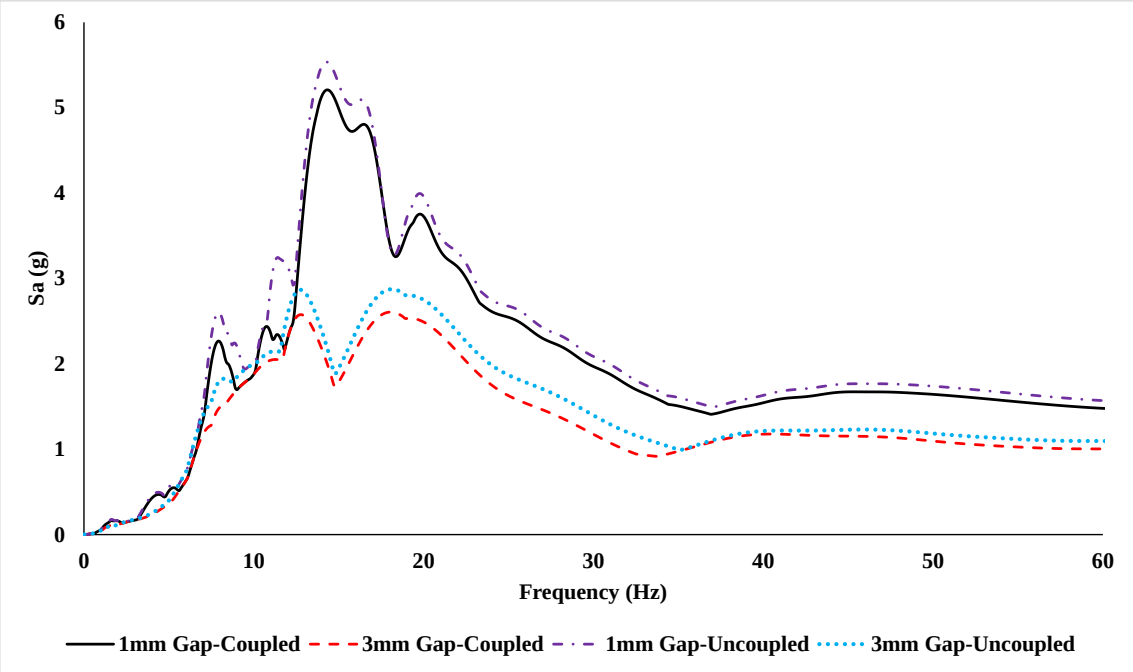


**Figure. 27.** Comparison of ICRS obtained at Sixth DOF of Secondary System from Coupled and Uncoupled Nonlinear Analysis of System–2 subjected to High–Frequency Ground Motions

## 6. Conclusions

This study presents some important conclusions about the seismic behavior of electrical cabinets which have not been addressed in existing studies. In particular, the effects of localized nonlinearity in the cabinet mounting arrangement and the effect of equipment-structure interaction on ICRS are explored for both the cases of linear and nonlinear mounting arrangement. Existing studies on the seismic behavior of electrical cabinets do not consider the effect of interaction between the building and the cabinet. It is observed that for a linear case in which electrical cabinets can have modal mass interaction of about 1 to 2 percent between the tuned modes of the building and the cabinet, a significant reduction occurs in the ICRS due to equipment-structure interaction. The magnitude of reduction observed is even greater when the spectral amplitudes in ICRS get greater contribution from higher frequency modes of the building and cabinet and are

subjected to high frequency earthquake ground motions. The effect of equipment-structure interaction in the case of nonlinear mounting arrangement is highly dependent upon the degree of nonlinearity. In general, a localized nonlinearity in the cabinet base filters out the floor displacements. For systems in which the cabinet oscillates in free vibration for relatively large duration of time due to a gap in the mounting arrangement, its interaction with building reduces. Interaction occurs when the cabinet base is in contact with the building floor which then leads to a reduction in ICRS. Therefore, the effect of equipment-structure interaction is relatively less for the case of high frequency ground motions with relatively smaller floor displacements. In such cases, even greater reductions are observed because the smaller displacements gets filtered out by a nonlinearity in the cabinet mounting arrangement.

It is also observed that a low frequency ground motion leads to significantly large spectral accelerations in the ICRS when a nonlinearity is present in the cabinet mounting arrangement. This amplification occurs due to an impact between the anchor bolt and the cabinet base whenever the gap closes. Localized impact introduces a transient motion that tend to excite high frequency modes of the cabinet and repeated impacts lead to significantly higher amplifications. The high–frequency peaks in the ICRS due to such localized impacts are observed only at lower elevations of the cabinet model but not at the top of cabinet because the effect of high–frequency modes is more prominent at lower elevations.

The effect of localized impact due to nonlinearities is dependent on the amplitude of ground motion although a reduction in ground motion amplitude cannot be related directly to the corresponding reduction in spectral peaks of ICRS. It is observed that a reduction in ground motion amplitude leads to much greater reduction for the high frequency case compared to the corresponding reduction in the low frequency case. More specifically, it is observed that a

reduction in ground motion amplitude by a factor of 5 results in a reduction of spectral peaks in ICRS by a factor of only 2 for the case of low frequency systems. This reduction occurs primarily due to equipment-structure interaction. For the case of high frequency systems, the corresponding reduction in the peaks of ICRS is close to a factor of 20. Such a large reduction occurs because a low amplitude ground motion results in smaller floor displacements which are filtered out by the geometric nonlinearity at the cabinet base. Overall, ICRS is influenced in a complex manner due to the effects of ground motion amplitude and the length of the gap. In general, the higher the gap length, the lower the spectral amplitudes of ICRS as larger gaps filter out floor displacements. However, in some cases, a larger gap can also lead to an increase in spectral acceleration because it allows development of greater impact velocity which in turn leads to greater transient response.

## 7. Acknowledgement

This research was supported by Center for Nuclear Energy Facilities and Structures at North Carolina State University. Resources for the Center come from the dues paid by member organizations and from the Civil, Construction, and Environmental Engineering Department and College of Engineering in the University.

## 8. References


[1] Burdisso, R.A., Singh, M.P., (1987) “Seismic Analysis of Multiply Supported Secondary Systems with Dynamic Interaction Effects.” *Earthquake Engineering Structural Dynamics*, Volume 15, Pages 1005-1022.

[2] Computers and Structures Inc., (2011) “CSI Analysis Reference Manual for SAP2000, ETABS, SAFE and CSI Bridge,” *Computers and Structures, Inc.*, Berkeley, CA.

[3] Dubey, A.R., Bodda, S., Gupta, A., Vasquez, J., Bhargava, D., (2019) “Reduction in Seismic Demand by Using Equipment-Structure Interaction,” *In: Transactions of 25$^{th}$ Conference on Structural Mechanics in Reactor Technology (SMiRT-25), Charlotte, NC, USA,* August 4-9, 2019.

[4] EPRI, (2007) "Program on technology innovation: The effects of high-frequency ground motion on structures, components, and equipment in nuclear power plants," Palo Alto, CA: 2007.1015108.

[5] EPRI, (2013) “Seismic Evaluation Guidance: Screening, Prioritization and Implementation Details (SPID) for the Resolution of Fukushima Near-Term Task Force Recommendation 2.1: Seismic,” Palo Alto, CA: 2013.1025287.

[6] EPRI, (2014) "High frequency program: High frequency testing summary," Palo Alto, CA, 2014.3002002997.

[7] EPRI, (2015) "High frequency program: Application guidance for functional confirmation and fragility evaluation," Palo Alto, CA, 2015.3002004396.

[8] Gupta, A., Bose, M., (2017) “Significance of Non-Classical Damping in Seismic Qualification of Equipment and Piping,” *Nuclear Engineering and Design,* 317 (2017) 90–99.

[9] Gupta, A., Cho, S.-G., Hong, K.-J., Han, M., (2019) “Current State of In-Cabinet Response Spectra for Seismic Qualification of Equipment in Nuclear Power Plants,” *Nuclear Engineering and Design,* 343 (2019) 269–275.

[10] Gupta, A., Gupta, A.K., (1998) “Missing Mass Effect in Coupled Analysis I: Complex Modal Properties,” *Journal of Structural Engineering,* 124(5): 490–495.

[11] Gupta, A.K., Jaw, J.-W., (1986) “Coupled Response Spectrum Analysis of Secondary System Using Uncoupled Modal Properties,” *Nuclear Engineering and Design,* 92 (1986) 61–68.

[12] Gupta, A., Rustogi, S.K., Gupta, A.K., (1999) “Ritz Vector Approach for Evaluating Incabinet Response Spectra,” *Nuclear Engineering and Design,* Vol. 199, pp. 255-272, March 1999. DOI: 10.1016/S0029-5493(99)00076-X.

[13] Han, M., Cho, S.-G., Hong, K.-J., Gupta, A., (2018) “Rocking Stiffness of Electrical Cabinet Considering the Local Deformation at the Base,” *In: Transactions of the Korean Nuclear Society Spring Meeting*, Jeju, Korea, May 17–18, 2018.

[14] Herve, G., (2014) "Improvement of the evaluation of high frequency content in the calculation of impact floor response spectra," *In: 2nd Conference on Technical Innovation in Nuclear Civil Engineering TINCE 2014*, Paris.

[15] Lee, S.-M., Jung, W.-Y., (2020) “Evaluation of Anchorage Performance of the Switchboard Cabinet under Seismic Loading Condition,” *Advances in Mechanical Engineering,* 2020, Vol. 12(5) 1–12, DOI: 10.1177/1687814020926309.

[16] PEER, (2015) “NGA-East: Median Ground-Motion Models for the Central and Eastern North America Region,” *Pacific Earthquake Engineering Research Centre*, PEER Report No. 2015/04, April 2015.

[17] Rustogi, S., Gupta, A., (2004) “Modeling the Dynamic Behavior of Electrical Cabinets and Control Panels: Experimental and Analytical Results,” *Journal of Structural Engineering,* 2004, 130(3): 511–519, DOI: 10.1061/(ASCE)0733-9445(2004)130:3(511).

[18] SSHAC, (1997) “Recommendations for Probabilistic Seismic Hazard Analysis: Guidance on Uncertainty and Use of Experts,” NUREG/CR-6372, UCRL-ID- 122160, Vol. 1.

[19] Salman, K., Tran, T.-T., Kim, D., (2020) “Grouping Effect on the Seismic Response of Cabinet Facility considering Primary–Secondary Structure Interaction,” *Nuclear Engineering and Technology*, 52 (2020) 1318–1326.

[20] Singh, S., (2017) “Seismic Response of Electrical Equipment in Nuclear Power Plants,” M.S. Thesis, North Carolina State University.

[21] USNRC, (2011) “Recommendation for Enhancing Reactor Safety in 21st Century,” July 2011.

[22] USNRC, (2014) "Design Response Spectra for Seismic Design of Nuclear Power Plants," Reg. Guide 1.60, July 2014.

[23] Vlaski, V., (2013) "Reduction of External Hazard (Fast Impact) Induced Vibrations," F/AB-58, *In: 1st Conference on Technical Innovation in Nuclear Civil Engineering TINCE 2013, Paris,* October 28-31, 2013.

[24] Vlaski, V., Moersch, J., Sallmann, M., (2019) "Comparative Study for Reduction of APC Induced Vibrations," *In: Transactions of 25th Conference on Structural Mechanics in Reactor Technology (SMiRT-25), Charlotte, NC, USA,* August 4-9, 2019.

[25] Yang, J., Rustogi, S.K., Gupta, A., (2002) "Rocking Stiffness of Mounting Arrangements in Electrical Cabinets and Control Panels," *Nuclear Engineering and Design,* 219 (2002), 127–141.

[26] Xu, J., DeGrassi, G., Chokshi, N., (1999) "NRC-BNL Benchmark Program on Evaluation of Methods for Seismic Analysis of Coupled Systems," *USNRC,* BNL-NUREG-66409, Paper ID: K4-A6-US, 1999.

[27] Xu, J., DeGrassi, G., Chokshi, N., (2004) "A NRC-BNL Benchmark Evaluation of Seismic Analysis Methods for Non-classically damped coupled systems," *Nuclear Engineering and Design,* 228 (2004) 345–366.

[28] Yim, S. C.-S., Chopra, A. K., (1985) "Simplified earthquake analysis of multistory structures with foundation uplift," *Journal of Structural Engineering,* 111(12), 2708–2731.

# Chapter 4

## Quantification of the Contribution of Sedimentary Deposits to High–Frequency Attenuation in Low–to–Moderate Seismicity Regions via the Site Transfer Function

**Abstract**

The probabilistic seismic hazard analysis requires availability of abundant strong ground motion data which is not usually available at low–to–moderate seismicity regions. Stochastic simulation or host–to–target adjustment methods are used to evaluate seismic hazard at sites in low–to–moderate seismicity regions. For such methods, prior knowledge of site–specific attenuation factor, kappa ($\kappa_0$) is required. However, most commonly used method to evaluate site–specific kappa, acceleration spectrum method ($\kappa_{0\_AS}$) also requires abundant strong ground motions. In this study, we explore transfer function method to obtain site–specific kappa ($\kappa_{0\_TF}$). $\kappa_{0\_TF}$ represents the attenuation of seismic waves between the bedrock and ground surface which is equivalent to $\Delta\kappa_{0\_AS}$ (difference between $\kappa_{0\_AS}$ measured at bedrock and surface). For linear–elastic sites, $\kappa_{0\_TF}$ is calculated from recorded data as well as by conducting linear–elastic site response analysis from the site parameters. Probability density functions of empirical and theoretical estimates of $\kappa_{0\_TF}$ at various sites are compared and uncertainty in damping ratio is quantified. The study further examines the approximation of soil profile by single layer proxies such as $V_{s30}$ and $V_{s\_mean}$ and uses closed–form equation to estimate $\kappa_{0\_TF}$. The probability density function of $\kappa_{0\_TF}$ estimates from closed–form equation is also compared with empirical and theoretical site response analysis. For single layer approximation, uncertainty in both shear–wave velocity proxy as well as damping is quantified. The probabilistic estimates of $\kappa_{0\_TF}$ can further be used to estimate $\kappa_{0\_AS}$ at the surface which is further used in probabilistic seismic hazard analysis at low–to–moderate seismicity regions.

## 1. Introduction

Kappa ($\kappa_{r\_AS}$; Anderson and Hough 1984) is a seismological parameter which characterizes the attenuation of seismic waves at high frequencies as they travel from the source to the ground surface. Kappa is most commonly calculated from the linear decay of the Fourier Amplitude Spectrum (FAS) of a recorded acceleration time history when plotted on natural log (amplitude) – linear (frequency) space. Kappa values evaluated from various recorded motions at a particular site are linearly correlated to the epicentral distance, $R_{epi}$ (Anderson and Hough, 1984; Ktenidou et al., 2012). The value of kappa evaluated at zero epicentral distance ($R_{epi}$=0) is called site–specific kappa, $\kappa_{0\_AS}$. The latter represents the attenuation of vertically propagating shear waves through the shallow geology of the soil profile (Anderson, 1991, Ktenidou et al., 2012) and describes the combined effect of material damping, scattering, etc., at the site (Parolai and Bindi, 2004; Cabas et al., 2017; Pilz and Fäh, 2017). Hence, previous studies have found estimates of kappa useful in the stochastic simulation of ground motions (e.g., Boore, 2003) and in empirical ground motion prediction equations (e.g., Laurendau et al., 2013)

Many studies have observed that the value of site–specific kappa affects the response spectral shape and specifically the frequency at which peak spectral acceleration occurs (Silva and Darragh, 1995; Boore and Joyner, 1997; Malagnini et al., 2000; Biro and Renault, 2012; Laurendau et al., 2013). For instance, for a low value of $\kappa_{0\_AS}$, which is mostly observed at rock sites, the peak spectral accelerations occur at higher frequencies. The safety–related equipment used in critical facilities such as nuclear power plants, electrical substations, data centers, etc., are sensitive to high–frequency accelerations thus, affecting safety and functionality of the facility. Moreover, the seismic response of small concrete dams, which may have high modal frequencies, is also affected by high–frequency ground motions (Ktenidou et al., 2016; Muto and Duron, 2015). Hence, $\kappa_{0\_AS}$

is an important factor to evaluate the ground motion response spectrum (GMRS) for engineering design purposes.

The design GMRS at a site is usually evaluated from ground motion prediction equations (GMPE) which relates a ground motion parameter such as spectral acceleration or peak ground acceleration to various seismological parameters based on global or regional empirical strong ground motion data. In low–to–moderate seismicity regions such as Central and Eastern United States (CEUS), France, Switzerland, etc., the recorded strong ground motion data are scarce. Hence, compared to analyses conducted for sites located in active tectonic regions, such as Western United States or Japan, an appropriate estimation of design GMRS in low–to–moderate seismic regions requires stochastic simulations and contains larger uncertainties. Host–to–target adjustment methods have been proposed (e.g., Campbell, 2003) to adjust a GMPE developed for a region with abundant data (referred to as the host region), to evaluate ground motion parameters for a region with scarce data (referred to as the target region). The adjustment of GMPEs is achieved by accounting for differences in source, path, and local site factors between host and target regions. Accounting for differences in local site conditions often focuses on capturing first order effects, such as seismic impedance and attenuation.

Characterizing near–surface attenuation in low–to–moderate seismicity regions in terms of site–specific kappa continues to be challenging because most commonly used methods require multiple ground motion recordings at the site of interest. A recent study focused on rock sites in the NGA–East database (Ktenidou et al., 2016) to estimate site–specific kappa ($\kappa_0$) values by using band–limited as well as broadband approaches. They found that broadband methods and mean $\kappa_{0\_AS}$ values provide similar estimates to the average $\kappa_0$ proposed for CEUS (i.e., 6±2 ms; Hashash et al., 2014). However, all the approaches considered still require the availability of ground motion

records. Our study aims to investigate the quantification of high–frequency attenuation via the site's theoretical linear–elastic transfer function ($\kappa_{0\_TF}$), which only requires knowledge of the subsurface conditions. Notably, we quantify the uncertainty throughout our characterization of near–surface attenuation to provide probability distributions of our $\kappa_{0\_TF}$ estimates instead of deterministic values. Comparisons with available empirical transfer functions at selected sites are used to evaluate the appropriateness of the proposed approach, not only in terms of mean values but also in terms of how well the variability in situ is captured. Ultimately, this work provides recommendations to quantify high–frequency attenuation informed by the large uncertainties associated with low–to–moderate seismicity regions.

The following sections provide a summary of previously proposed approaches to compute kappa in low–to–moderate seismicity regions. Then we describe our selected study sites and explain the fundamentals of our approach. Comparisons between our proposed method and the commonly used acceleration approach to compute kappa (by Anderson and Hough, 1984) are presented, followed by a simplified analytical solution for site–specific kappa estimations. Finally, recommendations based on our uncertainty quantification analyses are provided to help guide future research on specific parameters and the associated uncertainties that need to be studied in greater detail.

## 2. Background

Campbell (2003) introduced a hybrid empirical method to adjust a GMPE develop for a host region (e.g., Western North America) to the target region (e.g., Eastern North America). This hybrid method requires a full seismological model for the stochastic parameters (e.g., stress drop, whole-

path attenuation, etc.) of both, the host and target regions. Al Atik et al. (2014) directly adjusts the high–frequency slope of the acceleration FAS (obtained from the response spectrum via random vibration theory; Cartwright and Longuet-Higgins, 1956) generated from a host GMPE for Western United States (and multiple magnitude and distance scenarios), to the acceleration FAS (and then the response spectrum via inverse random vibration theory) consistent with site attenuation (i.e., short-distance kappa that approximates $\kappa_0$) at a target site in Switzerland. For both host–to–target adjustments (i.e., as proposed by Campbell, 2003 and Al Atik et al., 2014), prior knowledge of attenuation characteristics at the host and target region is required.

Ktenidou et al. (2014) explored various methods to evaluate site–specific kappa. Values of $\kappa_{r\_AS}$ evaluated from the acceleration spectrum method as proposed by Anderson and Hough (1984) are linearly correlated to epicentral distance, while $\kappa_{0\_AS}$ is calculated by extrapolating to zero epicentral distance. $\kappa_{0\_AS}$ can be computed at host regions because the recorded strong ground motion data are abundant, but that is not the case at target regions. Similarly, values of kappa can also be obtained from the displacement spectrum method (i.e., $\kappa_{r\_DS}$) where the decay on the displacement FAS at low frequencies is computed (Biasi and Smith, 2001). This method can be used for lower magnitude seismic events, which are more abundant in low–to–moderate seismicity regions. The corresponding site–specific kappa (i.e., $\kappa_{0\_DS}$) is calculated by extrapolating the linear relationship between $\kappa_{r\_DS}$ and $R_{epi}$ to $R_{epi}$=0. However, to use these approaches, an estimate of corner frequency is required which depends on the stress drop parameter. The latter is generally unknown without the availability of abundant strong ground motion data, especially in low–to–moderate seismicity region (Ktenidou et al., 2016). Ktenidou et al. (2014; 2016) also explored using broadband approaches such as broadband inversion ($\kappa_{0\_BB}$) and response spectral ($\kappa_{0\_RS}$) methods which are not affected by the selected frequency band of FAS to compute kappa values.

However, the broadband approaches also require availability of ground motions at the site to evaluate site–specific kappa, which is challenging for target regions.

Drouet et al. (2010) proposed an evaluation of $\kappa_0$ from the decaying slope of the site linear transfer function ($\kappa_{0\_TF}$) observed for low-magnitude earthquakes in France (i.e., with moment magnitudes from 3 to 5). This method quantifies the attenuation of seismic waves taking place between a reference rock horizon and the ground surface. The difference between $\kappa_{0\_AS}$ (or $\kappa_{r\_AS}$) calculated for bedrock conditions and its counterpart obtained at the ground surface, known as $\Delta\kappa_{0\_AS}$ (Cabas and Rodriguez-Marek, 2017) has also been proposed as a metric to capture the contribution of sedimentary deposits to overall path attenuation. Thus, $\kappa_{0\_TF}$ estimates should be theoretically equivalent to $\Delta\kappa_{0\_AS}$. In this study, we propose a methodology to evaluate $\kappa_{0\_TF}$ as a function of site parameters (i.e., without ground motions). Thus, we explore how to evaluate $\kappa_{0\_TF}$ from theoretical linear transfer functions and investigate the appropriateness of the resulting $\kappa_{0\_TF}$ based on its relationship with other $\kappa_0$ estimates and the associated uncertainties within our model.

## 3. Study Sites

The KiK–net database is the largest network of recording stations where both surface and downhole recordings are available for each event at each site (Aoi et al., 2004; Fujiwara et al., 2004). The database also provides the shear–wave velocity ($V_s$) profile of each site from downhole logging. The availability of a dense network with surface and borehole records makes it suitable to study discrepancies between theoretical and empirical transfer functions at multiple sites.

The four sites selected for the purposes of this study include sites with a uniform $V_s$ profile, and $V_s$ gradient with depth. The empirical site response of each selected site can be represented by

a one–dimensional (1D) theoretical linear elastic analysis. Stations FKSH14 and IBRH10 were classified as sites with low inter–event variability and a good fit to 1D theoretical formulations of wave propagation (LG) by Thompson et al. (2012), which make them suitable for linear elastic site response validation analysis. Sites OSKH01 and SZOH25 were not included in the Thompson et al. (2012) study. However, after comparing 1D linear–elastic theoretical and empirical transfer functions at the two sites, they were also deemed suitable for linear elastic site response validation analysis. While the intent of this research is not to assess the appropriateness of 1D site response models, it is important to select study sites with compatible theoretical and empirical transfer functions. The aforementioned agreement will allow the investigation of the sources of uncertainty in $\kappa_{0\_TF}$ values to remain independent from the chosen site response model. The $V_s$ profiles of our study sites are shown in Figure. 1.

Site OSKH01 is a single layer site, hence there is no gradient in $V_s$ throughout the depth of the soil profile, however, there are uncertainties associated with the $V_s$ measurements. On the other hand, site SZOH25 is a multiple–layer site with a smooth $V_s$ gradient. At FKSH14, there is an impedance contrast (calculated as the ratio between the product of density and $V_s$ of the overlying layer and the product of the density and $V_s$ of the underlying layer; hence, the lower the ratio, the stronger the impedance contrast) of 0.24 at 52m depth. At IBRH10, the $V_s$ gradient is slightly higher than for SZOH25 and the impedance contrast at bedrock is significant (i.e., 0.31). Values of $V_{s30}$, $V_{s\_mean}$ (time–averaged $V_s$ for entire depth of soil profile), depth to bedrock and NEHRP (National Earthquake Hazards Reduction Program) site classification (FEMA 450) for each site are stated in table 1.

## Table 1

**Selected Site Details and Classification**

| Site Name | Depth to Bedrock (m) | $V_{s30}$ (m/s) | $V_{s\_mean}$ (m/s) | NEHRP Site Classification |
|---|---|---|---|---|
| OSKH01 | 550 | 500 | 500 | C |
| SZOH25 | 328 | 347.3 | 589.1 | D |
| FKSH14 | 106 | 251.3 | 654 | D |
| IBRH10 | 518 | 200 | 531.3 | D |

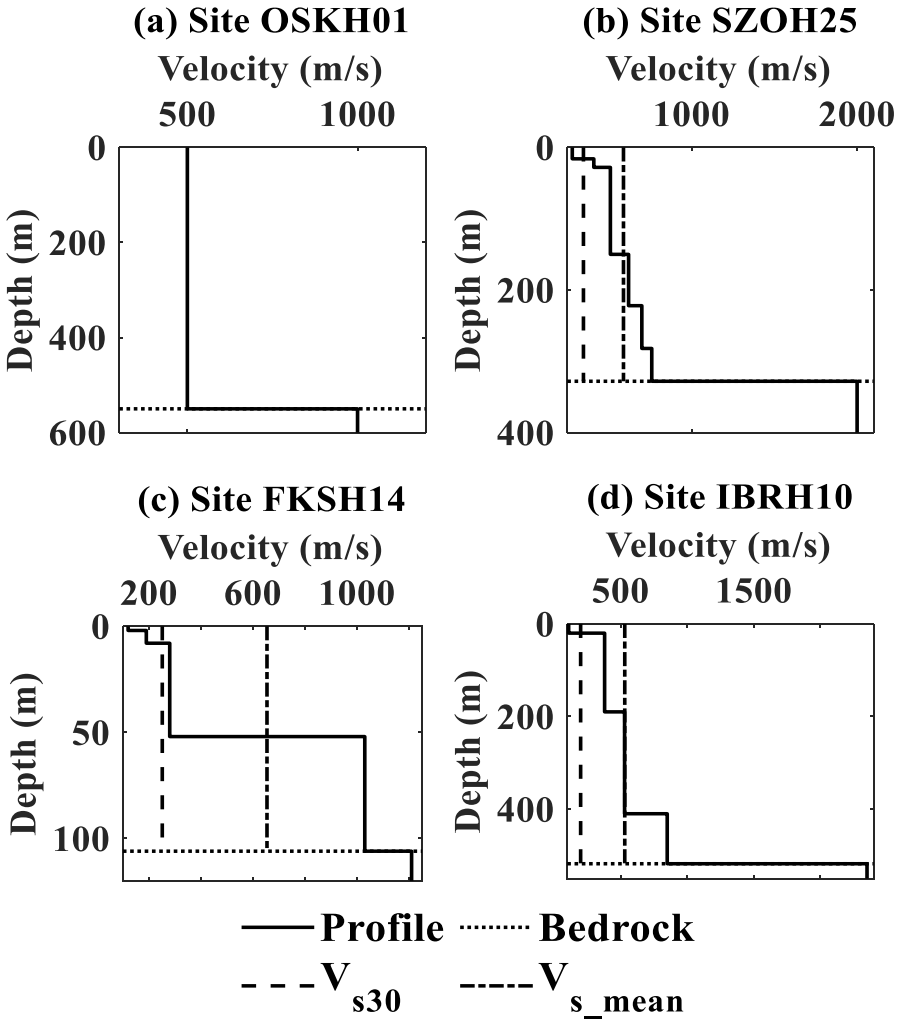


**Figure. 1.** Shear–Wave Velocity Profile of Selected KiK–net Sites

## 4. Ground Motion Selection

We compute $\kappa_{0\_TF}$ for at least 10 ground motion pairs at each site. We use both horizontal components of the recorded motions and values of $\kappa_{0\_TF}$ are reported as the average per horizontal component orientation. Each selected record is processed following protocols in Dawood et al. (2016) to comply with signal processing recommendations, such as baseline corrections and adequate noise windows (Ktenidou et al., 2012). The initial selection criteria of processed ground motions is based on peak ground accelerations lower than $10cm/s^2$ (to avoid the onset of soil nonlinear behavior), moment magnitudes between 3 and 5, epicentral distances less than 180 km (to avoid bias by multiple seismic ray paths) and shear strain index, $I_\gamma$ (defined as the ratio of peak ground velocity and $V_{s30}$; Chandra et al., 2016) less than 0.1% (to further constrain only linear motions) as shown in Table 2.

The values of $\kappa_{r\_AS\_bedrock}$, $\kappa_{r\_AS\_surface}$, and $\kappa_{0\_TF}$ are evaluated between 10Hz and 25Hz. For further screening, we identify amplification peaks on the empirical transfer functions taking place beyond 8Hz, so that $\kappa_{r\_AS\_bedrock}$, $\kappa_{r\_AS\_surface}$, and $\kappa_{0\_TF}$ are calculated for attenuating slopes not biased by high–frequency amplifications (Parolai and Bindi, 2004). Transfer functions are calculated using smoothed FAS of each horizontal component by applying the Konno–Ohmachi filter (Konno and Ohmachi, 1998). Any recording affected by site amplification peaks beyond 8Hz is rejected from our database (Parolai and Bindi, 2004).

## Table 2

**Initial Ground Motion Screening Criteria**

| Parameter | Value | Reference |
|---|---|---|
| SNR | <3 | Ktenidou et al. (2012) |
| PGA | <10cm/s$^2$ | Ktenidou et al. (2012) |
| Magnitude | 3-5 | Drouet et al. (2010) |
| Epicentral Distance | <180km | Anderson and Hough (1984) |
| Shear Strain Index | <0.1% | Cabas et al. (2017) |

## 5. Methodology

At every site, we estimate site–specific kappa from recorded motions. Since the FAS method is more commonly used, we calculate and compare values of $\Delta\kappa_{0\_AS}$ and $\kappa_{0\_TF}$ using the recorded motions at bedrock and at the ground surface. The recorded motion at bedrock is further used in 1D theoretical site response analysis to obtain theoretical estimates of $\kappa_{0\_TF}$ for each record. Finally, we use parameters from the soil profiles to evaluate $\kappa_{0\_TF\_Eqn}$ from a closed–form equation. The probability density function (PDF) of empirical, theoretical, and closed–form equation results are then compared to understand the uncertainties in the analyses.

### 5.1. Empirical Assessment of Site–Specific Kappa

Figure. 2 illustrates the procedure followed in this research for the calculation of $\kappa_{r\_AS\_bedrock}$, $\kappa_{r\_AS\_surface}$ and $\kappa_{0\_TF}$ at the study sites. For each recorded motion pair at the study sites, $\kappa_{r\_AS\_bedrock}$ is evaluated from the spectral decay of acceleration FAS evaluated from the recording observed at the bedrock. $\kappa_{r\_AS\_surface}$ is calculated from the spectral decay of acceleration FAS of the recording

at the surface. The site–specific kappa, $\Delta\kappa_{0\_AS}$ from the acceleration spectrum method is calculated by equation (1).

$$\Delta\kappa_{0\_AS} = \kappa_{r\_AS\_surface} - \kappa_{r\_AS\_bedrock} \quad \textbf{(1)}$$

Where $\kappa_{r\_AS\_surface}$ is the value of $\kappa_{r\_AS}$ measured from the recorded motion at the surface of the site, and $\kappa_{r\_AS\_bedrock}$ is the value of $\kappa_{r\_AS}$ measured from the recorded motion at the bedrock depth of the site. Empirical transfer functions (ETF) are calculated by dividing acceleration FAS at the surface by the FAS at the bedrock for each recording pair. As proposed by Drouet et al. (2010), $\kappa_{0\_TF}$ is then calculated as the slope of the decaying peaks in the high-frequency range of the ETF. We hypothesize that the contribution of the sedimentary deposit to the overall attenuation can be captured by $\kappa_{0\_TF}$ analogously to the characterization provided by $\Delta\kappa_{0\_AS}$ (Cabas and Rodriguez-Marek, 2017).

The value of $\kappa_{r\_AS}$ from the acceleration spectrum method is determined by calculating the slope of the decaying FAS in log–linear space at high frequencies. Figure. 3 shows the FAS for a surface recording from KiK–net data plotted on log (amplitude) – linear (frequency) space. The starting frequency ($f_1$) and ending frequency ($f_2$) for the kappa calculation are usually selected by visual inspection at the start and end of the decay in FAS. Once the frequencies are selected, a linear regression of the data points between the two frequencies is conducted. The value of $\kappa_{r\_AS}$ is computed by dividing the slope of the fitted line by $-\pi$.

The selection of frequencies by visual inspection in the $\kappa_{r\_AS}$ calculation usually yields different values when evaluated by different analysts. Various studies (e.g., Sonnemann and Halldorsson, 2018; Pilz et al., 2019; Ji et al., 2020) have proposed an automated procedure the frequency selection process. In this research, we have used the procedure proposed by Ji et al. (2020) to determine the most appropriate frequencies for each recording. In the automated

procedure, various frequency pairs (i.e., $f_1$ and $f_2$) are tested between 10–25Hz. For every frequency pair, the algorithm conducts a linear regression between the selected frequencies on the smoothed FAS and finds the fitted line. The frequency pair with the lowest mean squared error between the smoothed FAS and fitted line is selected for calculating $\kappa_{r\_AS}$ for the recording. In this study, an additional condition is added to the Ji et al. (2020) procedure. The frequency pair for bedrock and surface time history in a record must be the same. Using the frequency pairs obtained for all the records in each direction, the values of $\Delta\kappa_{0\_AS}$ are calculated per Equation (1). Furthermore, the same frequency pairs (i.e., $f_1$ and $f_2$) are used to evaluate $\kappa_{0\_TF}$ from the ETF of each record.

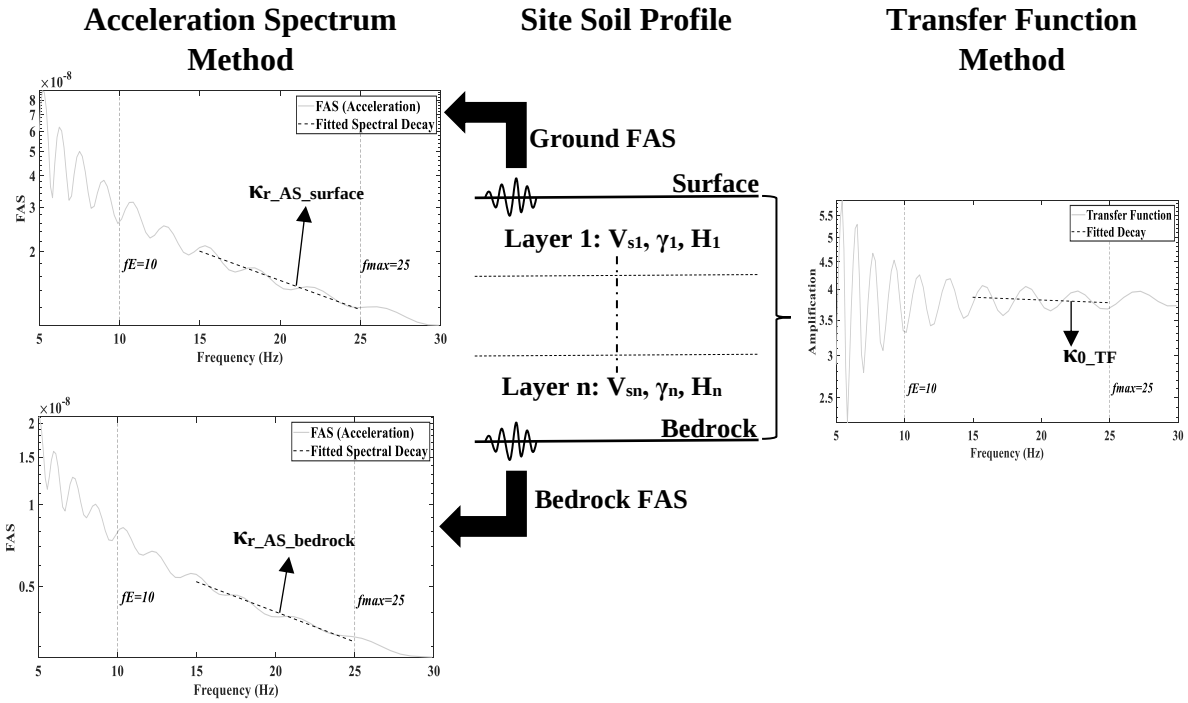


**Figure. 2.** Evaluation of Empirical Site–Specific Kappa using Two different Methods, the Acceleration Approach (Anderson and Hough, 1984) on the left, and the ETF for Transfer Function Approach (Drouet et al., 2010) on the right

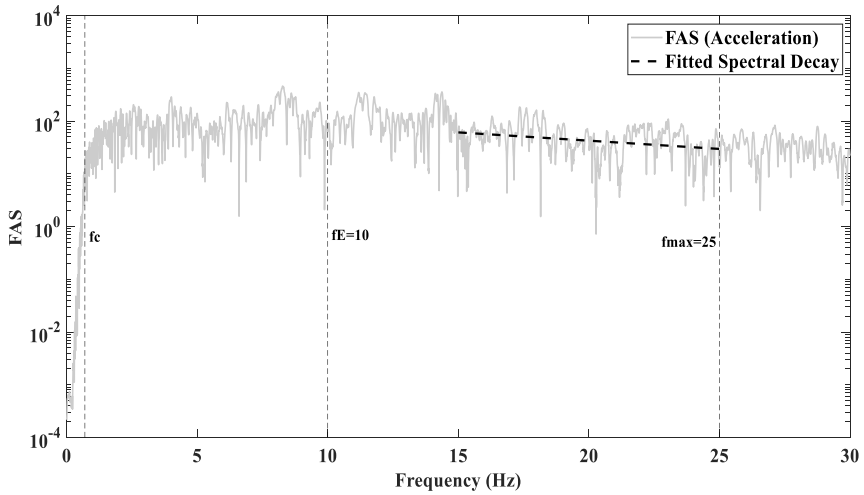


**Figure. 3.** Fourier Amplitude Spectrum of a Ground Motion Recording showing Evaluation of Kappa from Acceleration Spectrum Method

### 5.2. Site–Specific Kappa from Theoretical Evaluation of Site Response

Values of $\kappa_{0\_TF}$ are obtained from estimated 1D linear–elastic transfer functions at the study sites by means of a 1D formulation of wave propagation in layered media. Linear–elastic site response analyses are conducted using the program STRATA (Kottke and Rathje, 2008). Soils and rocks' unit weights are computed based on their reported $V_s$ and $V_p$ (Boore, 2016). For each layer of the profile, we calculate the minimum shear–strain damping based on the Darendeli and Stokoe (2001) model. However, these laboratory–based model only provides an estimate of material damping, and thus additional damping should be added to represent field observations of seismic attenuation (Cabas et al., 2017). Hence, we analyze the influence of various minimum shear–strain damping values by adding a constant damping ratio (i.e., from 1% to 4%) to the estimates of each layer obtained from Darendeli and Stokoe (2001) model.

Further, kappa–consistent damping is calculated for each record based on the formula proposed by Cabas et al. (2017) as shown in equation (2):

$$\xi = \frac{\Delta\kappa_{0\_AS}}{2\sum_{i=1}^{n}\frac{z_i}{V_{si}}} \quad \textbf{(2)}$$

Where, $\Delta\kappa_{0\_AS}$ is evaluated from site records. We hypothesize that values of $\Delta\kappa_{0\_AS}$ are theoretically equivalent to $\kappa_{0\_TF}$. $n$ is the number of layers, $V_{si}$ is the shear–wave velocity of $i^{th}$ layer and $z_i$ is the thickness of the $i^{th}$ layer. Mean and standard deviation in damping estimates are calculated for each site.

The input motions at the reference depth (i.e., the depth of the downhole sensor at each study site) correspond to the borehole records selected at each site under study. Such records, in both directions, are applied at the base of the soil columns of interest as within motions. Theoretical estimates of $\Delta\kappa_{0\_AS}$ are obtained by means of Equation (1) but using the FAS corresponding to the estimated surface motion from the 1D site response analysis. Similarly, theoretical values of $\kappa_{0\_TF}$ are computed from the theoretical linear–elastic transfer function at each site. We use the same frequency band for our site–specific kappa estimates based on theoretical formulations of site response to minimize the bias from the frequency range selection (Edwards et al., 2015).

### 5.3. Site-Specific kappa from Analytical Closed–Form Equation for a Single Layer

We derive an analytical closed–form equation to compute $\kappa_{0\_TF\_Eqn}$ for a single, homogeneous layer profile and compare it to theoretical multiple–layer analysis and single–layer approximations of the actual site's profile. The latter is achieved by assuming either $V_{s30}$ or $V_{s\_mean}$ characterizes the profile to the assumed reference depth. Uncertainty in site–specific input parameters affecting the variability in $\kappa_{0\_TF\_Eqn}$ is also quantified.

For a single–layer site as shown in Figure. 4a, the theoretical 1D linear–elastic transfer function is calculated using site parameters by using Equation 3 (Kramer, 1996):

$$Transfer\ Function, |F(\omega)| = \frac{2}{\cos\frac{\omega H}{V_s^*} + i\alpha^* \sin\frac{\omega H}{V_s^*}} \quad \textbf{(3)}$$

Where, $\omega$ is the frequency in rad/s; $H$ is the thickness of the soil layer; $V_s^*$ is the complex shear–wave velocity of the soil layer given by $V_s(1 + i\xi_s)$; $\alpha^*$ is the complex impedance ratio given by $\frac{\rho_s V_s^*}{\rho_b V_b^*}$; $\rho_s$ and $\rho_b$ are the density of the soil and the bedrock and $V_b^*$ is the complex shear–wave velocity of the bedrock given by $V_b(1 + i\xi_b)$; $\xi_s$ and $\xi_b$ are the damping ratio of the soil and the bedrock.

Figure. 4b shows the transfer function (from Equation 3) for two cases with the same soil damping ratio (ξ) and velocity ratio, $\beta$, which is the ratio between shear–wave velocity of soil, $V_s$ to the shear–wave velocity of the bedrock, $V_b$. However, the two cases have different $V_s$ of the soil layer and thus a different corresponding $V_b$ (to maintain the same $\beta$). As shown in Figure. 4c, when normalizing the X–axis by $\frac{\beta V_s}{H}$, the peaks of the theoretical transfer functions occur at the same normalized frequency with the same amplitude.

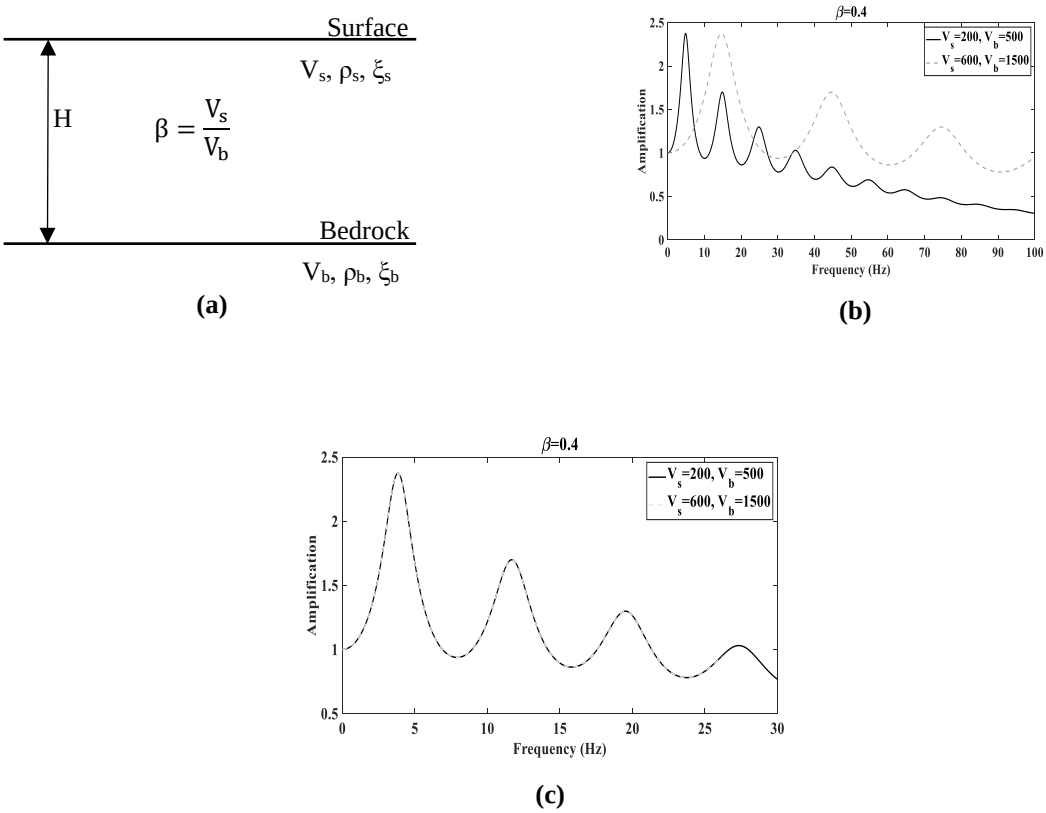


**Figure. 4. (a)** Single Layer Site Profile (**b)** Theoretical Transfer Function for Two Cases with the same Velocity ratio and Damping Ratio, but different Vs of the soil layer **(c)** Normalized Theoretical Transfer Function for Cases in previous figure.

Based on the properties of theoretical transfer function described by figure. 4, we derive a closed–form equation for calculating $\kappa_{0\_TF}$. As shown in figure. 5, $\kappa_{0\_TF}$ is evaluated between the starting ($n_1$) and ending ($n_2$) peaks. Hence, a peak occurs when:

$$\frac{\omega H}{V_s} = \frac{\pi}{2} + n\pi \quad \textbf{(4)}$$

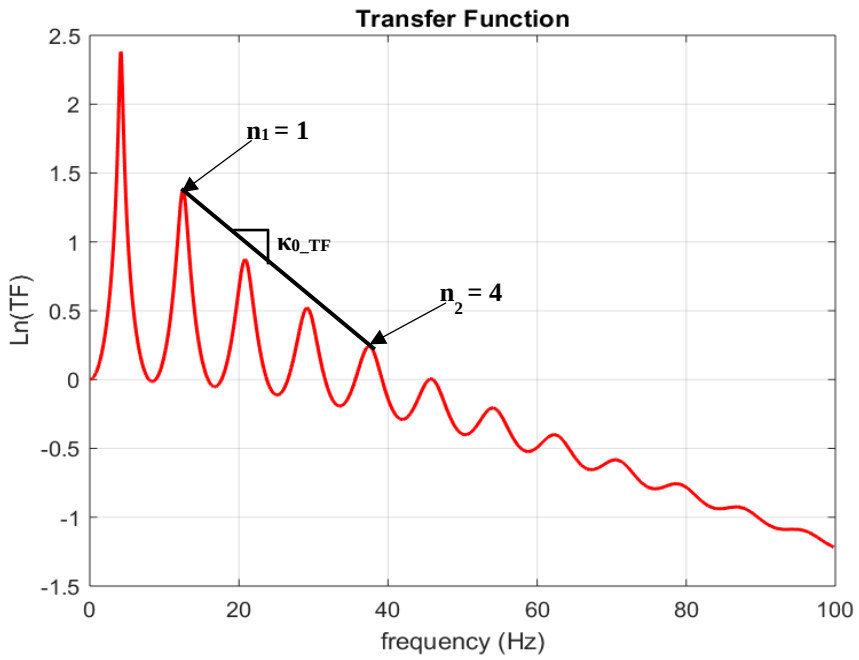


**Figure. 5.** Evaluation of Site–Specific Kappa, $\kappa_{0\_TF\_Eqn}$ from Theoretical Transfer Function

Hence, starting and ending peak frequencies are calculated as,

$$f_{n_1} = \frac{V_s}{4H}(1 + 2n_1)$$
$$f_{n_2} = \frac{V_s}{4H}(1 + 2n_2) \quad \textbf{(5)}$$

The site–specific kappa is computed as the slope between two peaks of the theoretical transfer function divided by π,

$$\kappa_{0\_TF\_Eqn} = -\frac{\ln TF(f_{n_2}) - \ln TF(f_{n_1})}{\pi(f_{n_2} - f_{n_1})} \quad \textbf{(6)}$$

Substituting equations (3) and (5) in equation (6),

$$\kappa_{0\_TF\_Eqn} = \frac{2H}{\pi V_s (n_2 - n_1)} \ln\left( \frac{\cos\frac{\pi}{2}\left(\frac{1+2n_2}{1+i\xi_s}\right) + i\alpha^* \sin\frac{\pi}{2}\left(\frac{1+2n_2}{1+i\xi_s}\right)}{\cos\frac{\pi}{2}\left(\frac{1+2n_1}{1+i\xi_s}\right) + i\alpha^* \sin\frac{\pi}{2}\left(\frac{1+2n_1}{1+i\xi_s}\right)} \right) \quad \textbf{(7)}$$

Using equation (7), $\kappa_{0\_TF\_Eqn}$ is calculated for the site parameters of the location of interest. Analogously to our previous estimations of site–specific kappa, we consider uncertainties in site parameters, $V_s$, and damping ratio in order to generate a probability density function of $\kappa_{0\_TF\_Eqn}$.

## 6. Uncertainty Quantification

In this study, we compare probability density functions (PDF) of empirical, theoretical, and closed–form equation results instead of comparing deterministic values. It is observed that even though the values of $\kappa_{r\_AS\_bedrock}$ and $\kappa_{r\_AS\_surface}$ change based on the seismic event, the value of $\Delta\kappa_{0\_AS}$ and $\kappa_{0\_TF}$, for linear soil response, should be approximately similar for different records. For theoretical estimations and the closed–form equation, $\kappa_{0\_TF}$ estimates only depend on site parameters such as $V_s$ and damping ratio. Uncertainties must account for variability in site parameter measurements. Comparisons among the PDFs of theoretical $\kappa_{0\_TF}$ and $\kappa_{0\_TF\_Eqn}$ with the PDF corresponding to empirical values of $\kappa_{0\_TF}$ allows for an assessment of the uncertainty in site parameters used in the analytical formulations and are presented in this section. By accounting for such uncertainties, a robust probabilistic estimate of $\kappa_{0\_TF}$ at a site can be obtained based on theoretical formulations.

First, a histogram of empirical $\kappa_{0\_TF}$ values obtained from the site–specific kappa estimates at each site is plotted. A normal as well as lognormal distribution are fitted to the data. As shown in Figure. 6, the PDF corresponding to a normal distribution fits better to the empirical data than

the lognormal distribution at SZOH25. Similarly, the PDF for a normal distribution also fits the empirical data at other sites better.

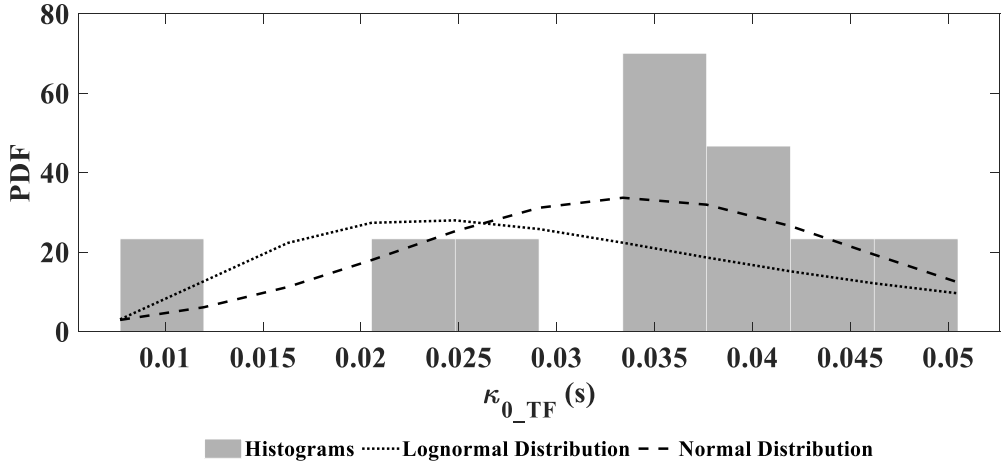


**Figure. 6.** Probability Density Function of Empirical $\kappa_{0\_TF}$ at Site SZOH25. The solid blocks show the histograms of data, Dotted line shows Lognormal Distribution fitted to the Data and Dashed line shows the Normal Distribution fitted to the Data

For site SZOH25, the theoretical analysis is conducted with the $V_s$ profile as shown in Figure. 1b and damping ratio values are assumed as described in section 6. A minimum shear–strain damping ratio is calculated according to Darendeli and Stokoe (2001) for each layer of the site profile. In Figure. 7, a constant damping of 1% is added to the minimum shear–strain damping ratio of each layer for case 1; a constant damping ratio of 2% is added in case 2; a constant damping ratio of 3% is added in case 3; and a constant damping ratio of 4% is added in case 4. None of the theoretical cases in Figure. 7 considers variability in damping ratio. Figure. 7 shows the comparison between empirical and theoretical estimates of $\kappa_{0\_TF}$ obtained from all the cases. Since the normal distribution fits the empirical data, the theoretical data is also fitted with a normal

distribution. Figure. 7 shows that there is a significant difference between empirical and theoretical estimates. Hence, theoretical analysis should consider variability in site parameters, namely $V_s$ and damping ratio. Figure. 7 also shows that the mean of the theoretical PDF changes with the damping. The mean of the PDFs corresponding to cases 2 and 3 are the closest to the empirical PDF. Hence, we add a constant damping of 2.5% to minimum shear–strain damping to further assess comparisons among empirical and theoretical PDFs at the site (Figure. 8).

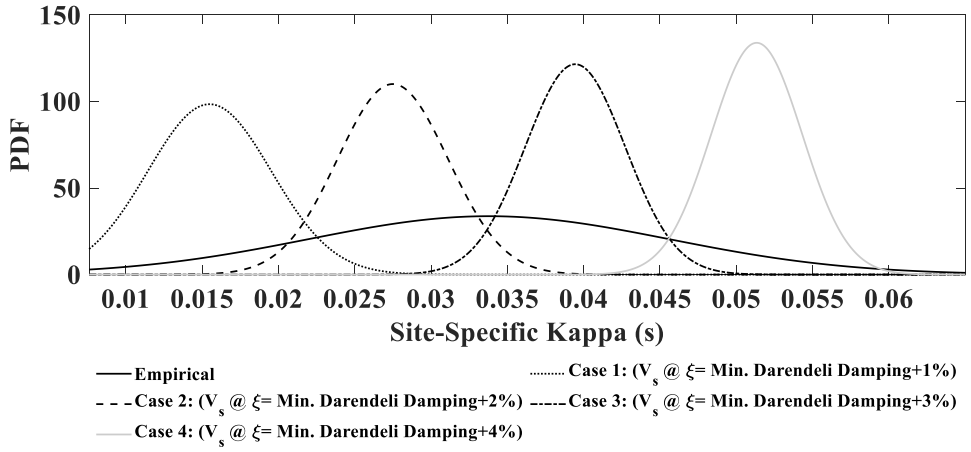


**Figure. 7.** Comparison of PDF of Empirical and Theoretical Site response analysis at Site SZOH25 without Uncertainty in input Site Parameters. Solid line represent the PDF of Empirical $\kappa_{0\_TF}$ estimates. Rest of the curves represent the cases represent theoretical estimates of $\kappa_{0\_TF}$ for different cases where constant 1% - 4% damping ratio is added to minimum shear–strain damping in each layer

Figure. 8 shows various cases where variability in site parameters is considered and PDFs of all the theoretical cases are compared with the empirical data. The variability considered in $V_s$ is assumed to be captured by a 15% variation around the mean value, and the variability in damping is the same as the coefficient of variation in kappa–consistent damping from empirical data. The variability in $V_s$ is assumed to account for the effect of uncertainty in $V_s$ measurements on the

PDF. However, as shown in Figure. 8, this variation in $V_s$ measurements does not appropriately reflect the uncertainty in empirical results. Hence, for theoretical site response analyses conducted at all remaining study sites, we do not consider the variation in $V_s$.

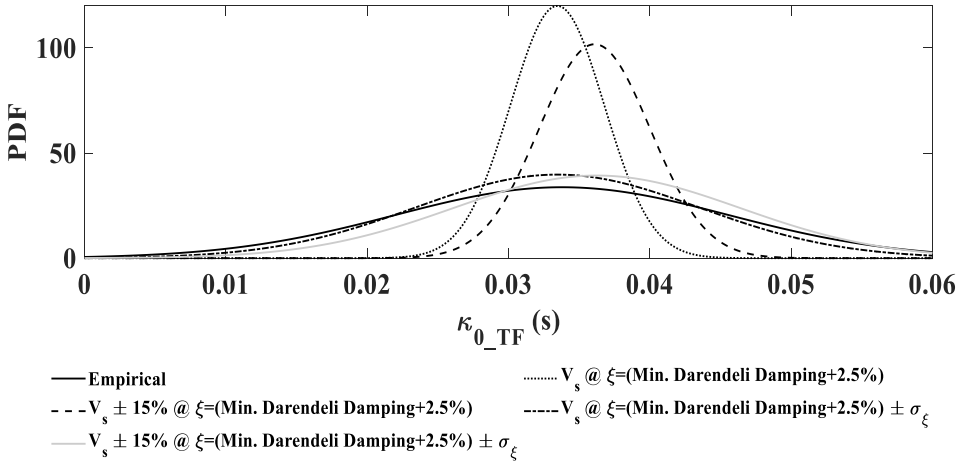


**Figure. 8.** Probability Density Function of Empirical and Theoretical Site Response Analysis at Site SZOH25 with Uncertainty in Site Parameters. $V_s$ refers to Shear–Wave Velocity Profile of site SZOH25

Estimates of $\kappa_{0\_TF\_Eqn}$ are evaluated from equation (7) by approximating the site as a single layer by using $V_{s30}$ or $V_{s\_mean}$ and kappa–consistent damping ratio. However, the equation does not require an input ground motion, so that for a single value of $V_s$ and damping ratio, we obtain one value of $\kappa_{0\_TF\_Eqn}$. To obtain probabilistic estimates of $\kappa_{0\_TF\_Eqn}$, Monte Carlo simulations are run for each study site. Similar to empirical and theoretical results, normal distribution for $V_s$ of the soil layer as well as the damping ratio for all the cases.

For this study, $V_{s30}$ and $V_{s\_mean}$ are assumed as proxies of the complete $V_s$ profile at the sites of interest. Standard deviations for the normal distribution of $V_s$ is calculated from the soil

profile where $V_s$ changes in each layer. The normal distribution for $V_s$ is bounded between the minimum and maximum $V_s$ of the soil profile. The mean and standard deviation for the normal distribution corresponding to the damping ratio is calculated from the empirical kappa–consistent damping as described by equation (2). $V_s$ and damping ratio are the independent random variables. For Monte Carlo simulations, random pairs of $V_s$ and damping ratios are selected from the respective distributions. The unit weight for all the pairs are calculated based on Boore (2016) proposed correlations with $V_s$ and $V_p$. Values of $\kappa_{0\_TF\_Eqn}$ for each pair are evaluated from equation (7). A PDF is then plotted using the values of $\kappa_{0\_TF\_Eqn}$ obtained for all the random pairs which is further compared with PDFs obtained from empirical data and site response analysis.

## 7. Discussion of Results

Various studies (Silva et al., 1998; Chandler et al., 2006; Drouet et al., 2010; Edwards et al., 2011; Van Houtte et al., 2011; Ktenidou et al., 2012; Ktenidou and Van Houtte, 2012) have proposed $\kappa_0$–$V_{s30}$ relationship to obtain $\kappa_{0\_TF}$ in low–to–moderate seismicity regions. In this study, we first examine the appropriateness of using $V_{s30}$ as a proxy for deeper $V_s$ profile. Figure. 9 shows the comparison of the PDF obtained from the empirical data, theoretical site response analysis and the closed–form equation results obtained by using $V_{s30}$ and $V_{s\_mean}$ as $V_s$ proxies and damping ratio calculated from empirical data at site SZOH25, which has a low $V_s$ gradient. The results from the closed–form equation based on $V_{s\_mean}$ as a single layer $V_s$ proxy for the soil profile's stiffness provides a better agreement with both, theoretical site response analysis and empirical data than $V_{s30}$. We observe the same trend in the remaining three study sites.

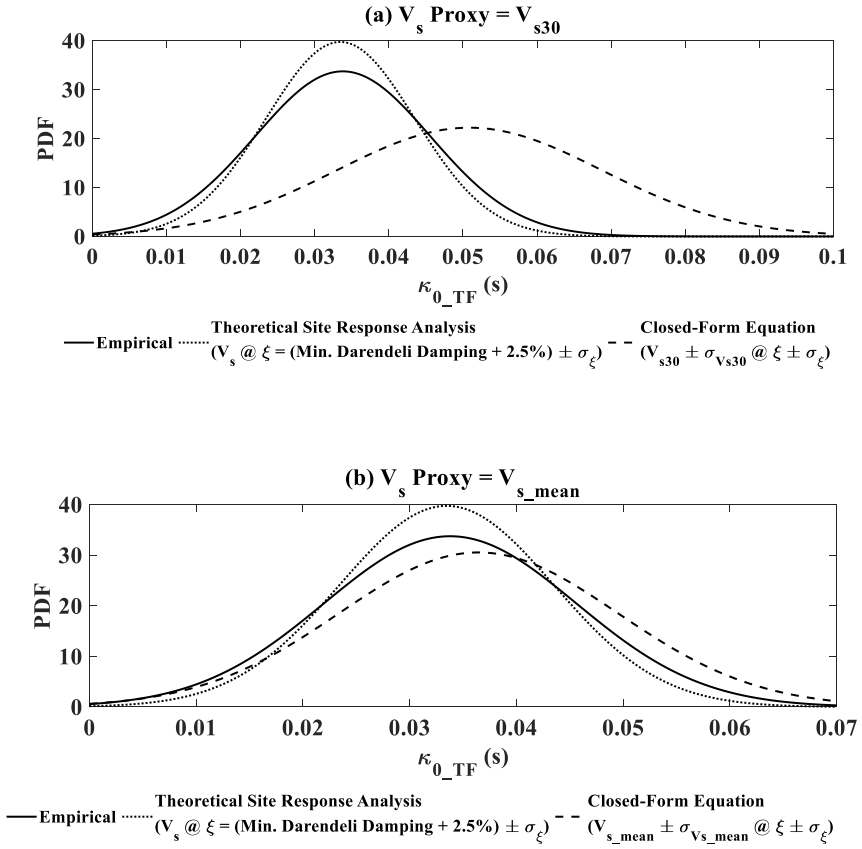


**Figure. 9.** Comparison of PDF obtained from Empirical, Theoretical Site response analysis and Closed–Form Equation for **(a)** $V_{s30}$ **(b)** $V_{s\_mean}$ at site SZOH25. The Damping for Site response analysis is same as that considered in Figure. 8. The Damping for Closed–Form Equation is Kappa–Consistent Damping calculated from equation (2)

The $V_s$ gradient at site SZOH25 is low. Hence, the PDF from closed–form equation for $V_{s\_mean}$ as site proxy and standard deviation in $V_s$ is in good agreement with empirical and theoretical site response analysis PDF. However, for sites such as FKSH14 where $V_s$ gradient is high, the coefficient of variation (CoV = 64%) in $V_s$ is large. It is thus important to identify appropriate standard deviation for use in the closed–form equation. Figure. 10 shows the PDF obtained from the empirical data compared with the closed–form equation results obtained when

considering uncertainty in shear–wave velocity with 100% and 50% of the coefficient of variation at the site FKSH14. Figure. 10 shows that the PDFs of the $\kappa_{0\_TF}$ from the empirical and the closed–form equation are more in agreement when standard deviation of the normal distribution of $V_s$ is 50% of the $V_s$ coefficient of variation (CoV). This observation relates to the empirical values of $\kappa_{0\_TF}$ where the CoV of the data at all sites is approximately 50%.

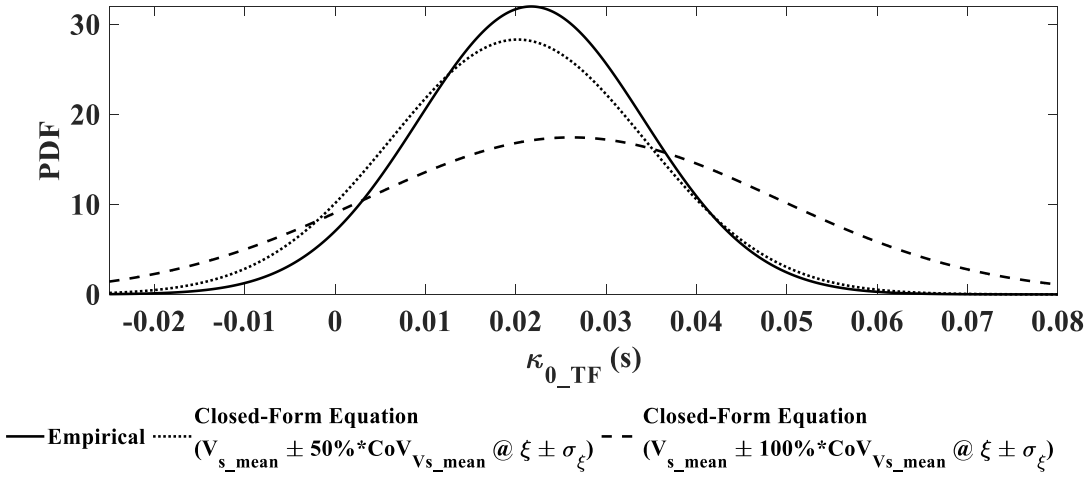


**Figure. 10.** Comparison of PDF for Empirical Data with Closed–Form Equation with Different Variability in Shear–Wave Velocity at site FKSH14

Figure. 11 shows the comparison of PDFs obtained from empirical, theoretical site response analysis and the closed–form equation results for all study sites. Site OSKH01 is a single layer profile, hence, uncertainty is only accounted for damping ratio estimates for both theoretical site response analysis and the closed–form equation. For sites SZOH25 and FKSH14, the approximation of soil profile with $V_{s\_mean}$ and the uncertainty in $V_s$ taken as 50% of the CoV compares well with the site response analysis and the empirical data. For site FKSH14, the difference between site response analysis and the closed–form equation PDF is larger than that at

SZOH25 because the $V_s$ gradient is higher at site FKSH14. Moreover, the damping ratio required for the site response analysis at site FKSH14 (i.e., 2% constant damping ratio added instead of 4.5% from kappa–consistent damping estimations) is much smaller than that corresponding to the kappa–consistent damping calculated from the empirical data. Finally, for site IBRH10, even though the PDF of empirical and closed–form equation results are comparable, the PDF from site response analysis is not compatible.

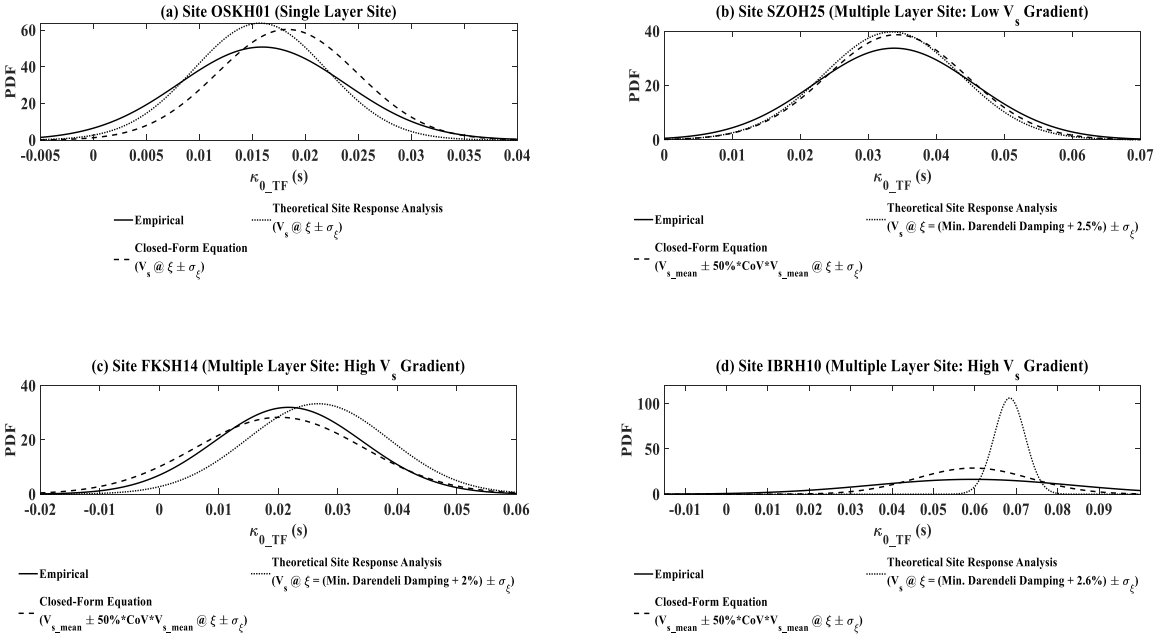


**Figure. 11.** Comparison of PDF of Empirical, Theoretical Site response analysis and Closed–Form Equation at sites **(a)** OSKH01 **(b)** SZOH25 **(c)** FKSH14 **(d)** IBRH10

We further examine the $\kappa_{0\_TF}$ obtained from the empirical data at site IBRH10 and find that the $\kappa_{0\_TF}$ estimates in north–south (NS) direction from two of the selected records is negative. A close observation of the transfer function of these two records in NS direction (Figure. 12) shows an amplification peak at a higher frequency, which makes the unbiased calculation of $\kappa_{0\_TF}$

between the frequencies 10–25Hz not feasible (Parolai and Bindi, 2004). Therefore, the corresponding $\kappa_{0\_TF}$ estimates obtained from these records are discarded. The revised PDFs are shown in Figure. 13, where the site response analysis and empirical data are compatible. However, the results from closed–form equation do not compare as well and shows that lower uncertainty in shear–wave velocity must be considered for IBRH10.

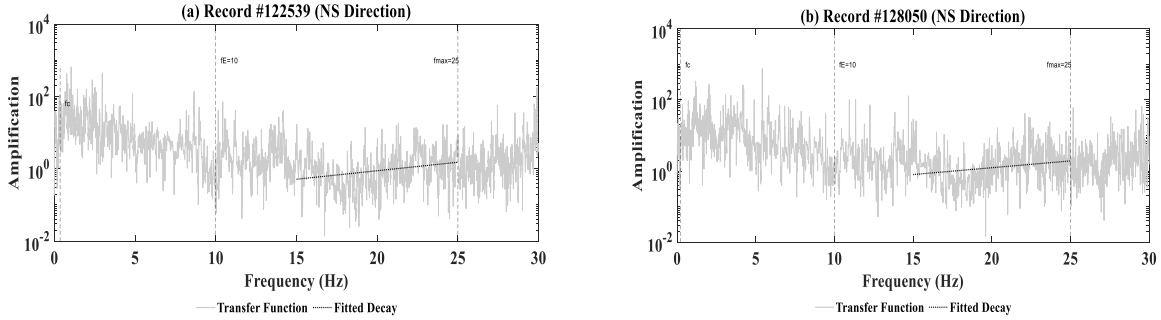


**Figure. 12.** Transfer Function for record number **(a)** 122539 **(b)** 128050 at Site IBRH10

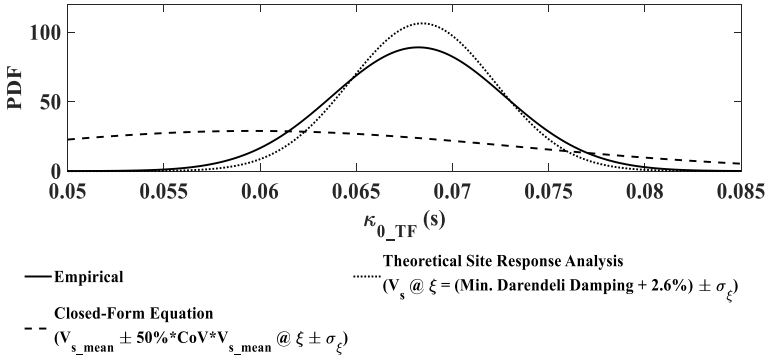


**Figure. 13.** Comparison of the PDF of Revised Empirical, Theoretical Site Response Analysis and Closed–Form Equation Data at site IBRH10

The empirical data at all sites (for site IBRH10, the data without rejecting $\kappa_{0\_TF}$ estimates from two records) have a coefficient of variation of approximately 50%. Hence, at site IBRH10, the PDF obtained from the closed–form equation, by assuming a variability of 50% of the CoV in $V_s$, were comparable with the empirical data. However, the empirical data at site IBRH10 show a very low CoV (6.32%) in the $\kappa_{0\_TF}$ estimates with the revised data. Figure. 14a shows the comparison between PDF for revised empirical data, theoretical site response analysis results and the closed–form equation results by assuming a variability in $V_s$ of 6.32% of CoV. The results further show that a higher damping ratio must be considered for the closed–form equation results and the comparison of such cases is shown in Figure. 14b.

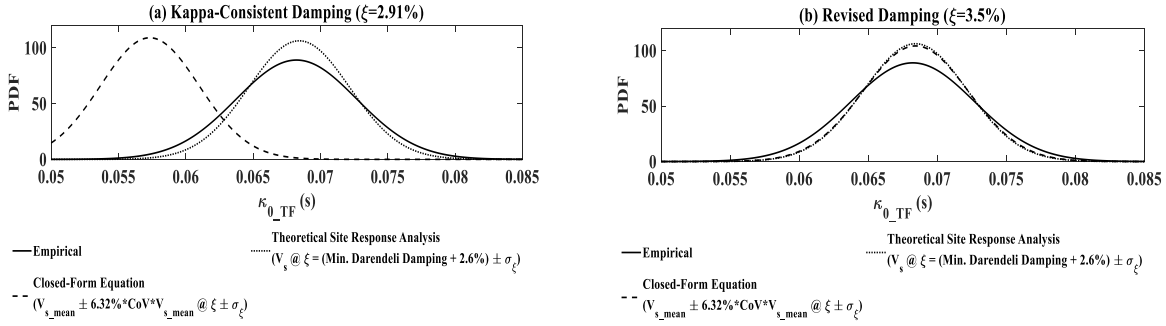


**Figure. 14.** Comparison of the PDFs corresponding to $\kappa_{0\_TF}$ estimates from the Revised Empirical, Theoretical Site Response Analysis and Closed–Form Equation Data with **(a)** $V_{s\_mean}$ Variability of 6.32% of CoV @ Kappa–Consistent Damping (2.91%) **(b)** $V_{s\_mean}$ Variability of 6.32% of CoV @ Revised Damping (3.5%) at Site IBRH10

The results from all sites show that the closed–form equation provides a first order approximation for probability distributions of $\kappa_{0\_TF}$ when knowledge of key site properties is available. Assumptions of damping ratio are still required, but the consideration of uncertainties in such values can prove beneficial in calculating preliminary estimates of $\kappa_{0\_TF}$. The $\kappa_{0\_TF}$ values

from the empirical transfer function at the site can capture the site–specific contribution of sedimentary columns to the overall path attenuation. Furthermore, our findings suggest that in the absence of surface and downhole records, theoretical formulations of 1D wave propagation at the site can provide a reasonable estimation of the $\kappa_{0\_TF}$ when the necessary subsurface characterization is available. The use of adjusted minimum shear–strain damping values (Cabas et al., 2017) in theoretical formulations of site response are found to provide a closer match to empirical $\kappa_{0\_TF}$ estimates. However, the differences in site parameters required for different sites show that further study is required for single layer approximations of soil profiles with Vs gradients.

## 8. Conclusions

The estimation of site–specific kappa from the acceleration spectrum method ($\kappa_{0\_AS}$) is needed for various engineering design purposes and requires availability of abundant ground motion data. At low–to–moderate seismicity regions such as Central and Eastern United States, abundant recorded data are not available to estimate $\kappa_{0\_AS}$. In this research, we have proposed a closed–form equation with consideration of uncertainty in site–specific parameters, namely Vs and damping, to provide a probabilistic representation of site–specific kappa via the transfer function method ($\kappa_{0\_TF}$). Values of $\kappa_{0\_TF}$ represent the attenuation between a reference rock horizon and the surface, at a specific site. $\Delta\kappa_{0\_AS}$ (the difference between surface and bedrock $\kappa_{0\_AS}$) as evaluated by equation (1) provides an equivalent characterization of the near-surface attenuation as $\kappa_{0\_TF}$.

In this research, we have first examined the equivalency between $\Delta\kappa_{0\_AS}$ and $\kappa_{0\_TF}$. Based on four sites and a total of 50 records, our study has found that the estimates of both $\Delta\kappa_{0\_AS}$ and

$\kappa_{0\_TF}$ agree if kappa at the bedrock ($\kappa_{r\_AS\_bedrock}$), the surface ($\kappa_{r\_AS\_surface}$) and the empirical transfer function ($\kappa_{0\_TF}$) are evaluated within the same frequency bands. Hence, the frequencies are selected such that the mean squared error between acceleration Fourier amplitude spectrum and the fitted line between the selected frequencies is minimum for both bedrock and surface recording.

We also compared the empirical and theoretical $\kappa_{0\_TF}$ estimates for the study sites to avoid sites not compatible with the 1D wave propagation assumption. The theoretical $\kappa_{0\_TF}$ estimates are obtained conducting 1D linear-elastic site response analysis. Moreover, we derived a closed–form equation to facilitate single layer approximation of the soil profile. In order to account for uncertainties in $\kappa_{0\_TF}$ estimates, we compared probability density functions of the empirical results with the theoretical results (from the site response analyses and the closed-form equation). The site response analysis results at all study sites accounted for the uncertainty in damping ratio whereas the closed–form equation results accounted for uncertainty in shear–wave velocity and damping ratio. The comparison of probability density functions corresponding to $\kappa_{0\_TF}$ at all the sites showed a good agreement between empirical and site response analysis results. The comparison between empirical and closed–form equation results also provided a good agreement. However, the site proxies required as input to the closed–form equation may vary as a function of the site' Vs profile (e.g., uniform single layer versus multi-layer sites with a $V_s$ gradient). More research is necessary to investigate systematic site conditions that require different parametrizations of be used in the closed-form equation to estimate $\kappa_{0\_TF}$. Although our study provides promising results regarding the practical use of the closed-form equation, expanding its implementation to a larger number of sites and ground motion records will further validate its ability to provide representative $\kappa_{0\_TF}$ values.

The probabilistic characterization of $\kappa_{0\_TF}$ resulting from this work can inform simulation of ground motions at low–to–moderate seismicity regions, and host-to-target adjustments of near-surface attenuation. In particular, the probabilistic distribution functions of $\kappa_{0\_TF}$ obtained from the closed–form equation as a function of site parameters only (i.e., without requiring ground motion records) shows promise toward analytical formulations that can be combined with probabilistic estimates of $\kappa_{0\_AS\_bedrock}$ in non-ergodic probabilistic seismic hazard analysis. Additionally, probabilistic estimates of $\kappa_{0\_AS}$ on the ground surface at the Central and Eastern United States region can be estimated using the probability density function of $\kappa_{0\_TF}$ couple with the distribution suggested by Hashash et al. (2014) for the reference rock, $\kappa_{0\_AS\_bedrock}$.

## 9. Acknowledgement

This research was supported by Center for Nuclear Energy Facilities and Structures at North Carolina State University. Resources for the Center come from the dues paid by member organizations and from the Civil, Construction, and Environmental Engineering Department and College of Engineering in the University.

## 10. References


[1] Al Atik, L., Kottke, A., Abrahamson, N., Hollenback, J., (2014) "Kappa (κ) Scaling of Ground-Motion Prediction Equations Using an Inverse Random Vibration Theory Approach," *Bulletin of the Seismological Society of America,* Vol. 104, pp. 336–346, February 2014, DOI: 10.1785/0120120200.

[2] Anderson, J.G., (1991) "A preliminary descriptive model for the distance dependence of the spectral decay parameter in southern California," *Bulletin of the Seismological Society of America,* Vol. 81, pp. 2186–2193.

[3] Anderson, J.G., Hough, S.E., (1984) "A Model for the Shape of the Fourier Amplitude Spectrum of Acceleration at High-Frequencies," *Bulletin of the Seismological Society of America,* Vol. 74, No. 5, pp. 1969–1993.

[4] Aoi, S., Kunugi, T., Fujiwara, H., (2004) "Strong-motion seismograph network operated by NIED: K-NET and KiK-net," *Journal of Japan Association for Earthquake Engineering,* Vol. 4, pp. 65–74.

[5] Biasi, G., Smith, K.D., Final Project Report, (2001) "Site effects for seismic monitoring stations in the vicinity of Yucca Mountain, Nevada," Prepared for the US DOE/UCCSN Cooperative Agreement Number DE-FC08-98NV12081, Task 12, Southern Great Basin Seismic Network Operations (SGBSN), MOL.20011204.0045.

[6] Biro, Y., P. Renault, P., (2012) "Importance and impact of host-to-target conversions for ground motion prediction equations in PSHA," *In: Proceedings of the 15th World Conference on Earthquake Engineering,* 1855, Lisbon, Portugal.

[7] Boore, D.M., (2003) "Simulation of Ground Motion Using the Stochastic Method," *Pure Applied Geophysics,* Vol 160, pp. 635-676.

[8] Boore, D.M., (2016) “Determining Generic Velocity and Density Models for Crustal Amplification Calculations, with an Update of the Boore and Joyner (1997) Generic Site Amplification for VS(Z) 760 m/s,” *Bulletin of the Seismological Society of America,* Vol. 106, No. 1, pp. 316–320, February 2016, doi: 10.1785/0120150229.

[9] Boore, D., Joyner, W., (1997) “Site amplifications for generic rock sites,” *Bulletin of the Seismological Society of America,* Vol. 87, No. 2, pp. 327–341.

[10] Building Seismic Safety Council, (2003) “NEHRP Recommended Provisions for Seismic Regulations for New Buildings and Other Structures (FEMA 450) Part 1: Provisions,” *Federal Emergency Management Agency*.

[11] Cabas, A., Rodriguez-Marek, A., (2017) “Vs-κ0 Correction Factors for Input Ground Motions Used in Seismic Site Response Analyses,” *Earthquake Spectra,* Volume 33, No. 3, Pages 917–941, August 2017, doi: 10.1193/22315EQS188M.

[12] Cabas, A., Rodriguez-Marek, A., Bonilla, L.F., (2017) “Estimation of Site-Specific Kappa (κ0)-Consistent Damping Values at KiK-Net Sites to Assess the Discrepancy between Laboratory-Based Damping Models and Observed Attenuation (of Seismic Waves) in the Field,” *Bulletin of the Seismological Society of America,* Vol. 107, No. 5, pp. 2258–2271, October 2017, doi: 10.1785/0120160370.

[13] Cartwright, D.E., Longuet-Higgins, M.S., (1956) “The statistical distribution of the maxima of a random function,” *In: Proceedings of the Royal Society of London. Series A, Mathematical and Physical Sciences,* Vol. 237, Issue 1209, pp. 212–232.

[14] Campbell, K.W., (2003) “Prediction of Strong Ground Motion Using the Hybrid Empirical Method and Its Use in the Development of Ground-Motion (Attenuation) Relations in

Eastern North America," *Bulletin of the Seismological Society of America,* Vol. 93, No. 3, pp. 1012-1033, June 2003.

[15] Chandler, A. M., Lamb, N.T.K., Tsang, H.H., (2006) "Near-surface attenuation modelling based on rock shear-wave velocity profile," *Soil Dynamics and Earthquake Engineering,* 26, pp. 1004–1014.

[16] Chandra, J., Guéguen, P., Bonilla, L.F., (2016) "PGA-PGV/Vs considered as a stress–strain proxy for predicting nonlinear soil response," *Soil Dynamics and Earthquake Engineering,* 85 (2016) 146–160.

[17] Darendeli, M. B., (2001) "Development of a new family of normalized modulus reduction and material damping curves," Ph.D. Thesis, Department of Civil Engineering, University of Texas, Austin, Texas.

[18] Dawood, H. M., Rodriguez-Marek, A., Bayless, J., Goulet, C., Thompson, E., (2016) "A flatfile of ground motions from the KiKnet array," *Earthquake Spectra,* Vol. 32, pp 1281–1302, DOI:10.1193/071214EQS106.

[19] Drouet, S., Cotton, F., Gueguen, P., (2010) "Vs30, κ, regional attenuation and Mw from accelerograms: Application to magnitude 3-5 French earthquakes," *Geophysical Journal International,* 182, 880–898.

[20] Edwards, B., Faeh, D., D. Giardini, D., (2011) "Attenuation of seismic shear wave energy in Switzerland," *Geophysical Journal International,* 185, pp. 967–984.

[21] Edwards, B., Ktenidou, O.-J., Cotton, F., Abrahamson, N., Van Houtte, C., Fäh, D., (2015) "Epistemic Uncertainty and Limitations of the κ0 Model for Near-Surface Attenuation at Hard Rock Sites," *Geophysical Journal International,* (2015) 202, 1627–1645.

[22] Fujiwara, H., S. Aoi, T. Kunugi, Adachi, S., (2004) “Strong-motion observation networks of NIED: K-NET and KiK-net, Technical Report, Consortium of Organizations for Strong-Motion Observation Systems (COSMOS),” available at http://www.cosmos-eq.org/events/wkshop_ records_processing/presentations/Fujiwara.pdf (last accessed January 2016).

[23] Hashash, Y.M.A., Kim, B., Kottke, A.R., Rathje, E.M., Silva, W.J., Stewart, J.P., Campbell, K.W., (2014) “Reference-Rock Site Conditions for Central and Eastern North America: Part II – Attenuation (Kappa) Definition,” *Pacific Earthquake Engineering Research Centre*, PEER 2014/12, August 2014.

[24] Ji, C., Cabas, A., Bonilla, F., Gelis, C., (2020) “Quantifying the High-Frequency Spectra Decay Parameter Beyond the Linear-Elastic Regime,” *Manuscript in Preparation*, 2020.

[25] Konno, K., Ohmachi, T., (1998) “Ground-motion characteristics estimated from spectral ratio between horizontal and vertical components of microtremor,” *Bulletin of the Seismological Society of America*, 88 (1), 228–241.

[26] Kottke, A. R., Rathje, E. M., (2008a) “Strata, Version alpha, Revision 381,” *University of Texas,* Austin, TX.

[27] Kottke, A. R., Rathje, E.M., (2008b) “Technical Manual for Strata, Report 2008/10,” *Pacific Earthquake Engineering Research (PEER) Center,* University of California, Berkeley, CA.

[28] Kramer, S., (1996) “Geotechnical Earthquake Engineering,” Prentice Hall, Upper Saddle River, NJ.

[29] Ktenidou, O.-J., Abrahamson, N.A., Darragh, R.B., Silva, W.J., (2016) “A Methodology for the Estimation of Kappa (κ) from Large Datasets: Example Application to Rock Sites in the

NGA-East Database and Implications on Design Motions," *Pacific Earthquake Engineering Research Centre,* PEER Report No. 2016/01, April 2016.

[30] Ktenidou, O.-J., Cotton, F., Abrahamson, N.A., Anderson, J.G., (2014) "Taxonomy of κ: A Review of Definitions and Estimation Approaches Targeted to Applications," *Seismological Research Letters,* Vol. 85, No. 1, January/February 2014, doi: 10.1785/0220130027.

[31] Ktenidou, O.-J., Gélis, C., Bonilla, L.-F., (2012) "A Study on the Variability of Kappa (κ) in a Borehole: Implications of the Computation Process," *Bulletin of the Seismological Society of America,* Vol. 103, No. 2a, doi: 10.1785/0120120093.

[32] Ktenidou, O.-J., Van Houtte, C., (2012) "Empirical Estimation of kappa from Rock Velocity Profiles at the Swiss NPP Sites (19.02.2012)," Report TP2-TB-1090, *PEGASOS Refinement Project*.

[33] Laurendeau, A., Cotton, F., Ktenidou, O.-J., Bonilla, L.-F., Hollender, F., (2013) "Rock and Stiff-Soil Site Amplification: Dependency on VS30 and Kappa (κ0)," *Bulletin of the Seismological Society of America,* Vol. 103, No. 6, December 2013, doi: 10.1785/0120130020.

[34] Malagnini, L., Herrmann, R., Bona, M.D., (2000) "Ground-motion scaling in the Apennines (Italy)," *Bulletin of the Seismological Society of America,* Vol. 90, No. 4, 1062–1081.

[35] Muto, M., Duron, Z., (2015) "High-frequency seismic hazard estimation and impact on seismic evaluation for dams," *In: Proceedings of SSA Annual Meeting,* Pasadena, CA.

[36] Parolai, S., Bindi, D., (2004) "Influence of Soil Layer Properties on κ evaluation," *Bulletin of the Seismological Society of America,* 94:349–356.

[37] Pilz, M., Cotton, F., Zaccarelli, R., Bindi, D., (2019) “Capturing Regional Variations of Hard-Rock Attenuation in Europe,” *Bulletin of the Seismological Society of America,* Vol. 109, No. 4, pp 1401–1418, August 2019, DOI: 10.1785/0120190023.

[38] Pilz, M., Fäh, D., (2017) “The Contribution of Scattering to Near–Surface Attenuation,” *J Seismol,* (2017) 21:837-855, DOI 10.1007/s10950-017-9638-4.

[39] Silva, W., Darragh, R., (1995) “Engineering characterization of earthquake strong ground motion recorded at rock sites,” *Electric Power Research Institute,* Report TR-102261, Palo Alto, California.

[40] Silva, W., Darragh, R., Gregor, N., Martin, G., Abrahamson, N., Kircher, C., (1998) “Reassessment of Site Coefficients and Near-Fault Factors for Building Code Provisions,” Technical Report Program Element II: 98-HQGR-1010, Pacific Engineering and Analysis, El Cerrito, U.S.A.

[41] Sonnemann, T., Halldorsson, B., (2018) “Towards an Automated Kappa Measurement Procedure,” *In: Proceedings of the International Conference on Earthquake Engineering and Structural Dynamics,* Geotechnical, Geological and Earthquake Engineering 47, https://doi.org/10.1007/978-3-319-78187-7_4.

[42] Thompson, E.M., Baise, L.G., Tanaka, Y., Kayen, R.E., (2012) “A Taxonomy of Site Response Complexity,” *Soil Dynamics and Earthquake Engineering,* 41 (2012) 32–43.

[43] Van Houtte, C., Drouet, S., Cotton, F., (2011) “Analysis of the origins of κ (kappa) to compute hard rock to rock adjustment factors for GMPEs,” *Bulletin of the Seismological Society of America,* Vol. 101, pp. 2926–2941.

# Chapter 5

## Summary and Conclusions

## 1. Summary and Conclusions

This dissertation discusses various factors that affect the seismic response of electrical equipment and thus inform the risk of failure of equipment. The probabilistic characterization of site – specific kappa for near–surface attenuation can be used for simulation of a suite of ground motions at the nuclear power plant (NPP) site and generate design spectrum. The NPP building–cabinet system are analyzed by considering building–cabinet interaction along with localized geometric nonlinearity and subjected to ground motion obtained from simulations. An in–cabinet response spectrum (ICRS) obtained from the analysis is used to compare seismic capacity of equipment from shake table tests. The dissertation includes manuscripts for three key topics:

- The effects of geometric nonlinearity on ICRS– In this chapter, we study the effect of localized geometric nonlinearity such as gaps on the ICRS. It is found that as the gap closes, the transient response of the cabinet increases due to an impact between cabinet base and the anchor bolt. The interaction between transient and steady–state response governs the total response so that a periodic pattern of peaks and valleys is observed in the ICRS.
- Understanding the seismic response of electrical equipment subjected to high–frequency ground motions– In this chapter, we considered the effects of building–cabinet interaction along with localized geometric nonlinearity such as gaps on the ICRS. The study mainly concludes that even though the spectral amplitudes of ICRS are lower because of the interaction between building and cabinet, the interaction plays a role only when the gap is closed. The effect of interaction is thus dependent on the displacements induced by high–frequency accelerations and the gap length.
- Evaluating Site–Specific Attenuation Factor, Kappa from Site Transfer Function– This chapter explores site–specific transfer function method for calculating site attenuation factor, kappa

($\kappa_{0\_TF}$) as it is an important factor in evaluating ground motions via stochastic simulations or host–to–target adjustment methods. The study also studies the effects of factors such as shear – wave velocity (Vs) and soil damping ratio ($\xi$) on estimates of $\kappa_{0\_TF}$.

### 1.1. Effects of Boundary Conditions on Seismic Response of Electrical Equipment subjected to High-Frequency Ground Motions

The ground motion studies (SSHAC, 1997; EPRI, 2013; PEER, 2015) conducted at nuclear power plant (NPP) sites in Central and Eastern United States indicate that the ground motion response spectra exceed the safe shutdown earthquake (SSE) suggested by Reg. Guide 1.60 in high–frequency content. The high–frequency ground motions induce low displacements and hence, do not result in structural damage. However, the functionality of safety–related equipment such as relays can be compromised by high–frequency accelerations. To qualify electrical equipment, the in–cabinet response spectra (ICRS) are usually evaluated by uncoupled linear analysis of building and electrical cabinets. However, study conducted by Singh (2017) indicates a significant difference in the ICRS obtained from linear and nonlinear models. A periodic pattern with multiple peaks and valleys at higher frequencies is observed in the ICRS for nonlinear models with gap. The reasons for the unique nature of ICRS for nonlinear gap model are explained in this research and can be enumerated as follows:

- Except for cases when excitation frequency is more than the natural frequency of a cabinet, the total response of the cabinet is not dominated by the transient response of linear cabinet. However, for nonlinear cabinet, the total response is dominated by the transient response due to the recurrent impact between the cabinet base and anchor bolt whenever the gap closes.

- In the ICRS obtained for nonlinear cabinet subjected to harmonic excitation, periodic pattern of peaks and valleys at high–frequencies is observed. This observation is similar to that in the study conducted by Singh (2017) for seismic excitations. For all cases, the peaks occur for oscillators whose natural frequencies are odd multiple of the excitation frequency while the valleys occur for oscillators whose natural frequencies are even multiple of the excitation frequency.
- The periodic pattern is explained by the interaction of steady–state response with the transient response for the oscillators. If the natural frequency of an oscillator is an odd multiple of the excitation frequency, the maximum amplitude of steady–state response coincides with maximum amplitude of transient response. On the contrary, for an oscillator with natural frequency which is an even multiple of the excitation frequency, the maximum amplitude of steady–state response does not coincide with the maximum amplitude of transient response. The total response of an oscillator with natural frequency which is an odd multiple of the excitation frequency is thus, more than that of an oscillator with natural frequency which is an even multiple of the excitation frequency leading to a periodic pattern of spectral peaks and valleys in the ICRS for nonlinear cabinet model.
- The interaction of excitation and natural frequency of the oscillator also determines the displacement response of the nonlinear cabinet. If excitation frequency is lower than the natural frequency, the total response of linear cabinet is not dominated by transient response while the transient response dominates the total response for linear cabinet cases with excitation frequency more than the natural frequency. For the nonlinear cabinet cases, the transient response of the cabinet initiates whenever the gap closes thereby resulting in an impact between cabinet base and anchor bolt. In such a case, the transient response of nonlinear

cabinet governs to the total response. For the cases where excitation frequency is equal to the natural frequency of cabinet, the total response of both linear and nonlinear cabinet increases up to a maximum amplitude. However, the transient response of nonlinear cabinet increases in each cycle due to repeated impact between cabinet base and anchor bolt while that of linear cabinet decays. Thus, the peak spectral acceleration of nonlinear cabinet is much higher than that of linear cabinet. This observation is especially important in cases where cabinet is subjected to low–frequency accelerations which induce higher displacements and the gap closes more frequently.

## 1.2. Understanding the Seismic Response of Electrical Equipment Subjected to High–Frequency Ground Motions

This study presents some important conclusions about the seismic behavior of electrical cabinets influenced by the effects of geometric nonlinearity in the cabinet mounting arrangement and the equipment–structure interaction. A significant reduction occurs in the ICRS due to equipment–structure interaction observed for a linear case with modal mass ratio of about 1 to 2 percent (or greater) between the tuned modes of the building and the cabinet. The magnitude of reduction observed is even greater when higher frequency modes of the building and cabinet are tuned, and the system is subjected to high–frequency ground motions. The main conclusions of this study are:

- The effect of equipment–structure interaction in the case of nonlinear mounting arrangement is highly dependent upon the degree of nonlinearity. In general, a localized nonlinearity in the cabinet base filters out the floor displacements. For nonlinear systems, the secondary system interaction with the building reduces when the cabinet oscillates in free vibration due to a gap

in the mounting arrangement. Since interaction occurs when the cabinet base is in contact with the building floor, the effect of equipment–structure interaction is relatively less for nonlinear systems. The effect of interaction decreases even more for high frequency ground motions which induces lower floor displacements.

- The study shows a larger spectral accelerations in the ICRS when a system with localized nonlinearity is subjected to low frequency ground motion. This amplification occurs due to an impact between the anchor bolt and the cabinet base whenever the gap closes. A transient motion excites high frequency modes of the cabinet due to localized impact. Due to higher displacement induced by low frequency ground motions, impacts are repeated frequently leading to significantly higher amplifications. Because the effect of high frequency modes are prominent at lower elevations, the high–frequency peaks in the ICRS due to localized impacts are observed only at lower elevations of the cabinet model compared to that at the top of cabinet.
- Even though the effect of localized impact due to nonlinearities depends on the amplitude of ground motion, a reduction in ground motion amplitude cannot be linearly related to the corresponding reduction in spectral peaks of ICRS. A larger reduction in spectral peaks is observed for high frequency systems subjected to high frequency ground motion as compared to low frequency system subjected to low frequency ground motion. Furthermore, as larger gaps filter out larger floor displacements, the spectral amplitudes of ICRS reduces as the gap length increases. However, in some cases, a larger gap can also lead to an increase in spectral acceleration because it allows development of greater impact velocity which in turn leads to greater transient response.

### 1.3. Quantification of the Contribution of Sedimentary Deposits to High–Frequency Attenuation in Low–to–Moderate Seismicity Regions via the Site Transfer Function

For various design purposes at a site, an estimate of site–specific kappa from the acceleration spectrum method ($\kappa_{0\_AS}$) is required. The estimation of $\kappa_{0\_AS}$ requires a profuse amount of ground motion data which is usually not available at low–to–moderate seismicity regions such as Central and Eastern United States. In this research, we explore using transfer function method ($\kappa_{0\_TF}$) and propose closed–form equation derived from site transfer function. $\kappa_{0\_TF}$ represents the attenuation between reference rock and the surface, at a specific site which is an equivalent characterization of $\Delta\kappa_{0\_AS}$ (the difference between surface and bedrock $\kappa_{0\_AS}$). For probabilistic representation of $\kappa_{0\_TF}$, the method proposed in this research considers uncertainty in site parameters, $V_s$, and damping ratio. The key conclusions of this research are as follows:

- First, an equivalency between $\Delta\kappa_{0\_AS}$ and $\kappa_{0\_TF}$ is examined. Our study finds a good agreement between the values of $\Delta\kappa_{0\_AS}$ and $\kappa_{0\_TF}$ if same frequency band is used to evaluate kappa at the bedrock ($\kappa_{r\_AS\_bedrock}$), the surface ($\kappa_{r\_AS\_surface}$) and the empirical transfer function ($\kappa_{0\_TF}$). The frequencies are thus selected accordingly.
- The theoretical $\kappa_{0\_TF}$ estimates are obtained by conducting 1D linear-elastic site response analysis of the $V_s$ profile as well as from closed–form equation to facilitate single layer approximation of the soil profile. The uncertainties in $\kappa_{0\_TF}$ estimates are accounted by comparing probability density functions of the empirical and theoretical results. At all study sites, the uncertainty in damping is considered for site response analysis while uncertainty in both $V_s$ and damping is considered for the closed–form equation. While the probability density functions of $\kappa_{0\_TF}$ obtained from empirical, site response analysis and closed–form equation

showed a good agreement, the $V_s$ and damping input for the closed–form equation may vary and requires further research to investigate systematic site conditions.

- The probabilistic representation of $\kappa_{0\_TF}$ can be used for ground motions simulation at low–to–moderate seismicity regions. The probabilistic density functions of $\kappa_{0\_TF}$ obtained from the closed–form equation may be combined with probabilistic estimates of $\kappa_{0\_AS\_bedrock}$ and obtain probabilistic estimates of $\kappa_{0\_AS}$ on the ground surface.

## 2. Recommendations for Future Work

Further research is required to understand factors affecting seismic response of electrical equipment when subjected to high–frequency ground motions as well as the determination of site–specific kappa from site parameters. Following are some of the recommended future work:

- Evaluation of effects of localized geometric nonlinearity such as gaps by considering friction on the surface where cabinet is mounted.
- Consideration of nonclassical damping in coupled analysis of multi–degree of freedom building and cabinet systems.
- Study of more sites for evaluation of site–specific kappa from closed–form equation and propose appropriate values for site parameters for use in the equation.
- Use kappa values obtained from closed–form equation for simulating ground motions at nuclear power plant sites and further apply simulated ground motions for analysis of building–cabinet system.

## 3. References


[1] EPRI, (2013) “Seismic Evaluation Guidance: Screening, Prioritization and Implementation Details (SPID) for the Resolution of Fukushima Near-Term Task Force Recommendation 2.1: Seismic,” *Electric Power Research Institute,* Palo Alto, CA: 2013.1025287.

[2] PEER, (2015) “NGA-East: Median Ground-Motion Models for the Central and Eastern North America Region,” *Pacific Earthquake Engineering Research Centre,* PEER Report No. 2015/04, April 2015.

[3] SSHAC, (1997) “Recommendations for Probabilistic Seismic Hazard Analysis: Guidance on Uncertainty and Use of Experts,” NUREG/CR-6372, UCRL-ID- 122160, Vol. 1, 1997.

[4] Singh, S., (2017) “Seismic Response of Electrical Equipment in Nuclear Power Plants,” M.S. Thesis, North Carolina State University.

# Appendix A

## Coupled and Uncoupled MDOF Primary–Secondary Systems Results

## A.1. System–1

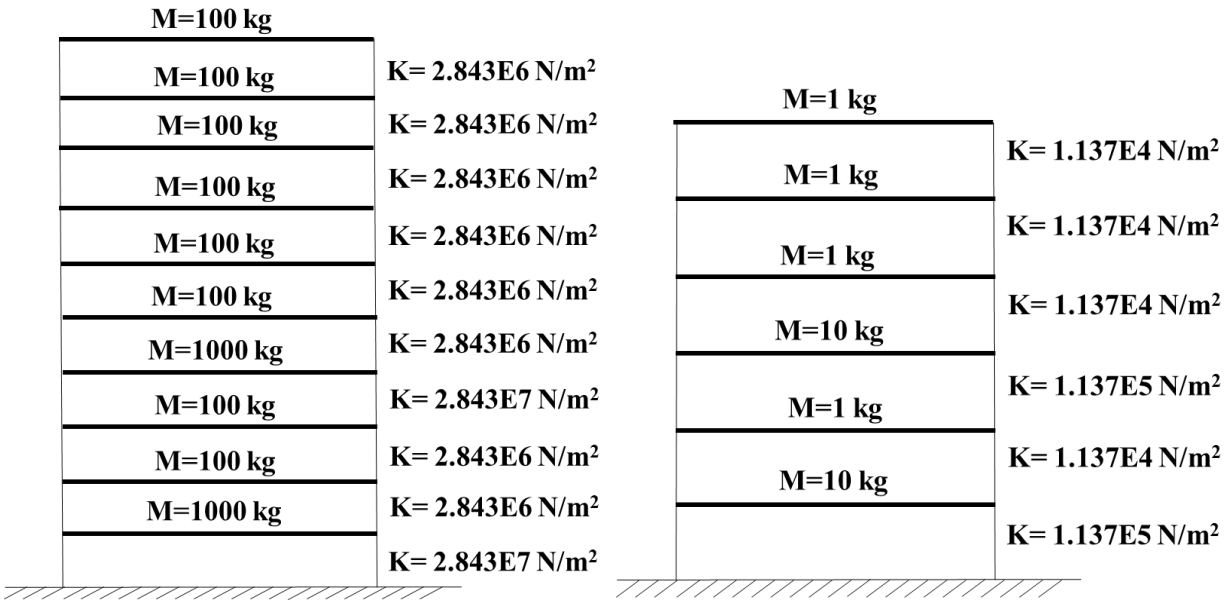


**Figure. A.1.** System–1: Uncoupled Primary and Secondary System. Secondary System Connected at 10th Floor of Primary System

**Table A.1.** Uncoupled and Coupled System Modal Frequencies for System–1

| Primary System | | Secondary System | | Coupled System | |
|---|---|---|---|---|---|
| **Mode #** | **Frequency (Hz)** | **Mode #** | **Frequency (Hz)** | **Mode #** | **Frequency (Hz)** |
| 1 | 4.00 | 1 | 4.00 | 1 | 3.72 |
| 2 | 8.42 | 2 | 8.42 | 2 | 4.26 |
| 3 | 19.52 | 3 | 19.52 | 3 | 8.32 |
| 4 | 26.84 | 4 | 26.84 | 4 | 8.78 |
| 5 | 30.72 | 5 | 30.72 | 5 | 17.29 |
| 6 | 38.42 | 6 | 38.42 | 6 | 20.29 |
| 7 | 40.32 | | | 7 | 21.40 |
| 8 | 47.57 | | | 8 | 26.84 |
| 9 | 52.12 | | | 9 | 30.63 |
| 10 | 93.02 | | | 10 | 30.86 |
| | | | | 11 | 38.43 |
| | | | | 12 | 40.38 |
| | | | | 13 | 47.60 |
| | | | | 14 | 52.13 |
| | | | | 15 | 58.62 |
| | | | | 16 | 93.03 |

### A.1.1. In–Cabinet Response Spectra (ICRS) at First Floor of Secondary System

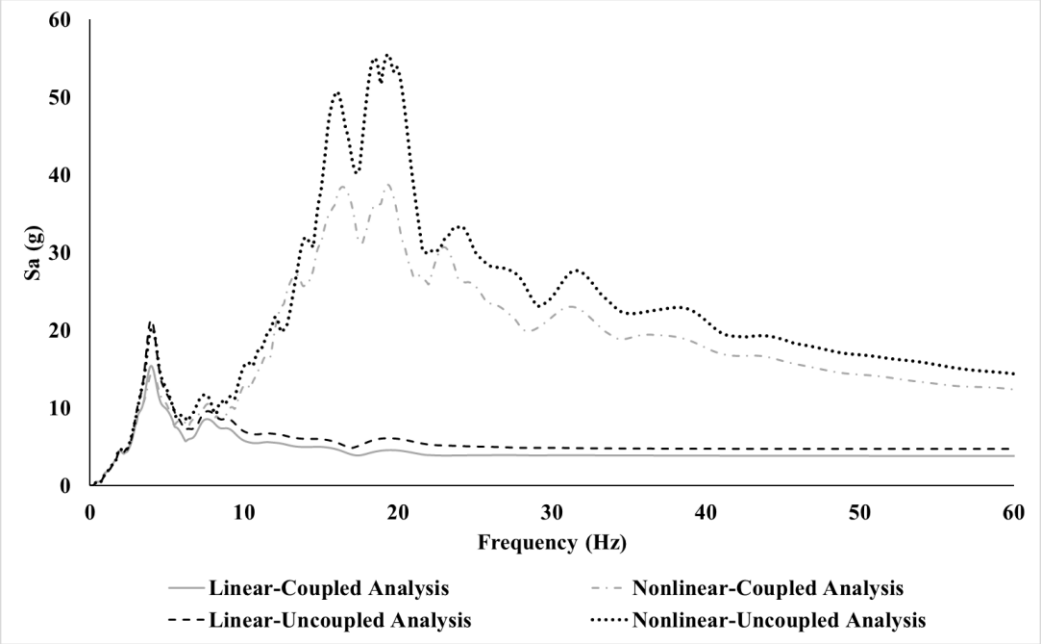


**Figure. A.2.** Comparison of ICRS at 1st Floor obtained from Coupled and Uncoupled Analysis of Linear and Nonlinear Models of System–1 Subjected to Low–Frequency Ground Motions

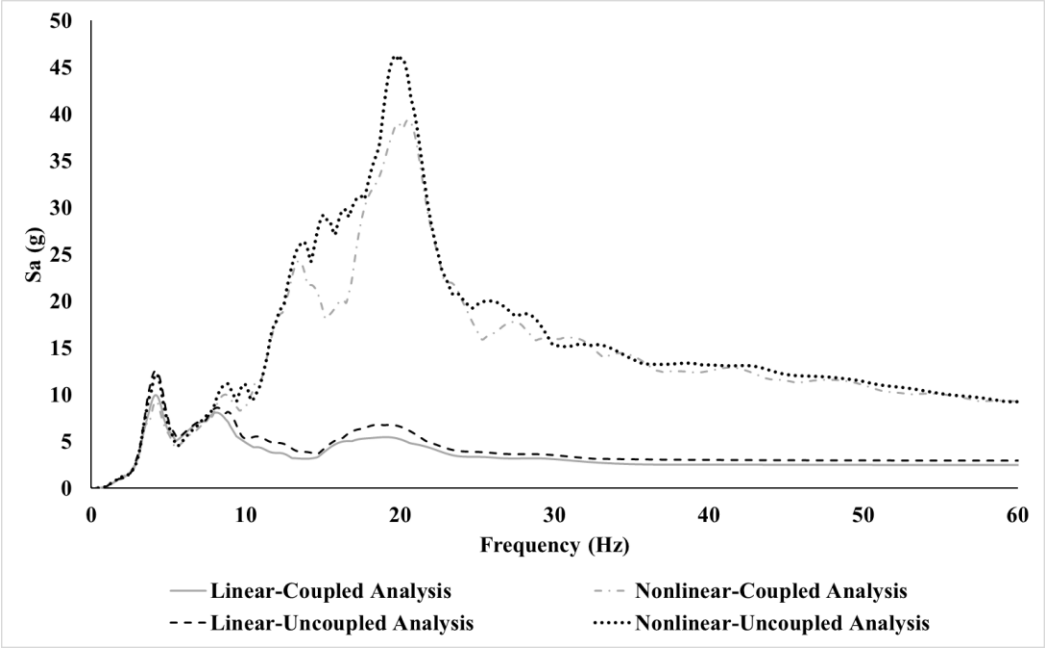


**Figure. A.3.** Comparison of ICRS at 1st Floor obtained from Coupled and Uncoupled Analysis of Linear and Nonlinear Models of System–1 Subjected to High–Frequency Ground Motions

### A.1.2. In–Cabinet Response Spectra (ICRS) at Sixth Floor of Secondary System

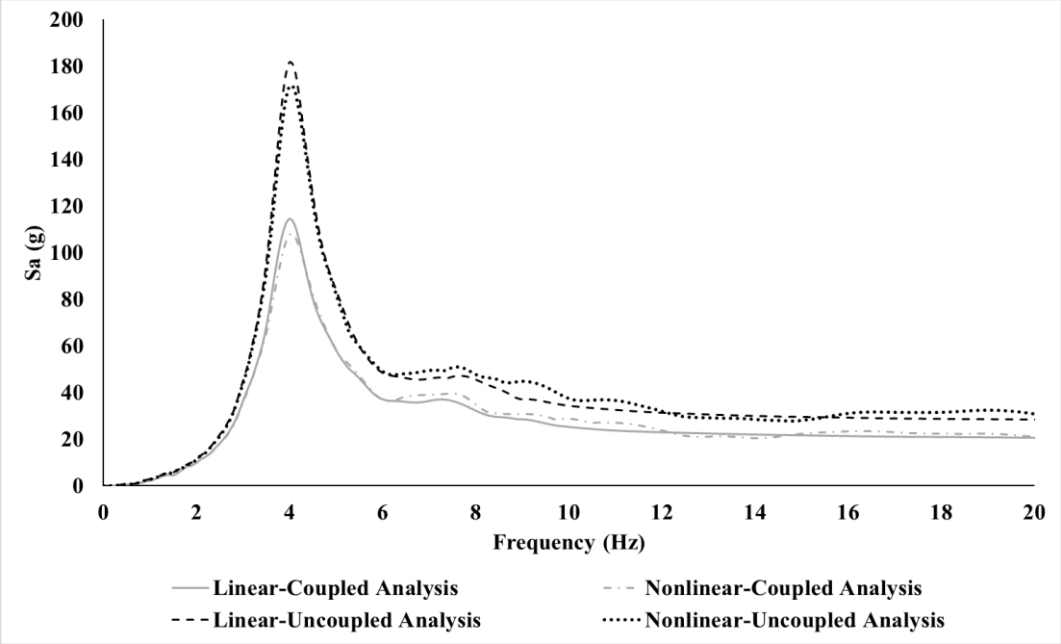


**Figure. A.4.** Comparison of ICRS at 6th Floor obtained from Coupled and Uncoupled Analysis of Linear and Nonlinear Models of System–1 Subjected to Low–Frequency Ground Motions

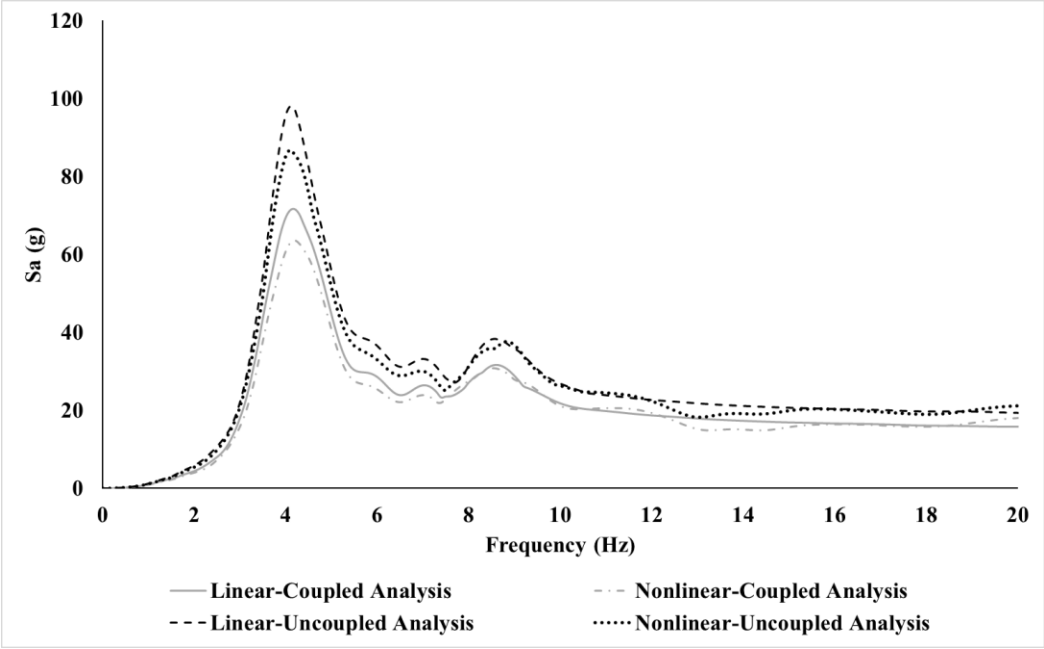


**Figure. A.5.** Comparison of ICRS at 6th Floor obtained from Coupled and Uncoupled Analysis of Linear and Nonlinear Models of System–1 Subjected to High–Frequency Ground Motions

## A.2. System–2

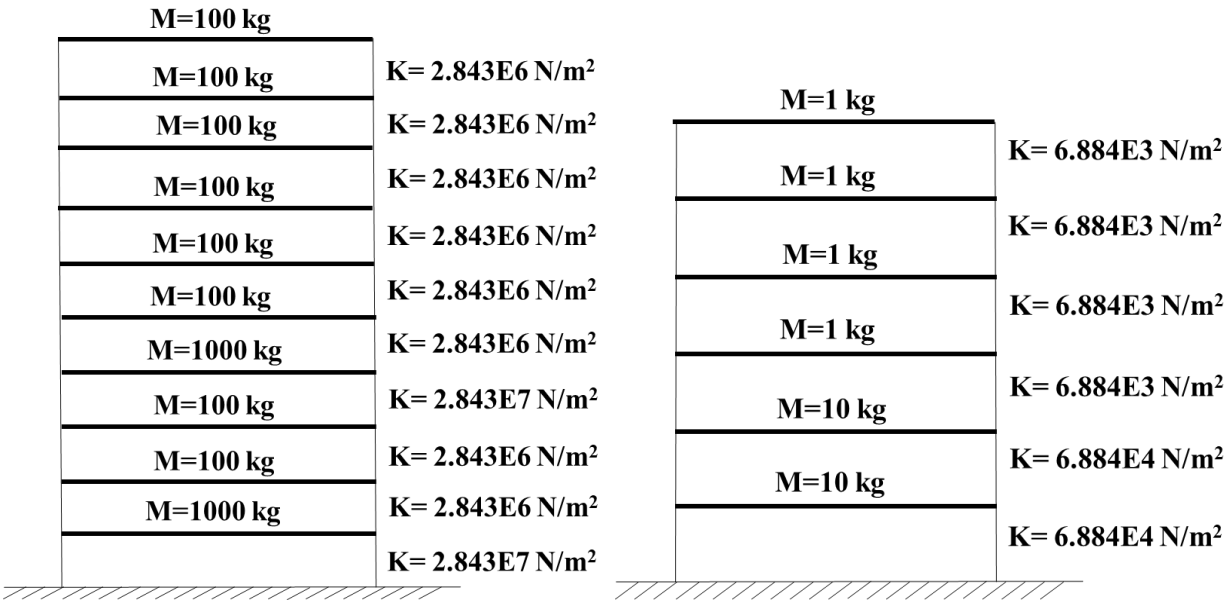


**Figure. A.6.** System–2: Uncoupled Primary and Secondary System. Secondary System Connected at 10$^{th}$ Floor of Primary System

**Table A.2.** Uncoupled and Coupled System Modal Frequencies for System–2

| Primary System | | Secondary System | | Coupled System | |
|---|---|---|---|---|---|
| **Mode #** | **Frequency (Hz)** | **Mode #** | **Frequency (Hz)** | **Mode #** | **Frequency (Hz)** |
| 1 | 4.00 | 1 | 4.33 | 1 | 3.86 |
| 2 | 8.42 | 2 | 8.42 | 2 | 4.42 |
| 3 | 19.52 | 3 | 13.42 | 3 | 7.75 |
| 4 | 26.84 | 4 | 20.13 | 4 | 9.2 |
| 5 | 30.72 | 5 | 21.64 | 5 | 13.43 |
| 6 | 38.42 | 6 | 24.85 | 6 | 19.44 |
| 7 | 40.32 | | | 7 | 20.20 |
| 8 | 47.57 | | | 8 | 21.77 |
| 9 | 52.12 | | | 9 | 24.85 |
| 10 | 93.02 | | | 10 | 26.84 |
| | | | | 11 | 30.80 |
| | | | | 12 | 38.42 |
| | | | | 13 | 40.35 |
| | | | | 14 | 47.59 |
| | | | | 15 | 52.13 |
| | | | | 16 | 93.02 |

### A.2.1. In–Cabinet Response Spectra (ICRS) at First Floor of Secondary System

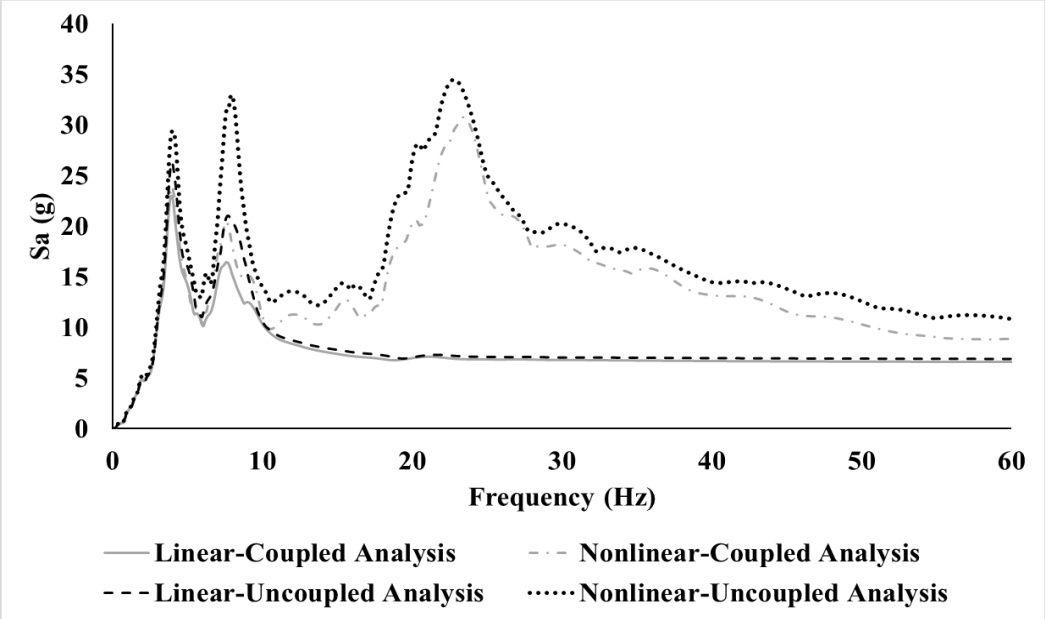


**Figure. A.7.** Comparison of ICRS at 1st Floor obtained from Coupled and Uncoupled Analysis of Linear and Nonlinear Models of System–2 Subjected to Low–Frequency Ground Motions

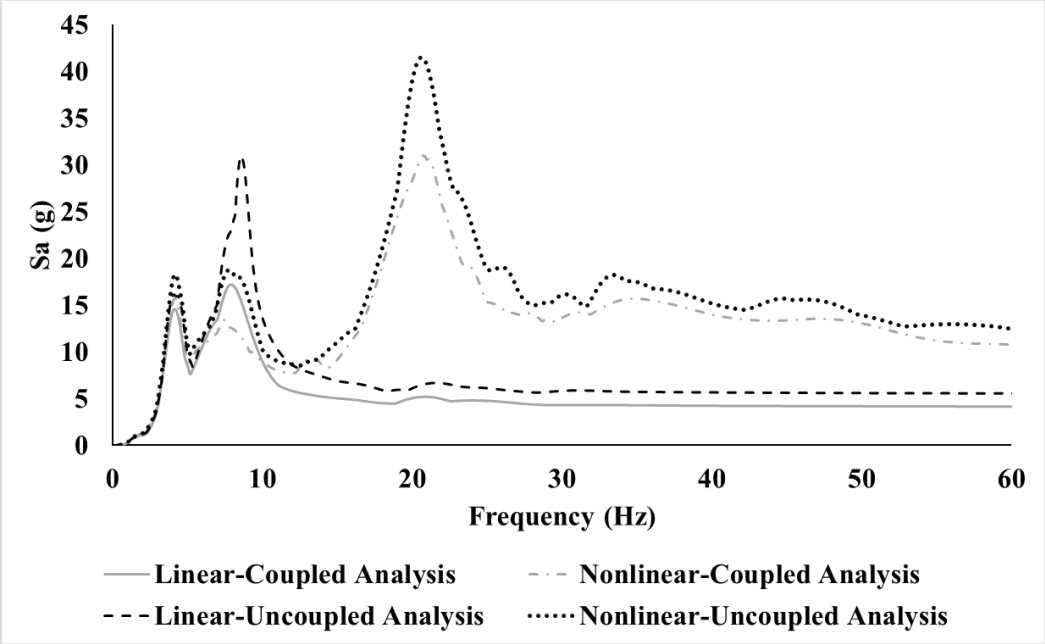


**Figure. A.8.** Comparison of ICRS at 1st Floor obtained from Coupled and Uncoupled Analysis of Linear and Nonlinear Models of System–2 Subjected to High–Frequency Ground Motions

### A.2.2. In–Cabinet Response Spectra (ICRS) at Sixth Floor of Secondary System

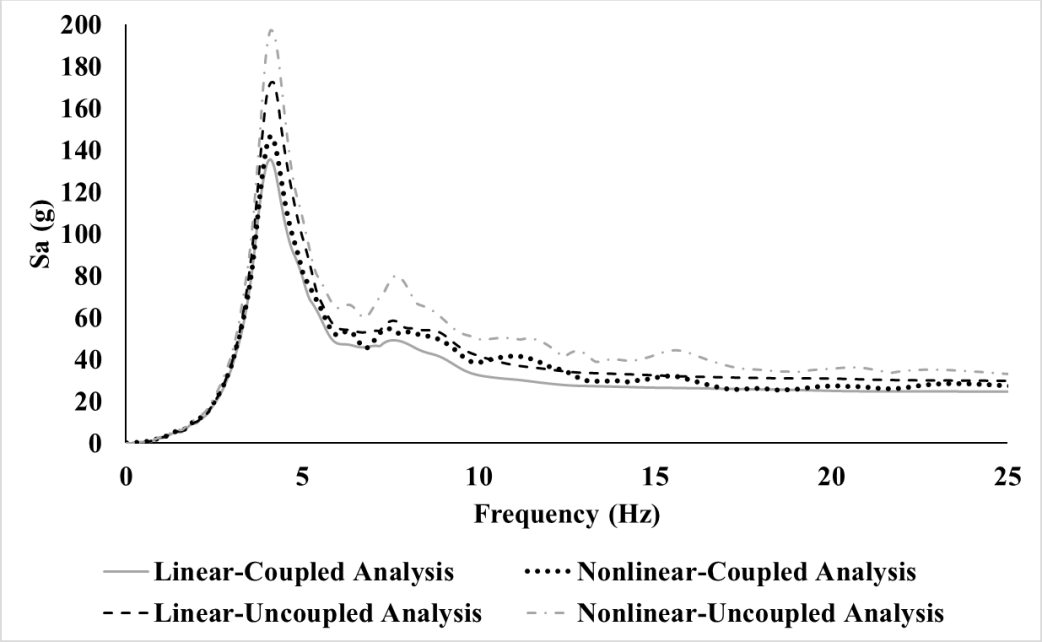


**Figure. A.9.** Comparison of ICRS at 6th Floor obtained from Coupled and Uncoupled Analysis of Linear and Nonlinear Models of System–2 Subjected to Low–Frequency Ground Motions

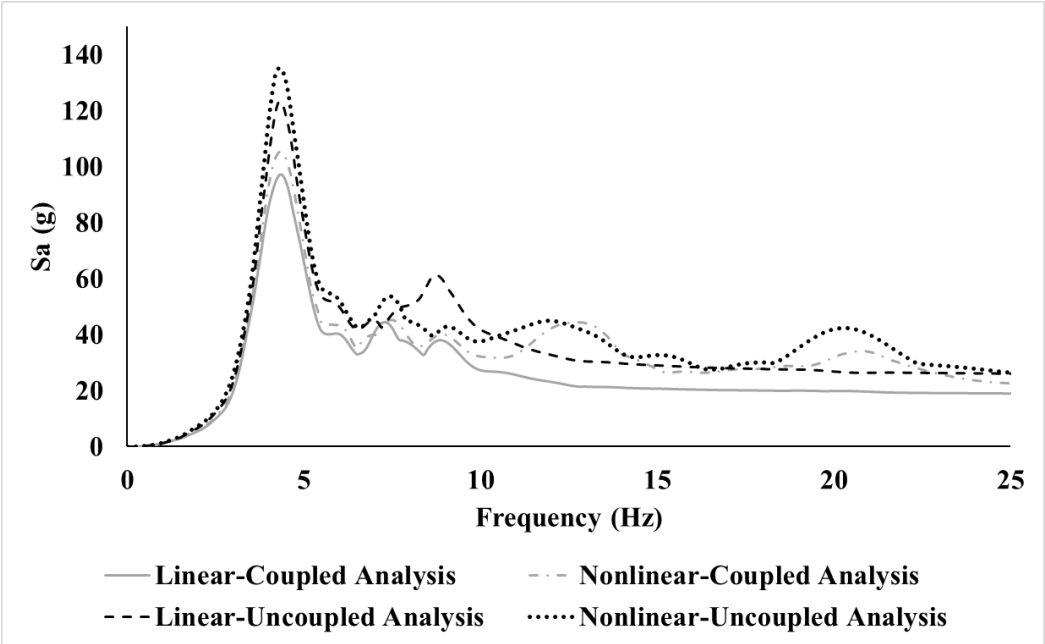


**Figure. A.10.** Comparison of ICRS at 6th Floor obtained from Coupled and Uncoupled Analysis of Linear and Nonlinear Models of System–2 Subjected to High–Frequency Ground Motions

## A.3. System–3

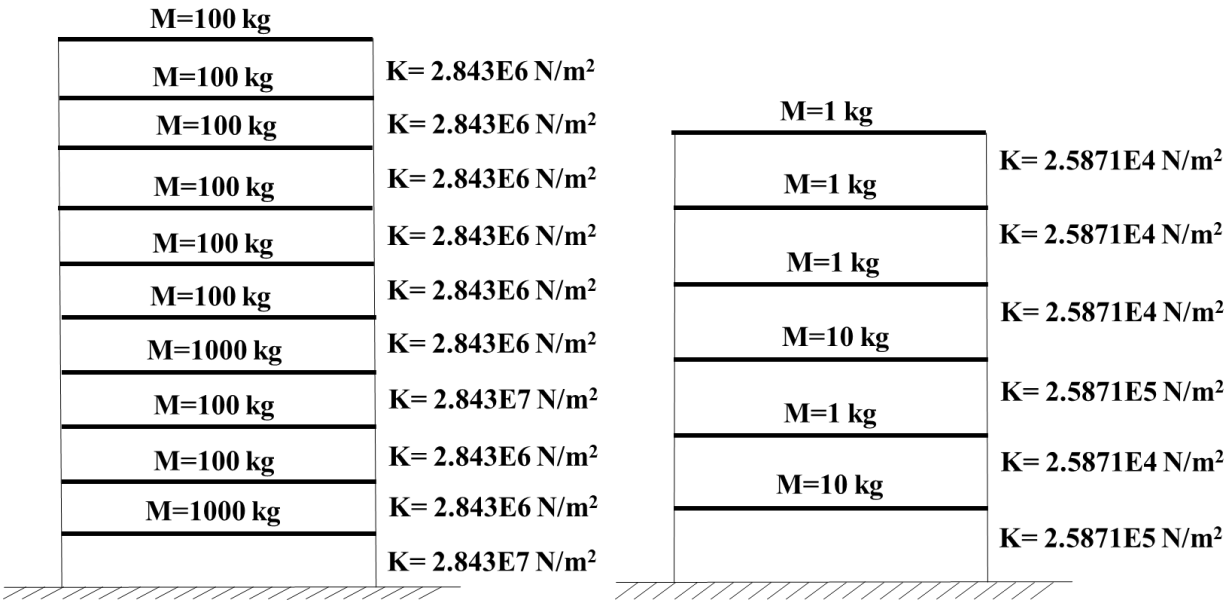


**Figure. A.11.** System–3: Uncoupled Primary and Secondary System. Secondary System Connected at 10th Floor of Primary System

**Table A.3.** Uncoupled and Coupled System Modal Frequencies for System–3

| Primary System | | Secondary System | | Coupled System | |
|---|---|---|---|---|---|
| **Mode #** | **Frequency (Hz)** | **Mode #** | **Frequency (Hz)** | **Mode #** | **Frequency (Hz)** |
| 1 | 4.00 | 1 | 6.03 | 1 | 3.92 |
| 2 | 8.42 | 2 | 13.18 | 2 | 6.02 |
| 3 | 19.52 | 3 | 26.84 | 3 | 8.47 |
| 4 | 26.84 | 4 | 32.28 | 4 | 13.18 |
| 5 | 30.72 | 5 | 46.20 | 5 | 19.17 |
| 6 | 38.42 | 6 | 88.43 | 6 | 26.77 |
| 7 | 40.32 | | | 7 | 26.98 |
| 8 | 47.57 | | | 8 | 31.53 |
| 9 | 52.12 | | | 9 | 32.28 |
| 10 | 93.02 | | | 10 | 38.43 |
| | | | | 11 | 40.52 |
| | | | | 12 | 46.20 |
| | | | | 13 | 47.64 |
| | | | | 14 | 52.14 |
| | | | | 15 | 88.43 |
| | | | | 16 | 93.03 |

### A.3.1. In–Cabinet Response Spectra (ICRS) at First Floor of Secondary System

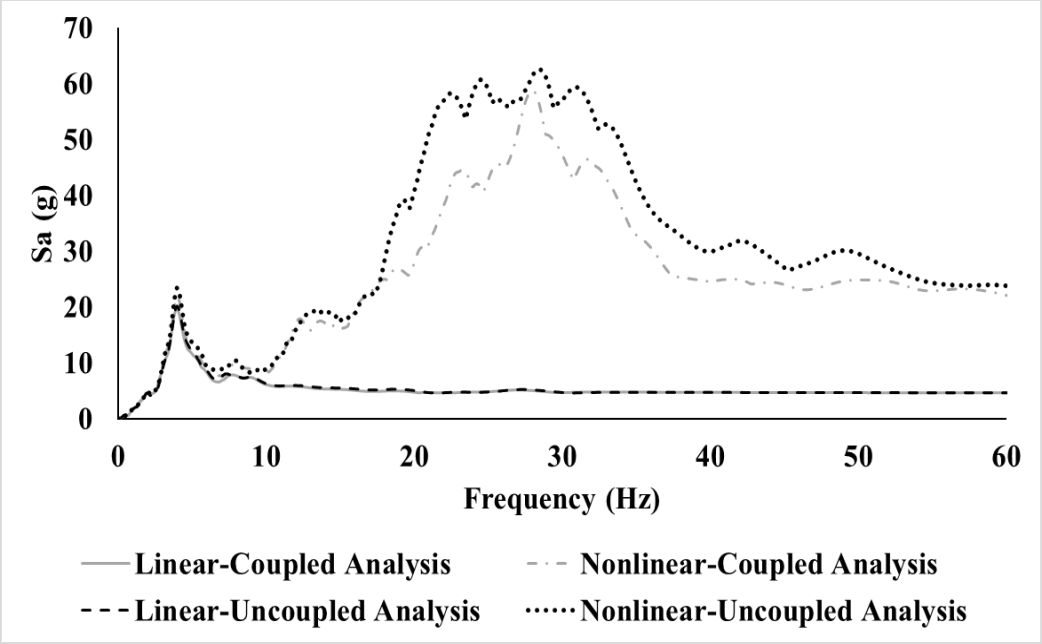


**Figure. A.12.** Comparison of ICRS at 1st Floor obtained from Coupled and Uncoupled Analysis of Linear and Nonlinear Models of System–3 Subjected to Low–Frequency Ground Motions

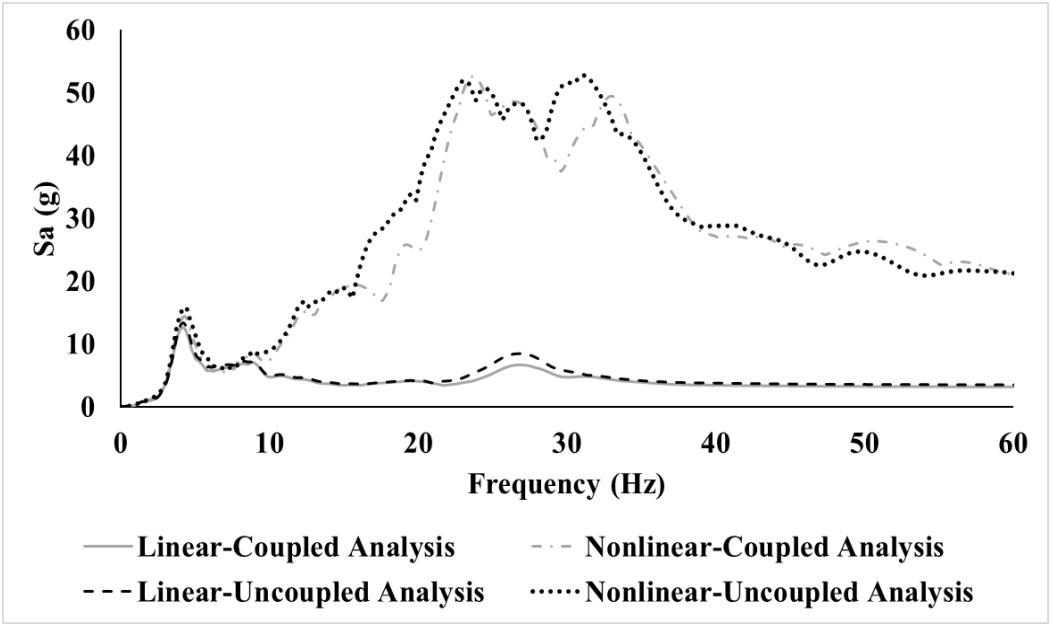


**Figure. A.13.** Comparison of ICRS at 1st Floor obtained from Coupled and Uncoupled Analysis of Linear and Nonlinear Models of System–3 Subjected to High–Frequency Ground Motions

### A.3.2. In–Cabinet Response Spectra (ICRS) at Sixth Floor of Secondary System

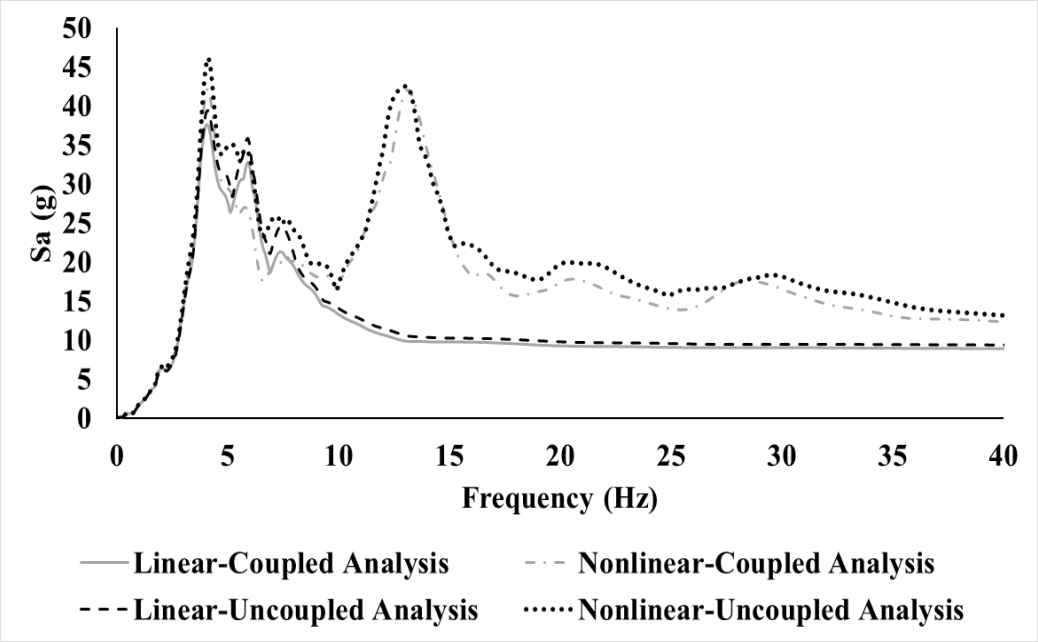


**Figure. A.14.** Comparison of ICRS at 6th Floor obtained from Coupled and Uncoupled Analysis of Linear and Nonlinear Models of System–3 Subjected to Low–Frequency Ground Motions

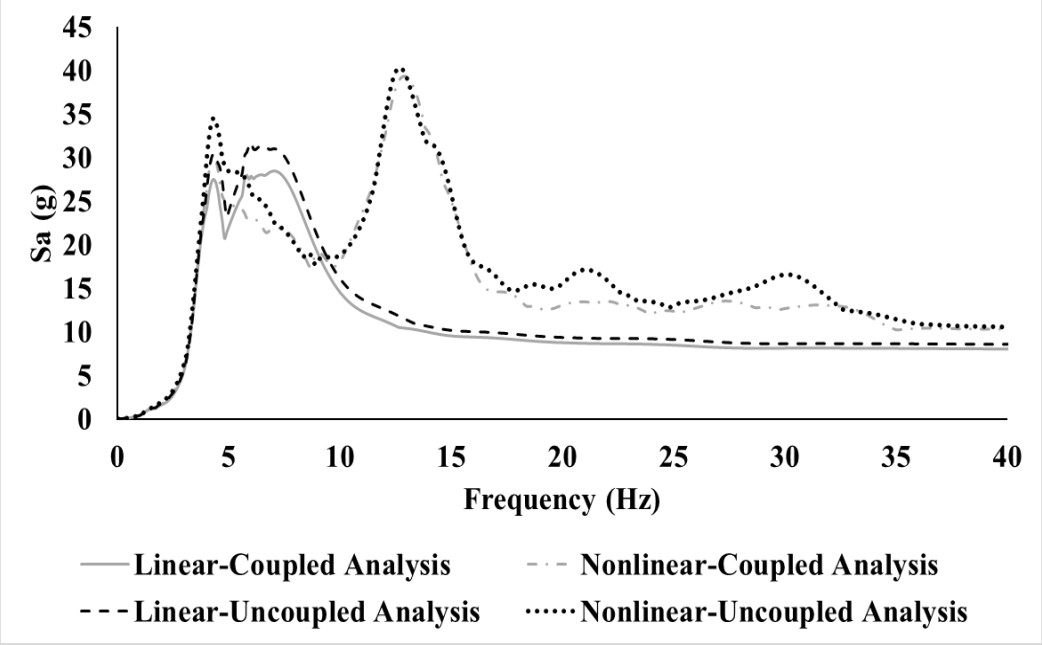


**Figure. A.15.** Comparison of ICRS at 6th Floor obtained from Coupled and Uncoupled Analysis of Linear and Nonlinear Models of System–3 Subjected to High–Frequency Ground Motions

## A.4. System–4

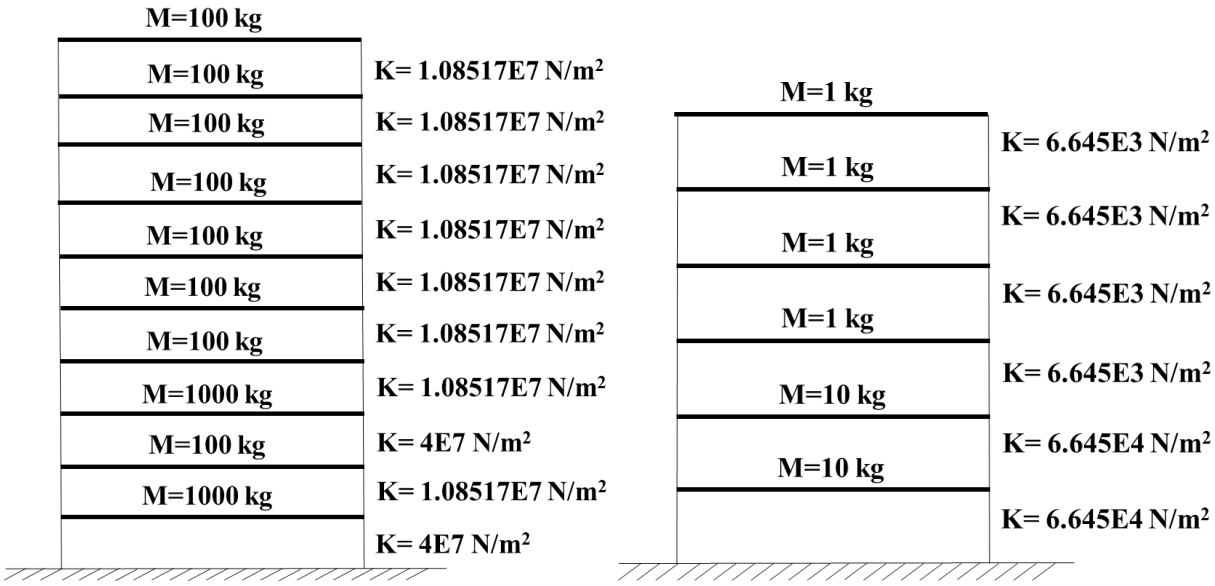


**Figure. A.16.** System–4: Uncoupled Primary and Secondary System. Secondary System Connected at 10th Floor of Primary System

**Table A.4.** Uncoupled and Coupled System Modal Frequencies for System–4

| Primary System | | Secondary System | | Coupled System | |
|---|---|---|---|---|---|
| **Mode #** | **Frequency (Hz)** | **Mode #** | **Frequency (Hz)** | **Mode #** | **Frequency (Hz)** |
| 1 | 8.27 | 1 | 4.26 | 1 | 4.25 |
| 2 | 16 | 2 | 8.27 | 2 | 7.64 |
| 3 | 33.20 | 3 | 13.19 | 3 | 8.91 |
| 4 | 35.98 | 4 | 19.78 | 4 | 13.19 |
| 5 | 52.98 | 5 | 21.26 | 5 | 16.04 |
| 6 | 70.45 | 6 | 24.42 | 6 | 19.78 |
| 7 | 84.97 | | | 7 | 21.285 |
| 8 | 95.85 | | | 8 | 24.42 |
| 9 | 102.58 | | | 9 | 33.27 |
| 10 | 117.35 | | | 10 | 35.99 |
| | | | | 11 | 53.01 |
| | | | | 12 | 70.47 |
| | | | | 13 | 84.98 |
| | | | | 14 | 95.85 |
| | | | | 15 | 102.58 |
| | | | | 16 | 117.35 |

### A.4.1. In–Cabinet Response Spectra (ICRS) at First Floor of Secondary System

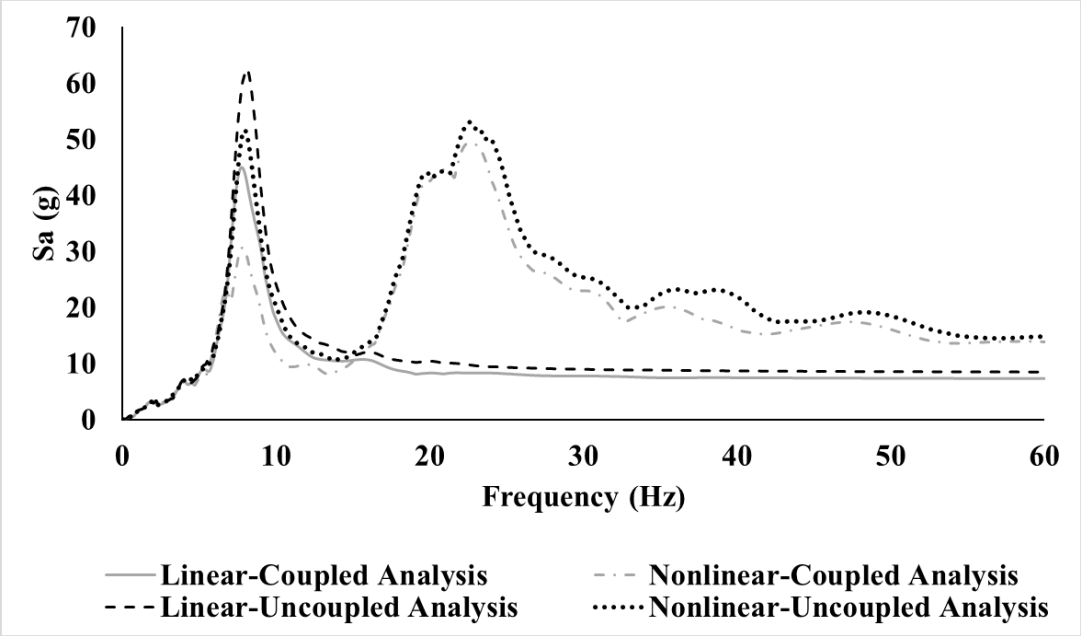


**Figure. A.17.** Comparison of ICRS at 1st Floor obtained from Coupled and Uncoupled Analysis of Linear and Nonlinear Models of System–4 Subjected to Low–Frequency Ground Motions

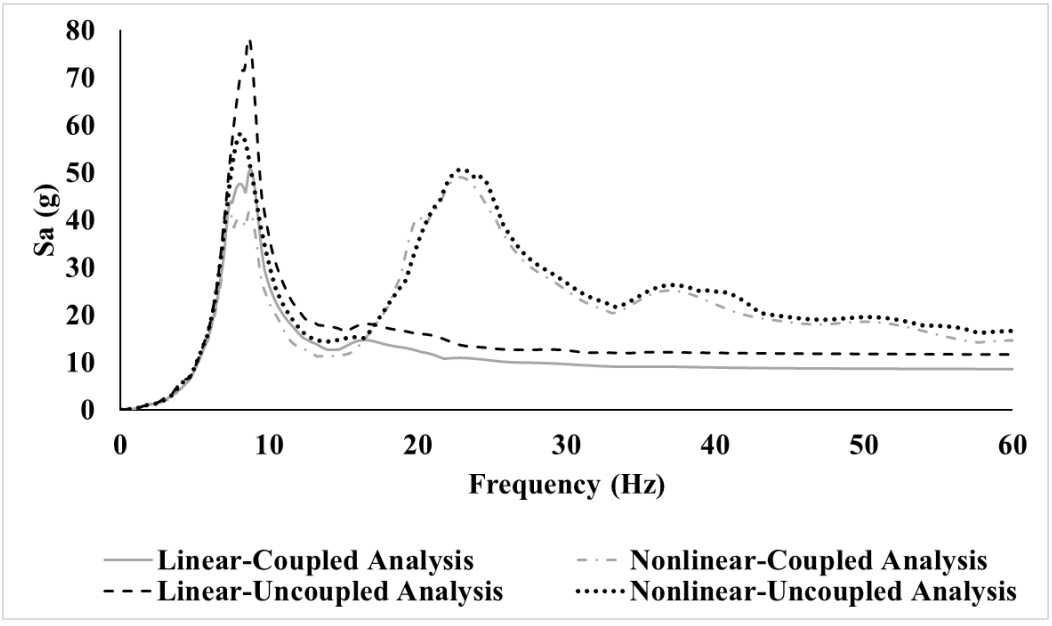


**Figure. A.18.** Comparison of ICRS at 1st Floor obtained from Coupled and Uncoupled Analysis of Linear and Nonlinear Models of System–4 Subjected to High–Frequency Ground Motions

### A.4.2. In–Cabinet Response Spectra (ICRS) at Sixth Floor of Secondary System

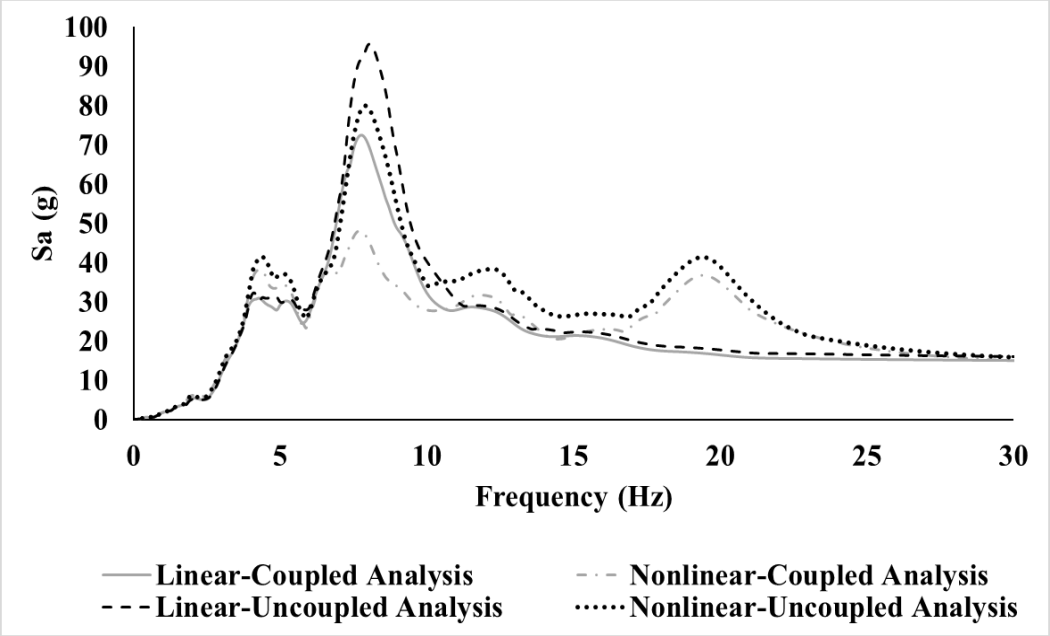


**Figure. A.19.** Comparison of ICRS at 6th Floor obtained from Coupled and Uncoupled Analysis of Linear and Nonlinear Models of System–4 Subjected to Low–Frequency Ground Motions

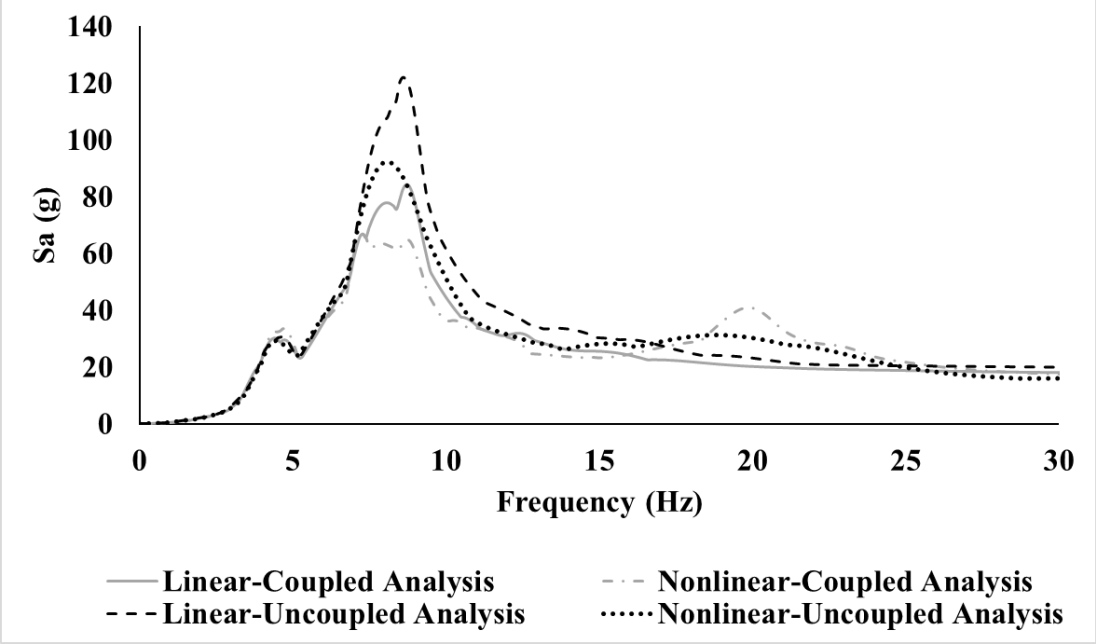


**Figure. A.20.** Comparison of ICRS at 6th Floor obtained from Coupled and Uncoupled Analysis of Linear and Nonlinear Models of System–4 Subjected to High–Frequency Ground Motions

## A.5. System–5

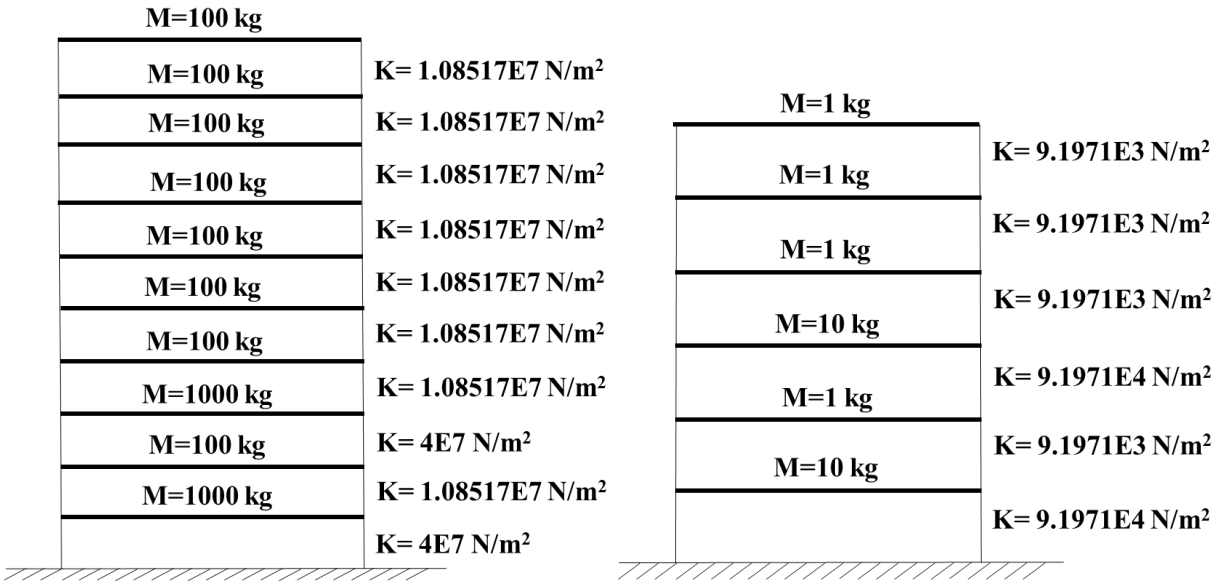


**Figure. A.21.** System–5: Uncoupled Primary and Secondary System. Secondary System Connected at 10th Floor of Primary System

**Table A.5.** Uncoupled and Coupled System Modal Frequencies for System–5

| **Primary System** | | **Secondary System** | | **Coupled System** | |
|---|---|---|---|---|---|
| **Mode #** | **Frequency (Hz)** | **Mode #** | **Frequency (Hz)** | **Mode #** | **Frequency (Hz)** |
| 1 | 8.27 | 1 | 3.60 | 1 | 3.59 |
| 2 | 16 | 2 | 7.86 | 2 | 7.83 |
| 3 | 33.20 | 3 | 16 | 3 | 8.25 |
| 4 | 35.98 | 4 | 19.25 | 4 | 15.25 |
| 5 | 52.98 | 5 | 27.55 | 5 | 16.87 |
| 6 | 70.45 | 6 | 52.73 | 6 | 19.25 |
| 7 | 84.97 | | | 7 | 27.55 |
| 8 | 95.85 | | | 8 | 33.29 |
| 9 | 102.58 | | | 9 | 35.99 |
| 10 | 117.35 | | | 10 | 52.73 |
| | | | | 11 | 53.03 |
| | | | | 12 | 70.47 |
| | | | | 13 | 84.99 |
| | | | | 14 | 95.85 |
| | | | | 15 | 102.58 |
| | | | | 16 | 117.35 |

### A.5.1. In–Cabinet Response Spectra (ICRS) at First Floor of Secondary System

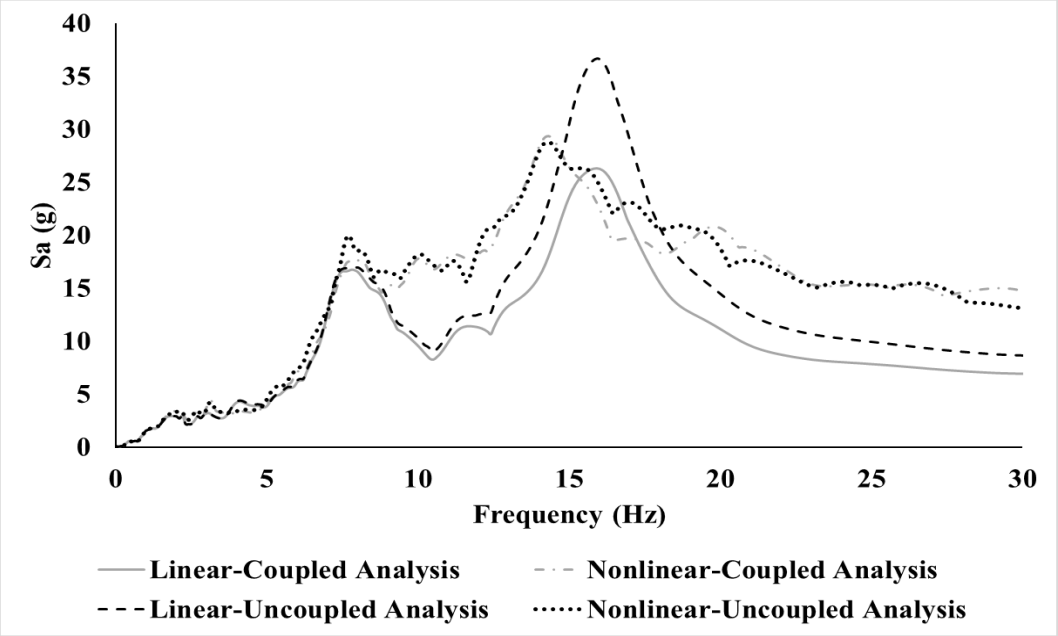


**Figure. A.22.** Comparison of ICRS at 1st Floor obtained from Coupled and Uncoupled Analysis of Linear and Nonlinear Models of System–5 Subjected to Low–Frequency Ground Motions

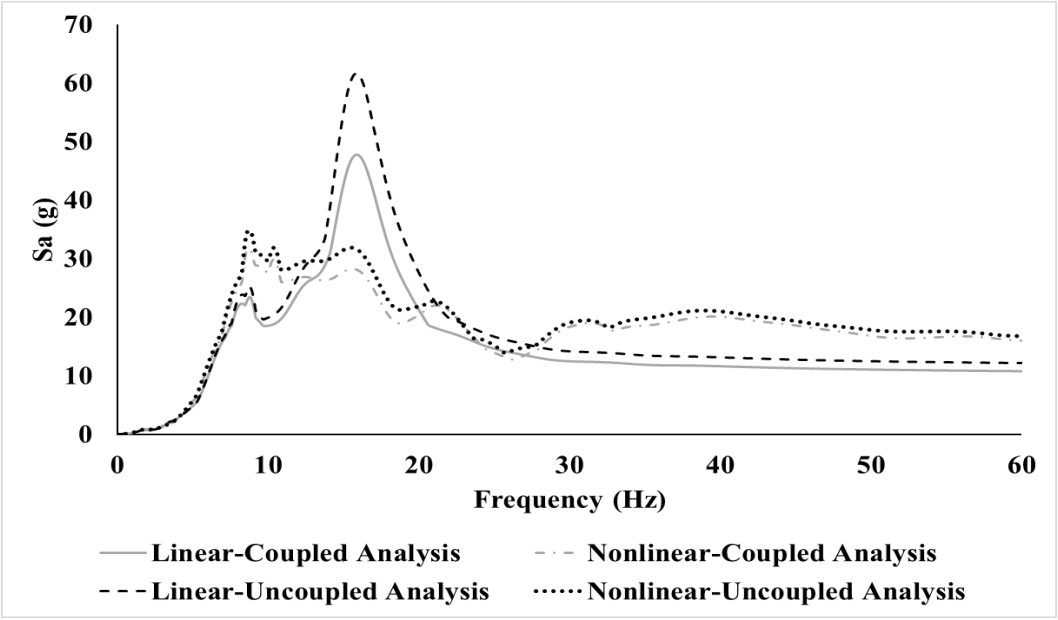


**Figure. A.23.** Comparison of ICRS at 1st Floor obtained from Coupled and Uncoupled Analysis of Linear and Nonlinear Models of System–5 Subjected to High–Frequency Ground Motions

### A.5.2. In–Cabinet Response Spectra (ICRS) at Sixth Floor of Secondary System

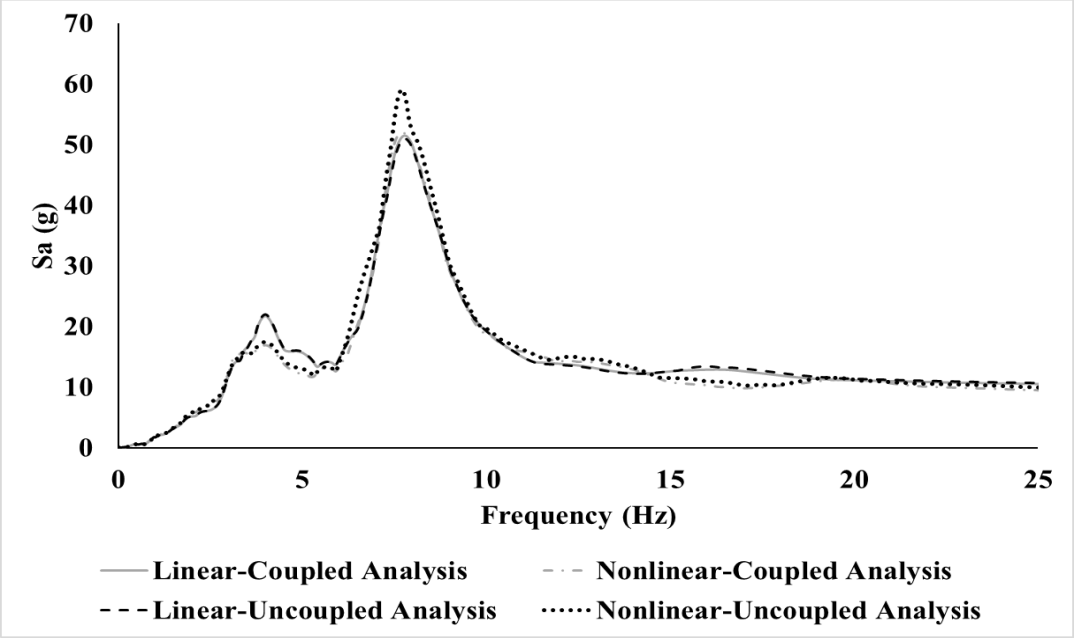


**Figure. A.24.** Comparison of ICRS at 6th Floor obtained from Coupled and Uncoupled Analysis of Linear and Nonlinear Models of System–5 Subjected to Low–Frequency Ground Motions

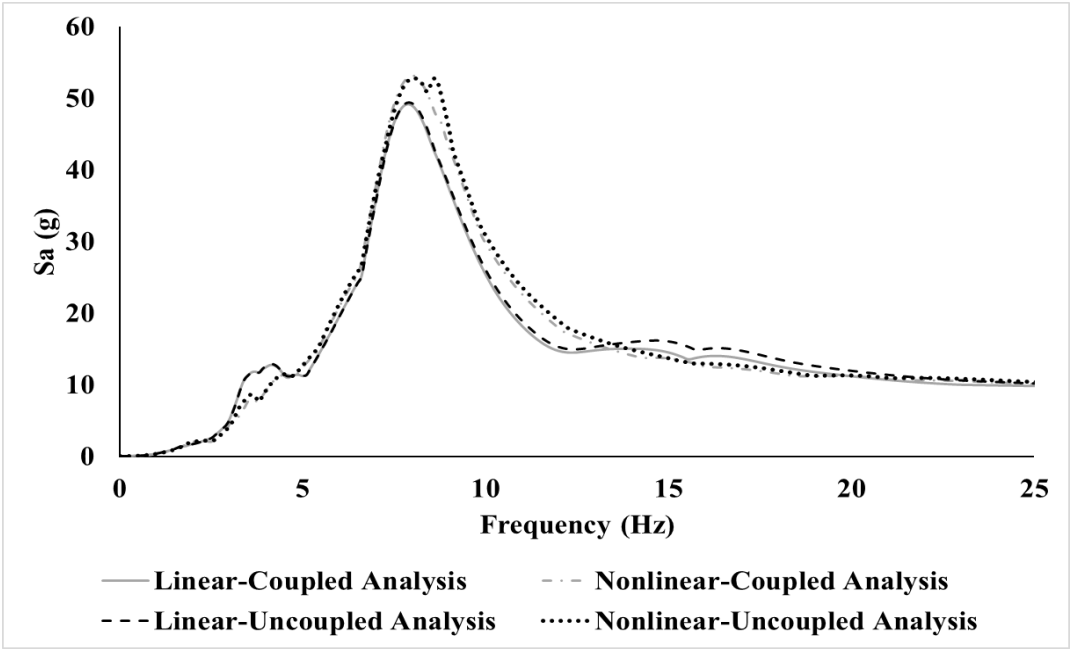


**Figure. A.25.** Comparison of ICRS at 6th Floor obtained from Coupled and Uncoupled Analysis of Linear and Nonlinear Models of System–5 Subjected to High–Frequency Ground Motions

## A.6. System–6

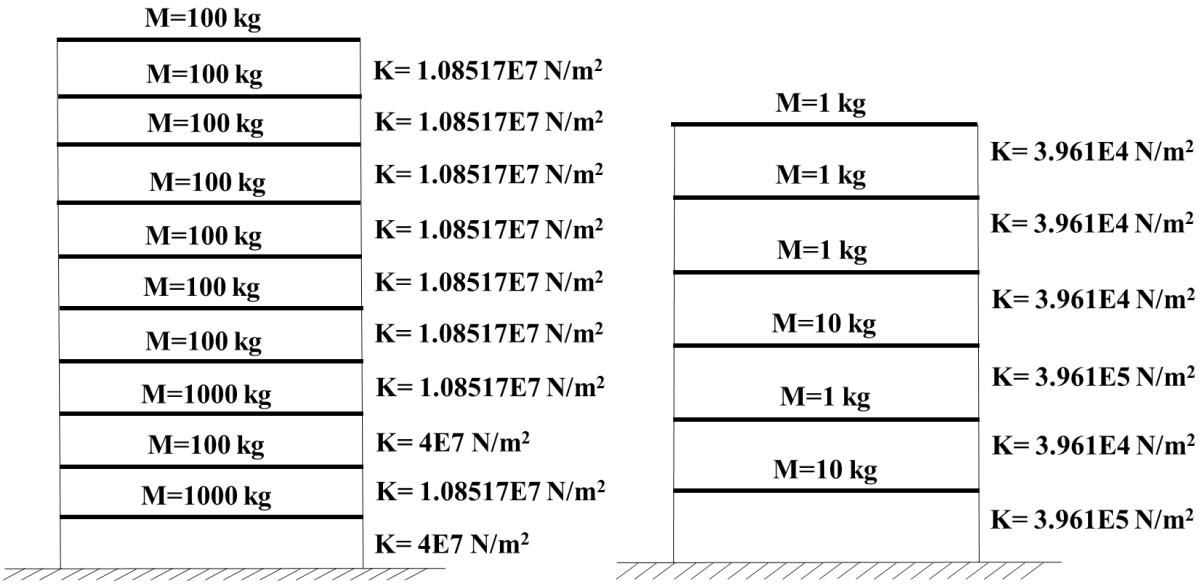


**Figure. A.26.** System–1: Uncoupled Primary and Secondary System. Secondary System Connected at 10th Floor of Primary System

**Table A.6.** Uncoupled and Coupled System Modal Frequencies for System–6

| Primary System | | Secondary System | | Coupled System | |
|---|---|---|---|---|---|
| **Mode #** | **Frequency (Hz)** | **Mode #** | **Frequency (Hz)** | **Mode #** | **Frequency (Hz)** |
| 1 | 8.27 | 1 | 7.47 | 1 | 7.15 |
| 2 | 16 | 2 | 16.30 | 2 | 8.54 |
| 3 | 33.20 | 3 | 33.21 | 3 | 15.85 |
| 4 | 35.98 | 4 | 39.94 | 4 | 16.4 |
| 5 | 52.98 | 5 | 57.17 | 5 | 31.20 |
| 6 | 70.45 | 6 | 109.42 | 6 | 35.17 |
| 7 | 84.97 | | | 7 | 36.38 |
| 8 | 95.85 | | | 8 | 39.94 |
| 9 | 102.58 | | | 9 | 53.28 |
| 10 | 117.35 | | | 10 | 57.17 |
| | | | | 11 | 70.58 |
| | | | | 12 | 85.04 |
| | | | | 13 | 95.87 |
| | | | | 14 | 102.59 |
| | | | | 15 | 109.42 |
| | | | | 16 | 117.35 |

### A.6.1. In–Cabinet Response Spectra (ICRS) at First Floor of Secondary System

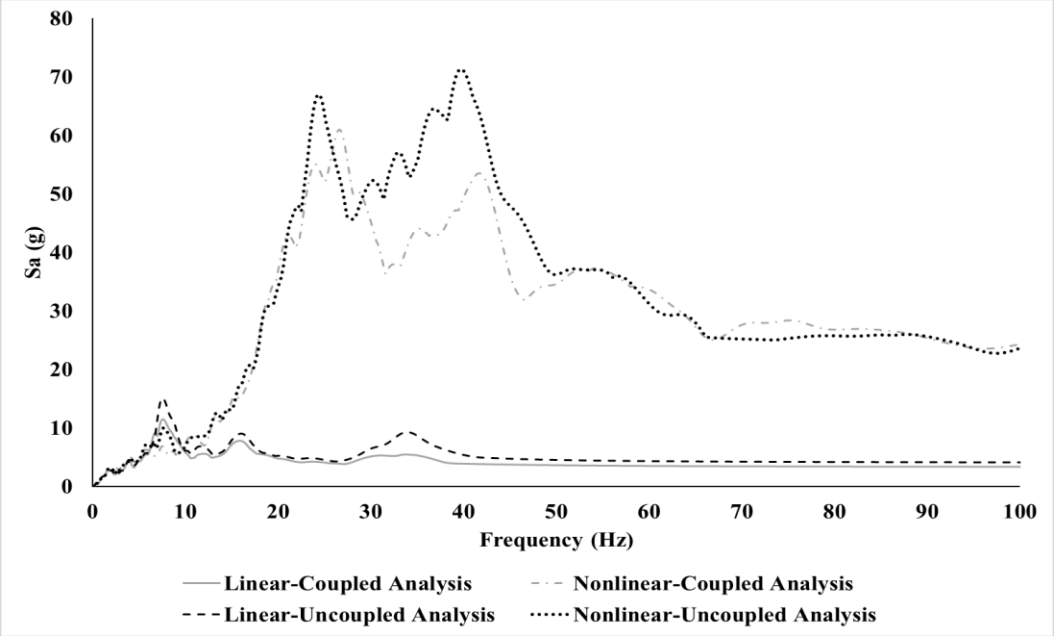


**Figure. A.27.** Comparison of ICRS at 1st Floor obtained from Coupled and Uncoupled Analysis of Linear and Nonlinear Models of System–6 Subjected to Low–Frequency Ground Motions

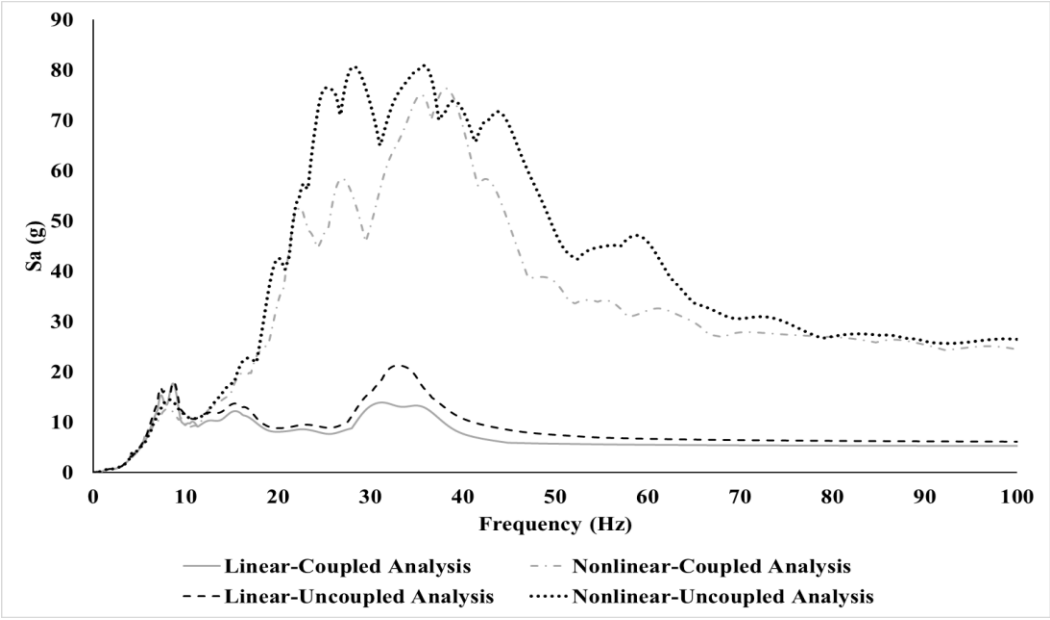


**Figure. A.28.** Comparison of ICRS at 1st Floor obtained from Coupled and Uncoupled Analysis of Linear and Nonlinear Models of System–6 Subjected to High–Frequency Ground Motions

### A.6.2. In–Cabinet Response Spectra (ICRS) at Sixth Floor of Secondary System

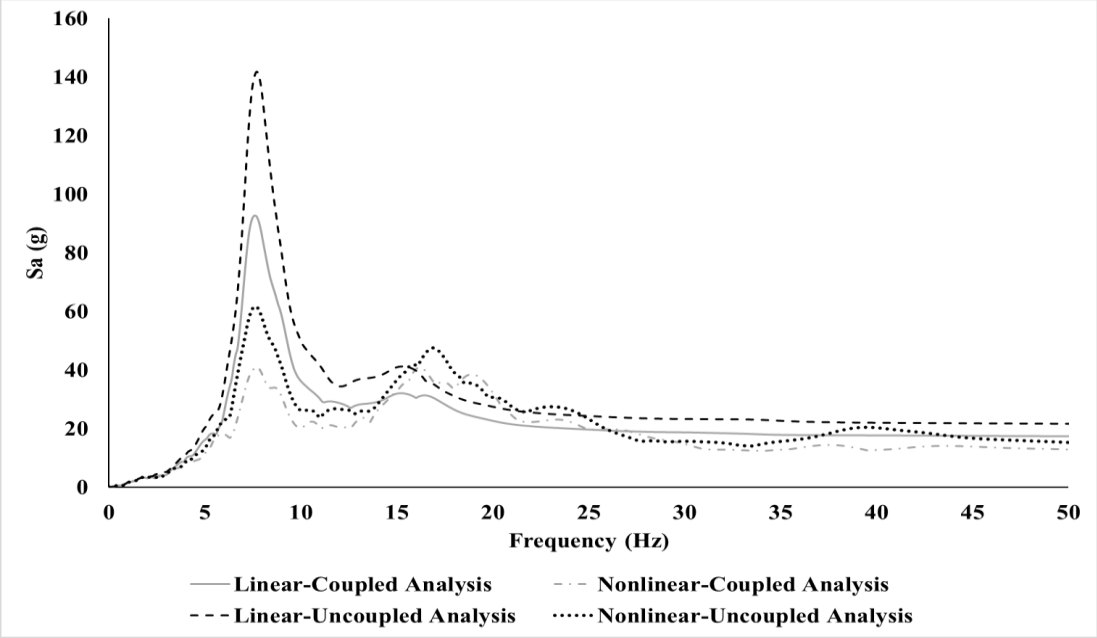


**Figure. A.29.** Comparison of ICRS at 6th Floor obtained from Coupled and Uncoupled Analysis of Linear and Nonlinear Models of System–6 Subjected to Low–Frequency Ground Motions

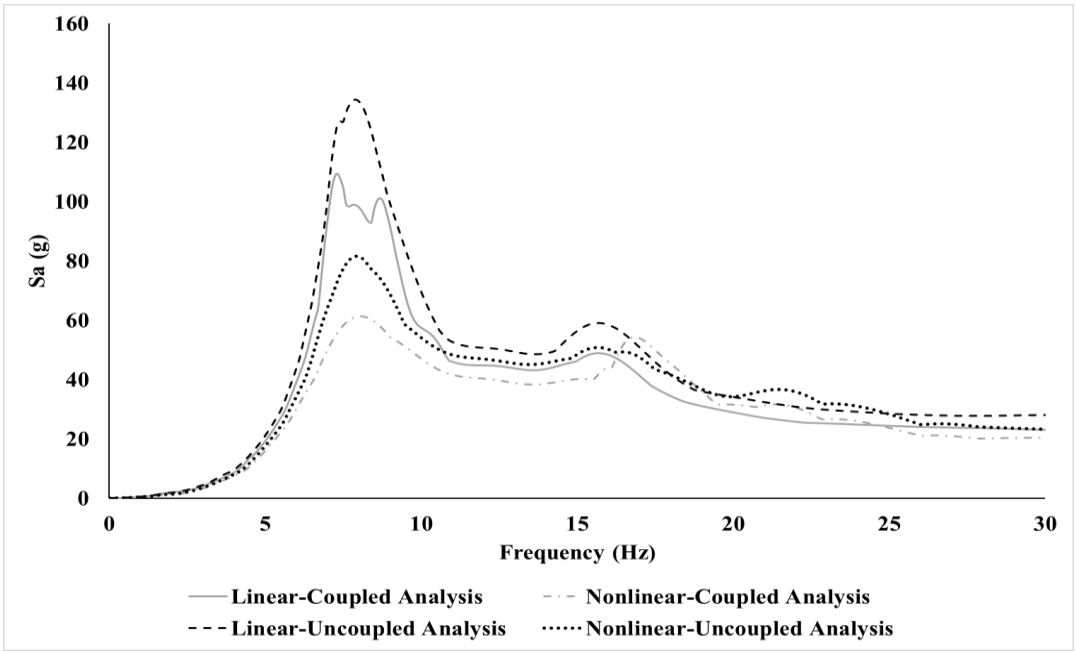


**Figure. A.30.** Comparison of ICRS at 6th Floor obtained from Coupled and Uncoupled Analysis of Linear and Nonlinear Models of System–6 Subjected to High–Frequency Ground Motions

## A.7. System–7

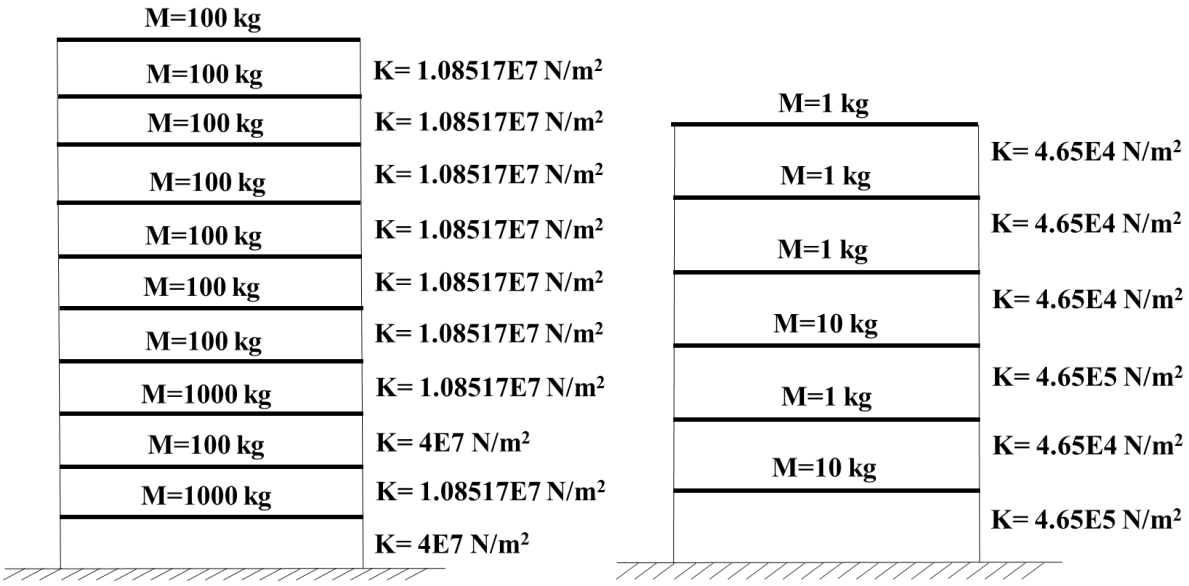


**Figure. A.31.** System–1: Uncoupled Primary and Secondary System. Secondary System Connected at 10th Floor of Primary System

**Table A.7.** Uncoupled and Coupled System Modal Frequencies for System–7

| Primary System | | Secondary System | | Coupled System | |
|---|---|---|---|---|---|
| **Mode #** | **Frequency (Hz)** | **Mode #** | **Frequency (Hz)** | **Mode #** | **Frequency (Hz)** |
| 1 | 8.27 | 1 | 8.09 | 1 | 7.53 |
| 2 | 16 | 2 | 17.67 | 2 | 8.78 |
| 3 | 33.20 | 3 | 35.98 | 3 | 15.92 |
| 4 | 35.98 | 4 | 43.28 | 4 | 17.70 |
| 5 | 52.98 | 5 | 61.94 | 5 | 32.01 |
| 6 | 70.45 | 6 | 118.56 | 6 | 35.73 |
| 7 | 84.97 | | | 7 | 37.73 |
| 8 | 95.85 | | | 8 | 43.28 |
| 9 | 102.58 | | | 9 | 53.37 |
| 10 | 117.35 | | | 10 | 61.94 |
| | | | | 11 | 70.61 |
| | | | | 12 | 85.05 |
| | | | | 13 | 95.88 |
| | | | | 14 | 102.59 |
| | | | | 15 | 117.35 |
| | | | | 16 | 118.56 |

### A.7.1. In–Cabinet Response Spectra (ICRS) at First Floor of Secondary System

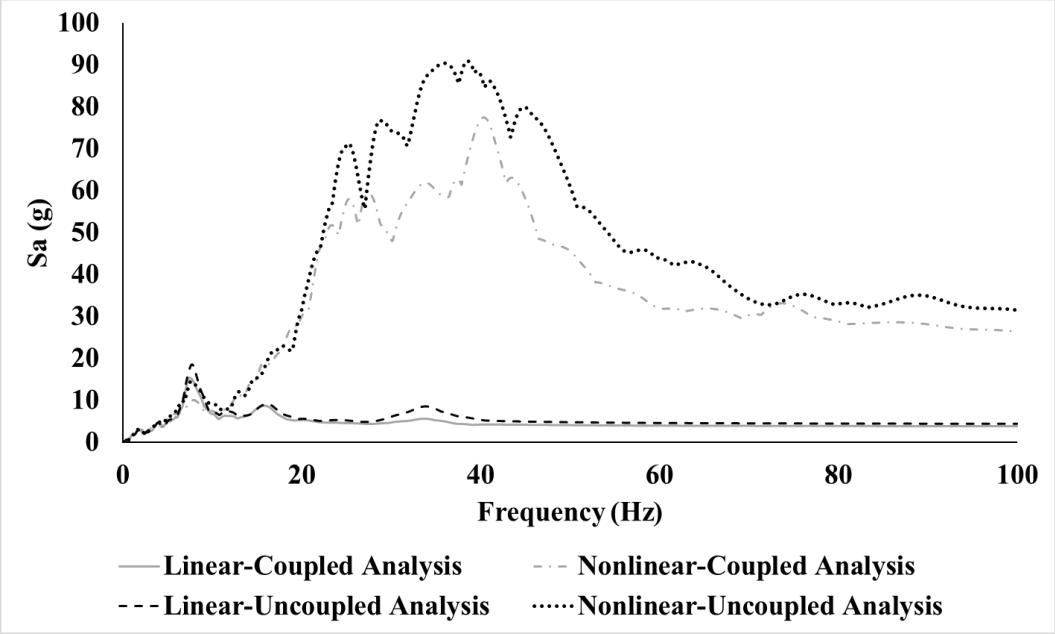


**Figure. A.32.** Comparison of ICRS at 1st Floor obtained from Coupled and Uncoupled Analysis of Linear and Nonlinear Models of System–7 Subjected to Low–Frequency Ground Motions

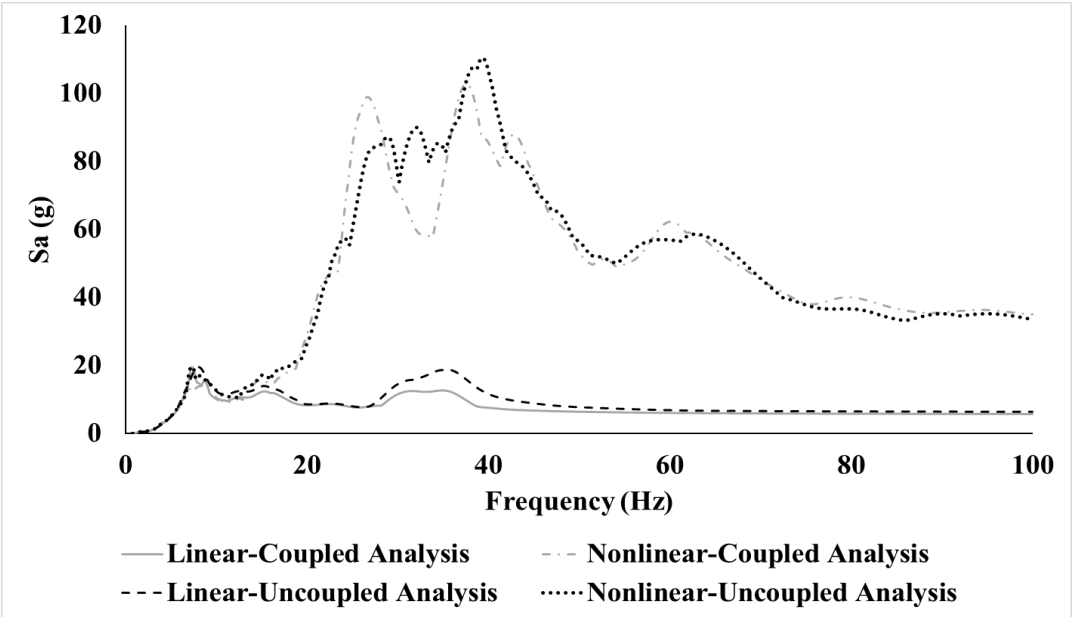


**Figure. A.33.** Comparison of ICRS at 1st Floor obtained from Coupled and Uncoupled Analysis of Linear and Nonlinear Models of System–7 Subjected to High–Frequency Ground Motions

### A.7.2. In–Cabinet Response Spectra (ICRS) at Sixth Floor of Secondary System

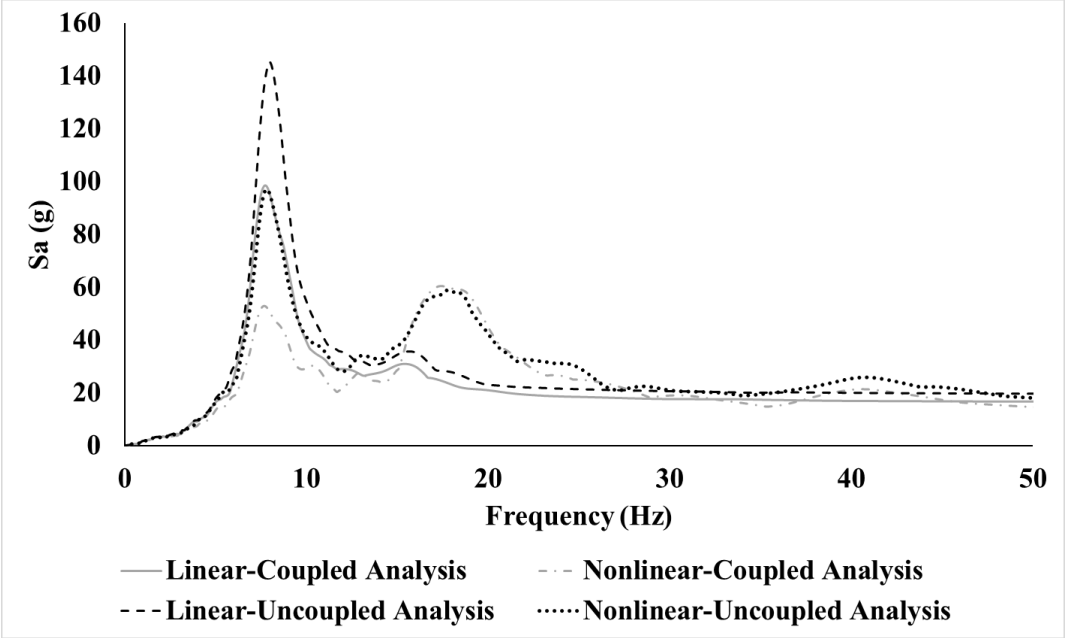


**Figure. A.34.** Comparison of ICRS at 6th Floor obtained from Coupled and Uncoupled Analysis of Linear and Nonlinear Models of System–7 Subjected to Low–Frequency Ground Motions

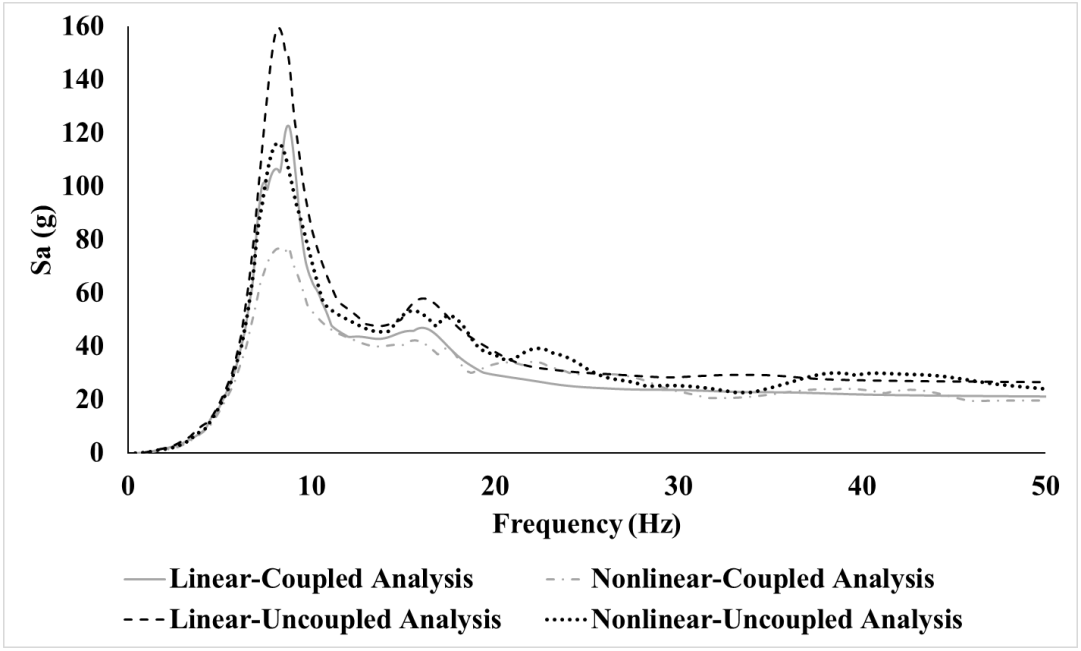


**Figure. A.35.** Comparison of ICRS at 6th Floor obtained from Coupled and Uncoupled Analysis of Linear and Nonlinear Models of System–7 Subjected to High–Frequency Ground Motions